NUMERICAL ANALYSIS OF WARM, TURBULENT SINKING JETS DISCHARGED INTO QUIESCENT WATER OF LOW TEMPERATURE

by

J. M. Peña and S. C. Jain

Prepared for
Commonwealth Edison Company
Chicago, Illinois

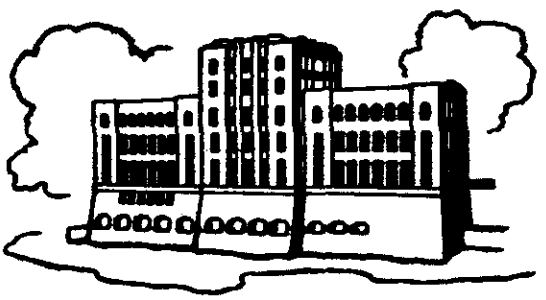

IIHR Report No. 154

Iowa Institute of Hydraulic Research
The University of Iowa
Iowa City, Iowa

February 1974

NUMERICAL ANALYSIS OF WARM, TURBULENT SINKING JETS DISCHARGED INTO QUIESCENT WATER OF LOW TEMPERATURE

by

J. M. Peña and S. C. Jain

Prepared for
Commonwealth Edison Company
Chicago, Illinois

IIHR Report No. 154

Iowa Institute of Hydraulic Research
The University of Iowa
Iowa City, Iowa

February 1974

NUMERICAL ANALYSIS OF WARM, TURBULENT SINKING JETS DISCHARGED INTO QUIESCENT WATER OF LOW TEMPERATURE

by

J. M. Peña and S. C. Jain

Prepared for
Commonwealth Edison Company
Chicago, Illinois

IIHR Report No. 154

Iowa Institute of Hydraulic Research
The University of Iowa
Iowa City, Iowa

December 1973

ACKNOWLEDGMENTS

This study was sponsored by the Commonwealth Edison Company, Chicago, Illinois. The authors wish to thank Mr. Byron Lee of Commonwealth Edison Company for his cooperation during this study. The authors gratefully acknowledge the guidance provided by Dr. John F. Kennedy, Director, Iowa Institute of Hydraulic Research.

ABSTRACT

This report is a summary of the numerical analysis of sinking jets in quiescent water of low temperature. Round jets (circular cross section) and two-dimensional slot jets are considered. The problem is analyzed by employing the integral approach and similarity conditions for velocity and temperature profiles. Results for the jet trajectory, width, and dilution are presented in graphical form. These solutions can be used to predict the behavior of warm, submerged jets discharging into lakes during winter season when the ambient temperature of the lake is near the freezing mark.

TABLE OF CONTENTS

LIST OF FIGURES

NUMERICAL ANALYSIS OF WARM, TURBULENT, SINKING JETS DISCHARGED INTO QUIESCENT WATER OF LOW TEMPERATURE

I. INTRODUCTION

Large quantities of waste heat from electric power plants are discharged into natural water bodies such as lakes, rivers and oceans. This method of "once through" cooling, being more economical than the "closed loop system" (i.e. cooling ponds, spray ponds, and cooling towers), is employed provided the temperature standards set by various regulatory agencies can be achieved. Due to the stringent temperature standards, submerged outlet or multi-port diffuser systems have been recently utilized in several installations (Jain et al. 1971, Vigander et al. 1970). Hitherto the outfall structures for thermal discharges were designed for the critical summer conditions. Lately some concerns have been expressed on the adverse effects of warm water on the ecology of lakes during winter when the ambient temperature of the lake water is near the freezing mark. Temperatures higher than the ambient temperature have been observed near the bottom of lakes (Pipes et al. 1973, Hogland and Spigarelli 1972).

As shown in Fig. 1 the density of water for a temperature less than 46.6°F (8°C) is always greater than that of water at 32°F (0°C) and the density is maximum at 39.2°F (4°C). During the winter the ambient temperature of lake water is about 32°F. If a discharge water temperature is less than 46.4°F (8°C), the plume will sink towards the bottom and stay there. Very few studies have been conducted on sinking plumes. The behavior of a sinking jet will be quite different from that of a buoyant jet in which the density of water can be assumed to be linearly decreasing with the increase of temperature.

This report is a summary of the numerical analysis of turbulent warm water jets discharging into stagnant water at freezing temperature.

The integral approach, assuming similarity in velocity and temperature profiles (Fan and Brooks 1969, Abraham 1963), is employed to solve the problem. The results are presented in graphical form showing the jet trajectories, the widths and the dilution ratios.

II. BASIC ASSUMPTIONS

The round and the two-dimensional slot jets are shown in figures 2 and 3, respectively. The flow is divided into two zones, (i) the zone of flow establishment and (ii) the zone of established flow. The flow leaves the nozzle with essentially uniform velocity and temperature. Due to lateral mixing the central core of constant velocity and temperature steadily decreases in lateral extent till the mixing region penetrates to the center-line of the jet. At that point the flow is considered to be fully established. Further entrainment of the ambient fluid steadily increases the jet spreading and reduces the velocity and temperature in the jet. The gross behavior of jet depends upon the buoyancy force acting on the jet and the initial momentum of the jet. The initial upward deflection of the jet axis due to the action of the buoyancy force depends upon the initial discharge temperature. If the net buoyancy force on the jet is positive (upward), the jet axis deflects upward and the vertical upward momentum flux of the jet increases. As the jet entrains ambient water, the jet temperature decreases. Due to the peculiar low temperature density behavior (figure 1), at a particular temperature for the jet the net buoyancy force on the jet becomes negative. The vertical momentum flux then begins to decrease, vanishing at the highest point of the jet-axis and finally increasing in the downward direction. Thereafter, the jet will sink.

The general assumptions, stated below, are common to both round and slot-jet problems:

1. The flow is fully turbulent and the effects of Reynolds number are negligible.

2. The pressure distribution is hydrostatic throughout the flow field.

3. Velocity profiles are assumed to be Gaussian and similar.

   (a) for round jet

$$u^*(s,r,\phi) = u(s)e^{-r^2/b^2} \qquad (1)$$

in which s: coordinate measured along axis of jet

r: radial distance from axis of jet

ϕ: angular co-ordinate shown in fig. 2

u^*: jet velocity at a local point

u: jet velocity at axis of jet

b: characteristic length defined by (1)

(b) for slot jet

$$u^*(s,n) = u(s)e^{-n^2/b^2} \tag{2}$$

in which n: distance from axis of jet in direction perpendicular to axis of jet (see Fig. 6)

b: characteristic length defined by (2)

4. Temperature profiles are assumed to be similar and Gaussian.

(a) for round jet

$$\frac{T^*(s,r,\phi) - T_a}{T_a} = \frac{(T(s) - T_a)e^{-r^2/(\lambda b)^2}}{T_a} \tag{3}$$

in which T^*: jet temperature at a local point

T : jet temperature at axis of jet

T_a: ambient temperature

λ^2: turbulent Schmidt number

(b) for slot jet

$$\frac{T^*(s,n) - T_a}{T_a} = \frac{(T(s) - T_a)e^{-n^2/(\lambda b)^2}}{T_a} \tag{4}$$

5. The entrainment velocity is assumed to be proportional to the jet velocity at axis of jet. The entrainment relation is given by the equation:

(a) for round jet

$$\frac{dQ}{ds} = 2\pi\alpha ub \tag{5}$$

in which Q: volume Flux across jet cross section

α: coefficient of entrainment

(b) for slot jet

$$\frac{dq}{ds} = 2\alpha u \tag{6}$$

in which q: volume flux per unit length along z-axis.

6. The effects of the curvature of jet trajectory are small.

The assumptions 3,4, and 5 are not valid in the zone of flow establishment. The theoretical analysis presented in the following sections is applicable to the zone of established flow. The initial value of the flow parameters for the zone of established flow are obtained from the initial values at the nozzle.

All these assumptions are essentially similar to those used by various earlier investigators for the case of a buoyant jet. The only difference is that in case of a buoyant jet the temperature density relation is assumed to be linear and the density deficiency profiles are then Gaussian by assumption 5. But this is not true in case of a jet at low temperature where the density temperature relation is nonlinear and multivalued.

In the following section a detailed analysis is performed for the case of a round heated water jet in quiescent water at low temperature. Since the analysis for a bidimensional slot jet is similar in almost all respects, the relevant equations are given in the Appendix, and numbered in such a way that they closely parallel the equations given in section III.

III. A ROUND HEATED WATER JET IN QUIESCENT WATER AT LOW TEMPERATURE

The three conservation equations for volume flux, momentum flux, and heat flux are used to analyze the problem.

A. Integral Formulation of the Problem.

Continuity equation: Using the entrainment relation (5) and neglecting the small variation in density, the equation of continuity can be expressed as

$$\frac{d}{ds}\int_0^{\infty}\int_0^{2\pi} u^* r\,dr\,d\phi = 2\pi\alpha u b \tag{7}$$

Integration of (7) on substituting for u^* from (1) yields

$$\frac{d}{ds}(ub^2) = 2\alpha u b \tag{8}$$

Momentum equation in horizontal direction:

$$\frac{d}{ds}\int_0^{\infty}\int_0^{2\pi} \rho^* u^* (u^* \cos\theta)\, r\, dr\, d\phi = 0 \tag{9}$$

in which ρ^*: density at a local point

θ : angle between the s-axis and horizontal

Substituting for u^* from (1) and neglecting the variation in ρ^*, (9) on integration reduces to

$$\frac{d}{ds}\left(\frac{u^2 b^2}{2}\cos\theta\right) = 0$$

or

$$\frac{u^2 b^2}{2}\cos\theta \text{ constant} \tag{10}$$

Momentum equation in vertical direction:

$$\frac{d}{ds}\int_0^{\infty}\int_0^{2\pi} \rho^* u^* (u^* \sin\theta)\, r\, dr\, d\phi$$

$$= g\int_0^{\infty}\int_0^{2\pi} (\rho_a - \rho^*)\, r\, dr\, d\phi \tag{11}$$

Using (1) and neglecting the variation in density in the inertia term (Boussinesq approximation), (11) on integration yields

$$\frac{d}{ds}\left(\frac{u^2b^2}{2}\sin\theta\right) = 2g\lambda^2b^2\beta(s) \tag{12}$$

in which

$$\beta(s) = \int_0^\infty \left(\frac{\rho_a-\rho^*}{\rho_a}\right) r'dr' \tag{13}$$

$$r' = r/\lambda b \tag{14}$$

Heat conservation equation:

$$\frac{d}{ds}\int_0^\infty \int_0^{2\pi} c\rho^*u^*(T^*-T_a)\, r\, dr\, d\phi = 0 \tag{15}$$

in which c: specific heat of water at constant pressure and is assumed constant.

Substituting for u^* from (1) and for T^* from (3) and integrating,

$$\frac{d}{ds}\left[ub^2(T-T_a)\right] = 0$$

or

$$ub^2(T-T_a) = \text{constant} \tag{16}$$

Further the geometric relations for the jet trajectory are

$$\frac{dx}{ds} = \cos\theta \tag{17}$$

and

$$\frac{dy}{ds} = \sin\theta \tag{18}$$

in which x: horizontal co-ordinate (see fig. 2)

y: vertical co-ordinate

Finally the density of water is a known function of temperature (Fig. 1), i.e.

$$\rho^* = f(T^*) \tag{19}$$

Equations 8, 10, 12, 16, 17, 18 and 19 contain seven unknowns, namely u, b, T, ρ, θ, x and y, which can be solved as functions of s for the following initial conditions.

$$\left.\begin{aligned} &u(0) = U_o,\ b(0) = b_o,\ \rho(0) = \rho_o \\ &T(0) = T_o,\ \theta(0) = \theta_o, \quad x = 0 \\ &y = 0 \end{aligned}\right\} \quad \text{at } s = 0 \tag{20}$$

in which suffix "o" denotes the initial conditions of jet at the beginning of the zone of established flow.

B. Normalized Governing Equations.

The governing equations are normalized to obtain the generalized solutions. It can be easily seen that (19) cannot be normalized because temperature is a double valued function of density at low temperatures. The system of the remaining six equations is transformed into normalized form (Fan and Brooks 1969) using the dimensionless parameters defined below.

Volume flux parameter:

$$\mu = ub^2/U_o b_o^2 \tag{21}$$

Momentum flux parameter:

$$m = \left| \frac{g\lambda^2 U_o^3 b_o^6}{2\sqrt{2}\alpha} \right|^{-2/5} \frac{u^2 b^2}{2} \tag{22}$$

$$h = m \cos\theta \tag{23}$$

$$v = m \sin\theta \tag{24}$$

Co-ordinates:

$$\zeta = \delta s \tag{25}$$

$$\eta = \delta x \tag{26}$$

$$\xi = \delta y \tag{27}$$

in which

$$\delta = \left| \frac{U_o^2 b_o^4}{64 g \alpha^4 \lambda^2} \right|^{-1/5} \tag{28}$$

Temperature:

$$\psi^* = \frac{T^* - T_a}{T_o - T_a} \tag{29}$$

Density:

$$\phi^* = \frac{\rho_a - \rho^*}{\rho_a} \tag{30}$$

Equations 8, 10, 12, 16, 17 and 18 then in non-dimensional form become

$$\frac{d\mu}{d\zeta} = \sqrt{m} \tag{31}$$

$$h = \sqrt{m^2 - v^2} = m_o \cos \theta_o = \text{constant} \tag{32}$$

$$\frac{dv}{d\zeta} = \frac{\mu^2}{m} \cdot \beta \tag{33}$$

$$\frac{d\eta}{d\zeta} = \frac{h}{m} \tag{34}$$

$$\frac{d\xi}{d\zeta} = \frac{v}{m} \tag{35}$$

$$\mu\psi = \mu_o \psi_o = \text{constant} \tag{36}$$

$$\text{The quantity } \beta = \int_0^\infty \phi^* r' dr' \tag{37}$$

The initial conditions corresponding to (20) are $\mu(0) = 1$, $m(0) = m_o$, $\theta(0) = \theta_o$, $\psi(0) = 1$, $\phi(0) = \phi_o$, $\xi = 0$, $\eta = 0$ at $\zeta = 0$ (38)

The governing parameters for a given ambient condition are m_o, θ_o, and ϕ_o. The parameter m_o is directly related to jet Froude number. It can be shown from (22) that

$$m_o^5 = \frac{\alpha^2}{4\lambda^4} \cdot \frac{U_o^4}{g^2 b_o^2} \tag{39}$$

Substituting fro b_o from (42),

$$m_o = \left(\frac{\alpha^2}{8\lambda^4}\right)^{1/5} F^{4/5} \tag{40}$$

in which

$$F = \frac{U_o}{\sqrt{gR}} \quad \text{(jet Froude number)} \tag{41}$$

$2R = D$ = initial jet diameter

C. Numerical Results:

The system of ordinary differential equations was solved numerically on IBM 360/65 computer using modified Euler predictor-corrector method. Solutions are obtained for the following conditions.

(i) $T_a = 32°F$ (0°C)

(ii) $\Delta T = 10°F$, 15°F, 20°F and 25°F

(iii) $F = 0.8$, 1.6, 2.4, 3.2, 4.0, and 6.0 (roundjet)

(iv) $F = 0.3$, 0.6, 0.9, 1.2, 1.5, and 2.25 (slot)

(vi) $\theta_o = 0°$, 15° and 30°

The centerline trajectory and the half width are presented, in Figs. 3(a) to 3(l) for the round jet and in Figs. 7(a) to 7(l) for the slot

jet. It should be noted that the jet trajectory for all conditions is deflected downward indicating a negative buoyancy force on the jet. For $\theta > 0^{o}$ the jet rises to a certain maximum height y_t due to initial positive vertical momentum. The variation of the maximum rise with the jet Froude number is shown in Fig. 4 for the round jet and in Fig. 8 for the slot jet. The maximum rise for a given jet angle and temperature difference varies linearly with the jet Froude number except at very low Froude numbers. The maximum rise is higher for smaller initial jet temperatures. The rate of dilution, S_o, along the jet trajectory is presented in Figs. 5(a) to 5(l) for the round jet and in Figs. 9(a) to 9(l) for the slot jet. These curves show that the dilution is minimum for some intermediate jet Froude number. The jet travels the shortest path at this jet Froude number.

D. Correction for Zone of Flow Establishment:

To make use of the results presented in the preceeding section, corrections must be made for the zone of flow establishment. The following corrections apply to the round jet. The corresponding corrections for the slot jet are given by equation (A 42) through (A 48) in the Appendix.

(i) Width Correction - The initial value of b_o is obtained from conservation of momentum between 0' and 0 neglecting buoyancy force in such a short region, i.e.

$$\pi \frac{D^2}{4} U_o^2 = \int_0^{\infty} \int_0^{2\pi} u^{*2} r dr \, d\phi \qquad \text{at } 0$$

$$= \frac{\pi}{2} b_o^2 U_o^2$$

Thus

$$b_o = \frac{D}{\sqrt{2}} \tag{42}$$

(ii) Correction for Dilution - The conservation of heat flux between 0 and 0' (fig. 2) gives

$$\rho_o' C(T_o' - T_a) \cdot \frac{\pi}{4} D^2 U_o = \int_0^{\infty} \int_0^{2\pi} c\rho^* u^* (T^* - T_a)\, r\, dr\, d\phi \qquad (43)$$

in which T_o' = initial jet temperature

ρ_o' = initial jet density

Substituting for u^* from (1), for $(T^* - T_a)$ from (3), and for b_o from (42), and neglecting the variation in density, (43) reduces to,

$$(T_o' - T_a) = \frac{2\lambda^2}{1+\lambda^2} (T_o - T_a) \qquad (44)$$

The dilution ratio S with respect to the initial temperature at the nozzle is

$$S = \frac{T_o' - T_a}{T - T_a} = \frac{2\lambda^2}{1+\lambda^2} \frac{T_o - T_a}{T - T_a} = \frac{2\lambda^2}{1+\lambda^2} S_o \qquad (45)$$

Hence the values of S_o given in figs. 5(a) to 5(l) must be multiplied by the factor $2\lambda^2/1+\lambda^2$ to obtain the correct centerline dilution.

(iii) Coordinate Correction for jet trajectory - From the experiments of Alberttson et al. (1950), the length of the zone of flow establishment is taken as 6.2 D. The non-dimensional coordinates with respect to the discharge point 0' (fig. 2), neglecting buoyancy effects in this zone, are

$$\frac{x'}{D} = \frac{x}{D} + 6.2 \cos \theta_o \qquad (46)$$

$$\frac{y'}{D} = \frac{y}{D} + 6.2 \sin \theta_o \qquad (47)$$

E. Entrainment and Spreading Coefficients:

In the present analysis the entrainment coefficient α has been assumed a constant. The experimental data for buoyant jets seem to justify

this assumption. The values for the entrainment coefficient α and spreading coefficient, λ, (turbulent Schmidt number λ^2) according to Rouse et al. (1952) results are

$$\alpha = 0.082 \text{ and } \lambda = 1.16 \tag{48}$$

These values have been adopted by various investigators. It is suggested that these values in the absence of better estimates may be used for sinking jets also.

IV. SUMMARY

In a certain range of low temperatures the density of the heated water discharged from power plant can be higher than that of the receiving water. Under those conditions a heated jet will sink rather than rising towards the surface. Numerical results in graphical form for a wide range of initial conditions are presented for round and slot jets. The ambient temperature of the receiving water is taken as $32^{\circ}F$. Four condenser water temperature increases; $10^{\circ}F$, $15^{\circ}F$, $20^{\circ}F$, and $25^{\circ}F$; are presented. It is observed that the jet trajectory is deflected downward for all the conditions. For the initial jet angles greater than zero, the jet rises to a maximum height due to initial vertical momentum and then starts sinking. The results can be used to design a submerged outfall structure for winter conditions.

APPENDIX

The equations for the two dimensional jet are listed below. These equations are numbered such that they correspond to the equations for the axisymetric jet given in the text.

$$\frac{d}{ds}\int_{-\infty}^{\infty} u^* dn = 2\alpha u \tag{A7}$$

$$\frac{d}{ds}(ub) = \frac{2\alpha u}{\sqrt{\pi}} \tag{A8}$$

$$\frac{d}{ds}\int_{-\infty}^{\infty} \rho^* u^* (u^* \cos\theta)\, dn = 0 \tag{A9}$$

$$\frac{d}{ds}\left(\frac{u^2 b}{\sqrt{2}} \cos\theta\right) = 0$$

$$\frac{u^2 b}{\sqrt{2}} \cos\theta = \text{constant} \tag{A10}$$

$$\frac{d}{ds}\int_{-\infty}^{\infty} \rho^* u^* (u^* \sin\theta)\, dn = g\int_{-\infty}^{\infty} (\rho_a - \rho^*) dn \tag{A11}$$

$$\frac{d}{ds}\left(\frac{u^2 b}{\sqrt{2}} \sin\theta\right) = \sqrt{\pi} g \lambda b\, \beta(s) \tag{A12}$$

$$\beta(s) = \int_{-\infty}^{\infty} \frac{\rho_a - \rho^*}{\rho_a} \, dn' \tag{A13}$$

$$n' = n/\lambda b \tag{A14}$$

$$\frac{d}{ds} \int_{-\infty}^{\infty} c\rho^* u^* (T^* - T_a) \, dn = 0 \tag{A15}$$

$$\frac{d}{ds} [ub(T - T_a)] = 0$$

$$ub(T - T_a) = \text{constant} \tag{A16}$$

$$\frac{dx}{ds} = \cos \theta \tag{A17}$$

$$\frac{dy}{ds} = \sin \theta \tag{A18}$$

$$\rho^* = f(T^*) \tag{A19}$$

$$\left.\begin{aligned} &u(0) = U_o, \; b(0) = b_o, \; \rho(0) = \rho_o \\ &T(0) = T_o, \; \theta(0) = \theta_o, \; x = 0, \\ &y = 0 \end{aligned}\right\} \text{at } s = 0 \tag{A20}$$

$$\mu = ub/U_o b_o \tag{A21}$$

$$m = \left| \frac{4\alpha}{\lambda g U_o^4 b_o^4} \right|^{1/3} \frac{u^2 b}{\sqrt{2}} \tag{A22}$$

$$h = m \cos \theta \tag{A23}$$

$$v = m \sin \theta \tag{A24}$$

$$\zeta = \delta' s \tag{A25}$$

$$\eta = \delta' x \tag{A26}$$

$$\xi = \delta' y \tag{A27}$$

$$\delta' = \left| \frac{4\sqrt{2} g \alpha^2 \lambda}{\pi \sqrt{\pi}\, U_o^2 b_o^2} \right|^{1/3} \tag{A28}$$

$$\psi^* = \frac{T^* - T_a}{T_o - T_a} \tag{A29}$$

$$\phi^* = \frac{\rho_a - \rho^*}{\rho_a} \tag{A30}$$

$$\frac{d\mu}{d\zeta} = \frac{m}{\mu} \tag{A31}$$

$$h = \sqrt{m^2 - v^2} = m_o \cos \theta_o = \text{constant} \tag{A32}$$

$$\frac{dv}{d\zeta} = \frac{\mu^2}{m}\beta \tag{A33}$$

$$\frac{d\eta}{d\zeta} = \frac{h}{m} \tag{A34}$$

$$\frac{d\xi}{d\zeta} = \frac{v}{m} \tag{A35}$$

$$\mu\psi = \mu_o\psi_o = \text{constant} \tag{A36}$$

$$\beta = \int_{-\infty}^{\infty} \phi^* d\eta' \tag{A37}$$

$$\mu(0) = 1,\ m(0) = m_o,\ \theta(0) = \theta_o,\ \psi(0) = 1,$$

$$\phi(0) = \phi_o, \quad \xi = 0 \qquad \eta = 0 \qquad \zeta = 0 \tag{A38}$$

$$m_o^3 = \frac{\sqrt{2\alpha}}{\lambda}\ \frac{U_o^2}{gb_o} \tag{A39}$$

$$m_o = \left(\frac{\sqrt{\pi\alpha}}{\lambda}\right)^{1/3} F^{2/3} \tag{A40}$$

$$F = \frac{U_o}{\sqrt{gB}} \quad \text{(jet Froude number)} \tag{A41}$$

B = initial jet width.

$$BU_o^2 = \int_{-\infty}^{\infty} u^{*2} dn$$

$$= \sqrt{\pi/2}\ U_o^2 b_o$$

$$b_o = \sqrt{2/\pi}\ B \tag{A42}$$

$$\rho_o' c(T_o' - T_a) \cdot BU_o = \int_{-\infty}^{\infty} c\rho^* u^* (T^* - T_a) dn \tag{A43}$$

$$(T_o' - T_a) = \sqrt{\frac{2\lambda^2}{1+\lambda^2}}\ (T_o - T_a) \tag{A44}$$

$$S = \frac{T_o' - T_a}{T - T_a} = \sqrt{\frac{2\lambda^2}{1+\lambda^2}}\ \frac{T_o - T_a}{T - T_a} = \sqrt{\frac{2\lambda^2}{1+\lambda^2}}\ S_o \tag{A45}$$

$$\text{for } \sqrt{\frac{2\lambda^2}{1+\lambda^2}}\ S_o \geq 1$$

$$\frac{x'}{D} = \frac{x}{D} + 5.2 \cos \theta_o \tag{A 46}$$

$$\frac{Y'}{D} = \frac{Y}{D} + 5.2 \sin \theta_o \tag{A47}$$

$$\alpha = 0.16 \quad \text{and} \quad \lambda = 0.89 \tag{A48}$$

REFERENCES

1. Abraham, G. 1963, "Jet Diffusion in Stagnant Ambient Fluid"- Delft-Hydraulic Laboratory, Publication No. 29.

2. Albertson, M.L., Dai, Y.B., Jensen, R.A., and Rouse, H., 1950, "Diffusion of Submerged Jets", Transactions, ASCE, 115.

3. Fan, L.N. and Brooks, N.H., 1969, "Numerical Solutions of Turbulent Buoyant Jet Problems," W.M. Keck Laboratory, California Institute of Technology, Report No. KH-R-18.

4. Hogland, B. and Spigarelli, S.A., 1972, "Studies of the Sinking Plumes Phenomenon", presented at the 15th Great Lakes Research Conference, Madison, Wisconsin.

5. Jain, S.C., Sayre, W.W., Adyeampong, Y.A., McDougall, D. and Kennedy, J.F., 1971, "Model Studies and Design of Thermal Outlet Structures Quad Cities Nuclear Plant", Iowa Institute of Hydraulic Research, University of Iowa, IIHR Report No. 135.

6. Pipes, W.O., Pritchard, D.W. and Beer, L.P., 1973, "Condenser Water Discharge Plumes from Waukegan Generating Station Under Winter Conditions", Commonwealth Edison Company, Chicago, Illinois.

7. Rouse, H., Yih, C.S., and Humphreys, W., 1952, "Gravitational Convection from a Boundary Source, Tellus, 4.

8. Vigander S., Elder, R.A. and Brooks, N.H., 1970, "Internal Hydraulics of Thermal Discharges Diffusers", Journal of the Hydraulic Division, ASCE, Vol. 96, No. HY2.

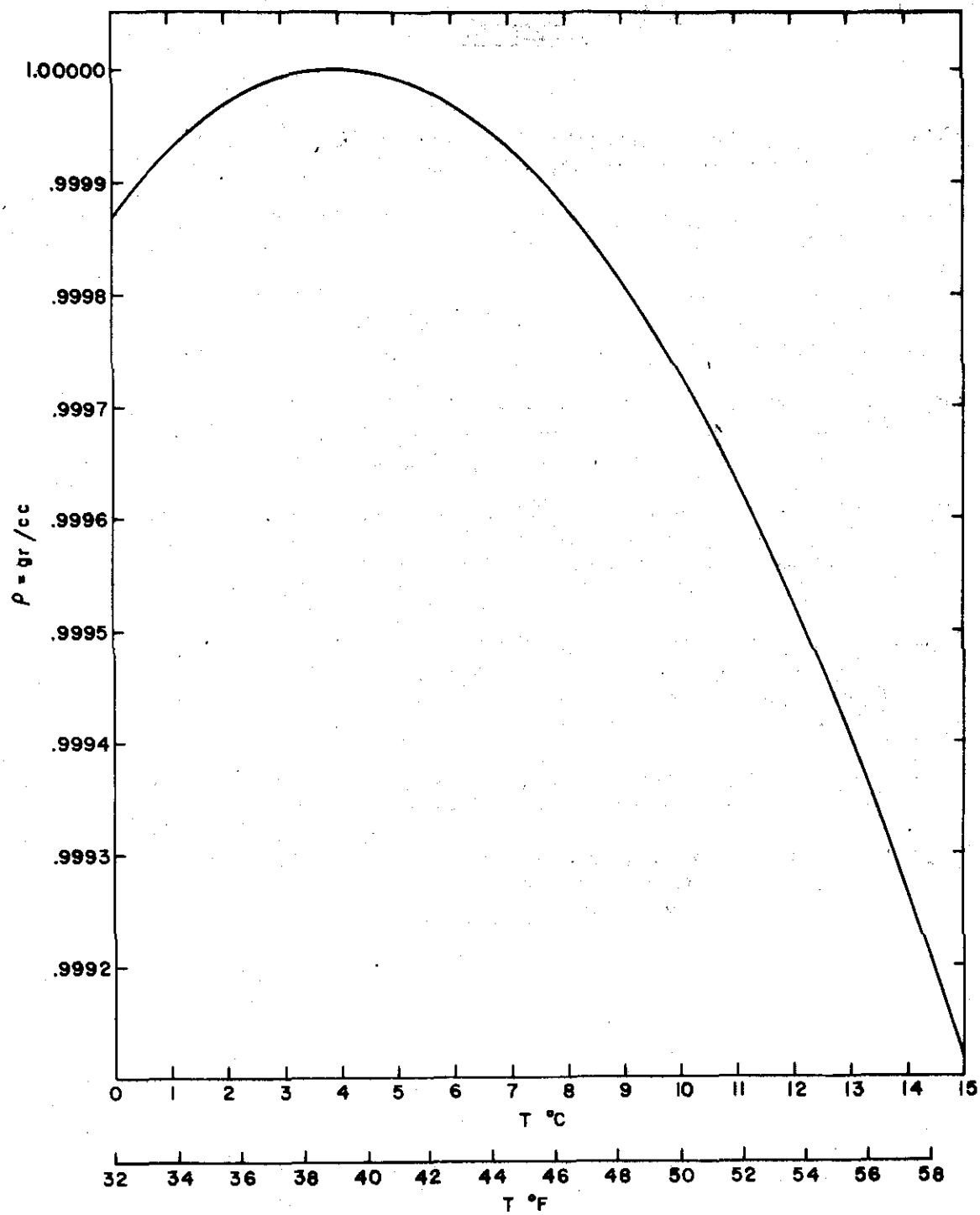

Fig. 1. Density of water as a function of temperature

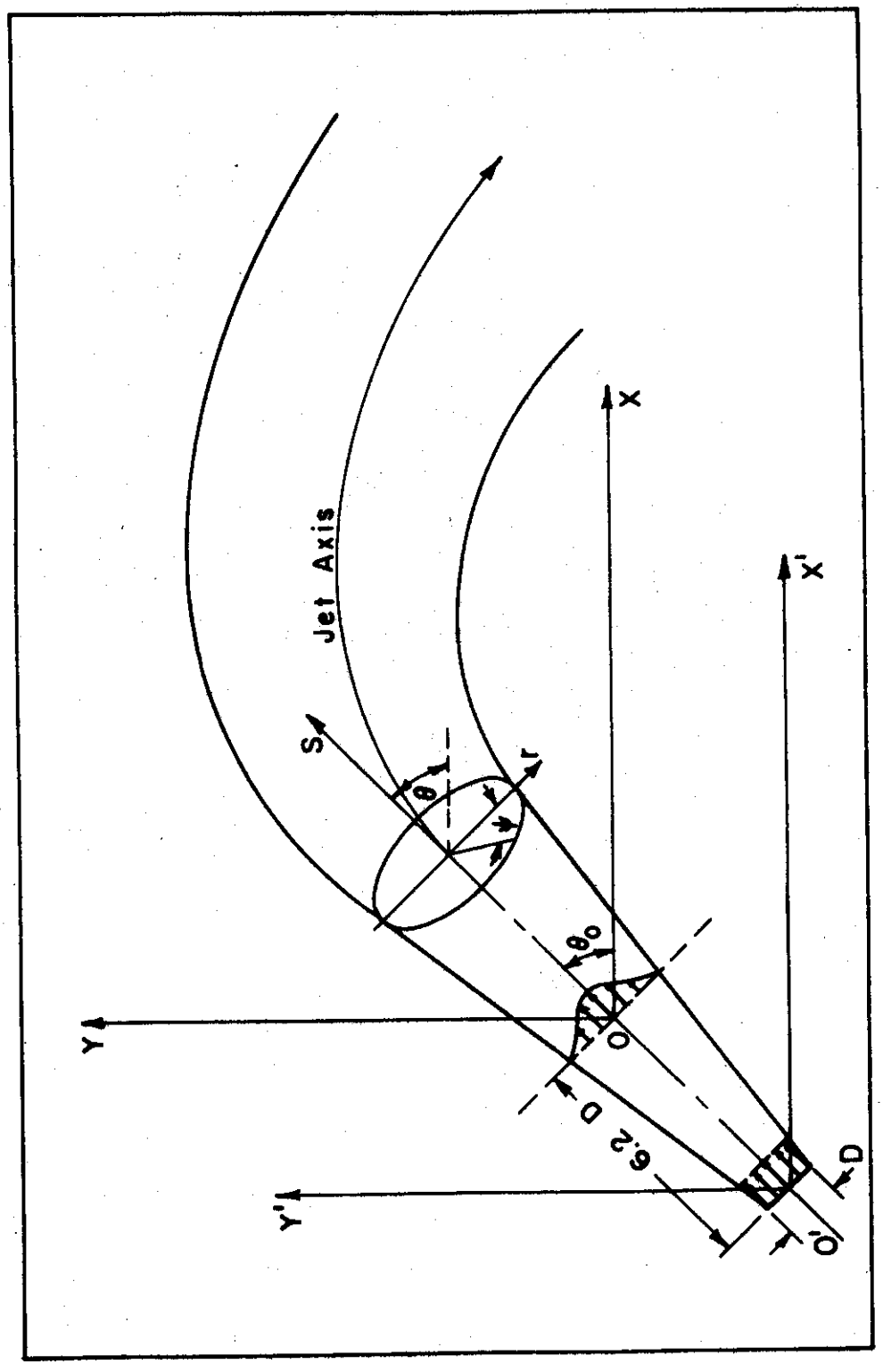

Fig. 2. Schematic diagram of round jet

Figs. 3. Centerline trajectory and half-width of round jet

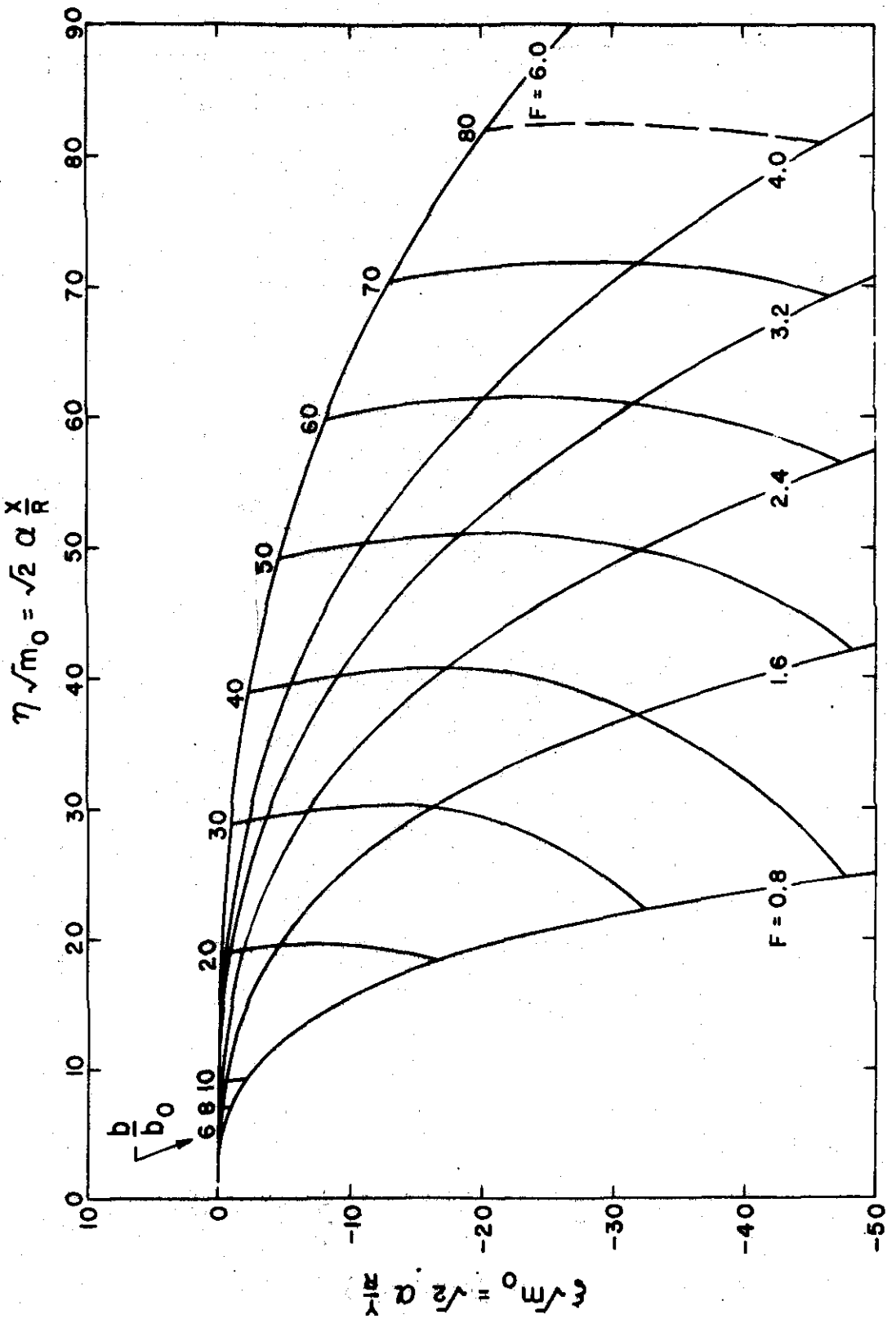

Fig. 3(a). $\theta = 0°$, $\Delta T = 10°F$

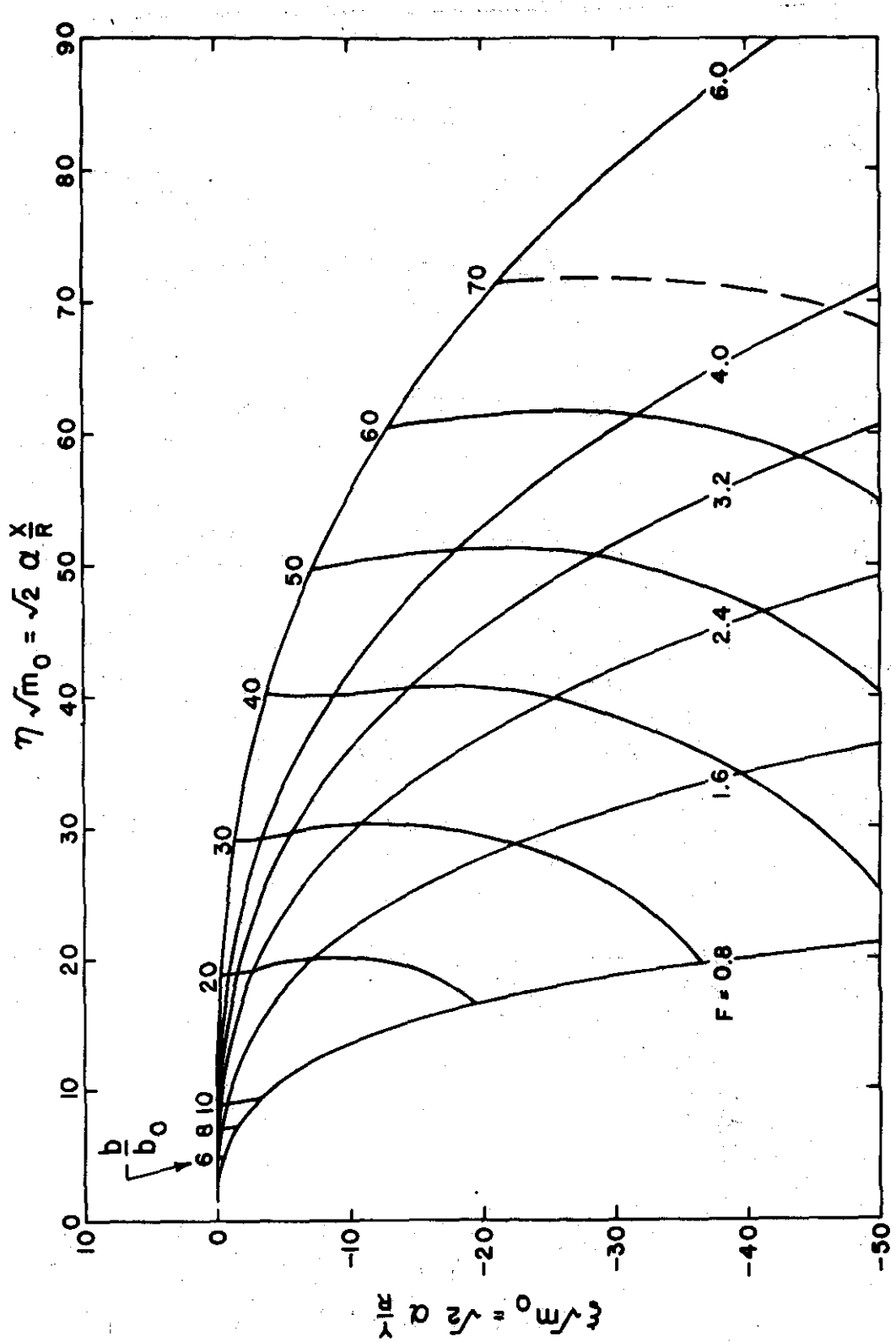

Fig. 3(b). $\theta = 0$, $\Delta T = 15°F$

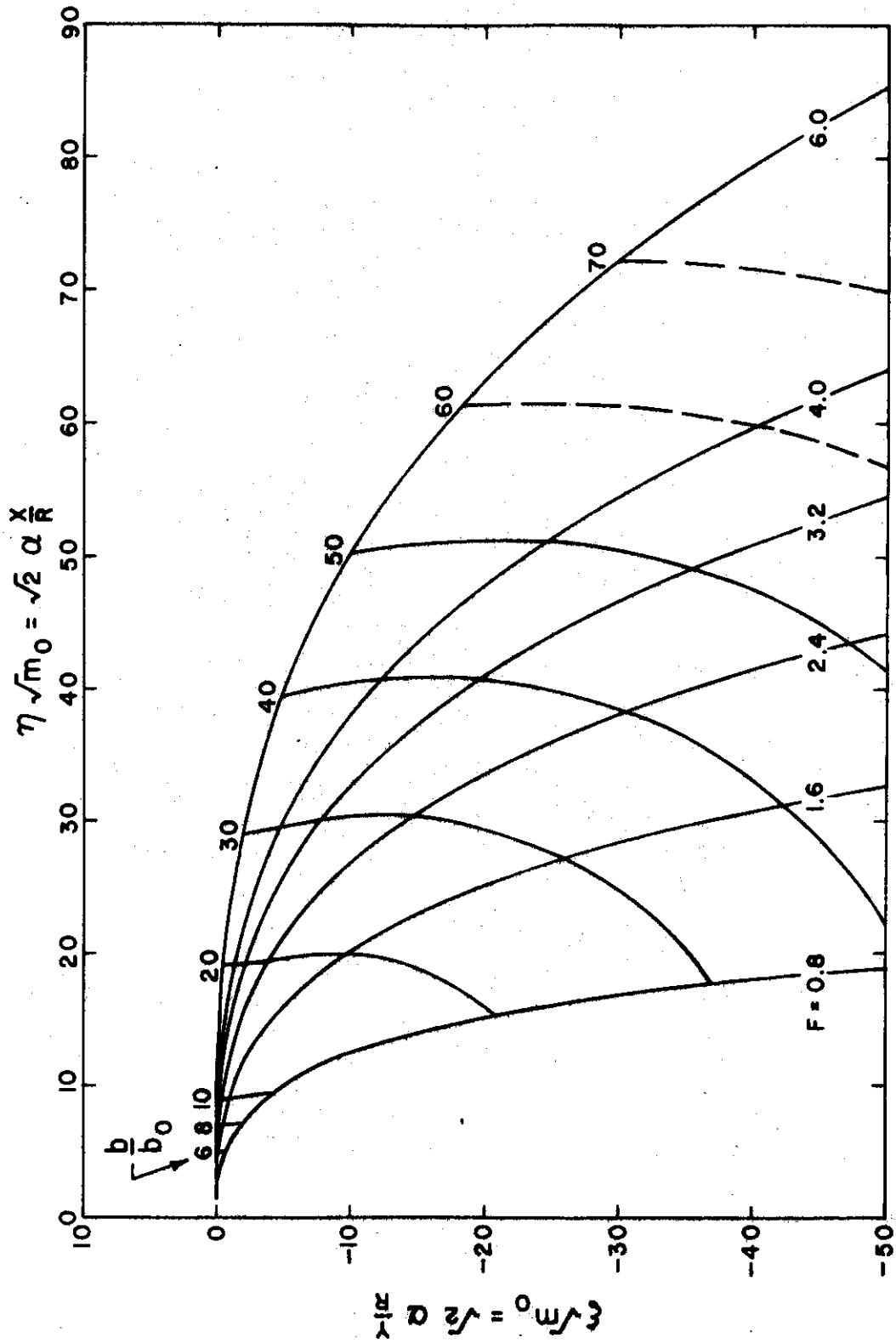

Fig. 3(c). $\theta = 0°$, $\Delta T = 20°F$

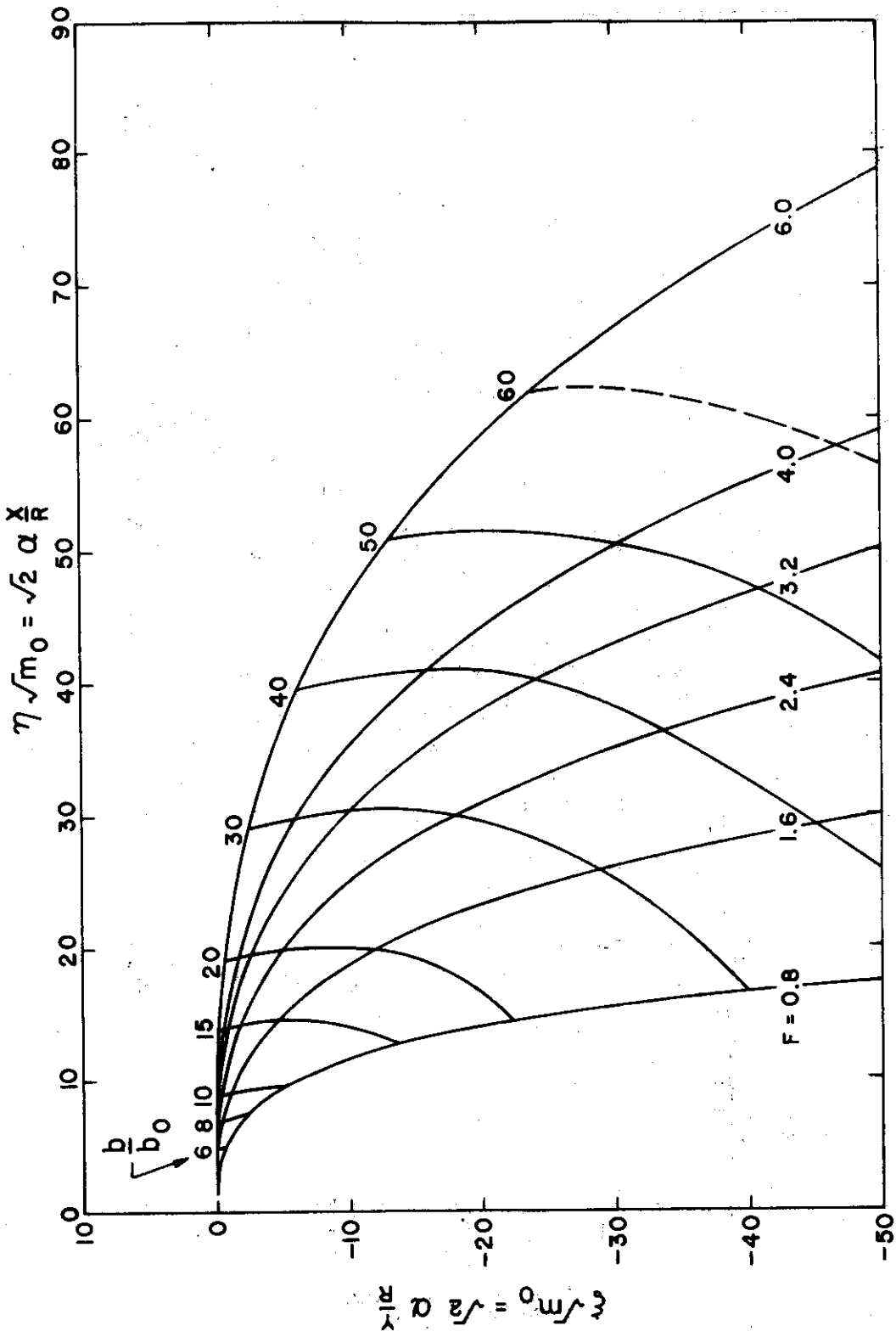

Fig. 3(d). $\theta = 0°$, $\Delta T = 25°F$

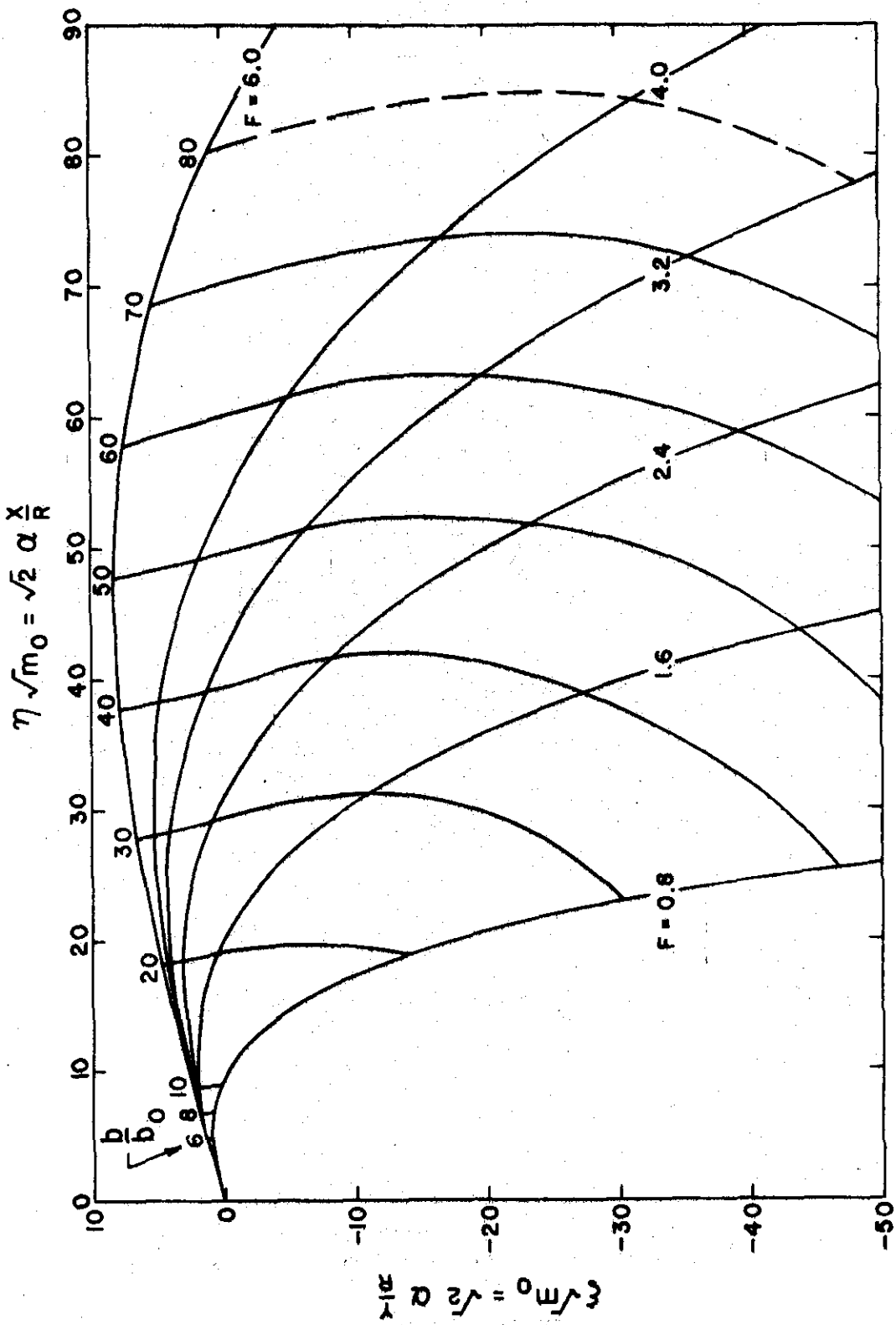

Fig. 3(e). $\theta = 15°$, $\Delta T = 10°F$

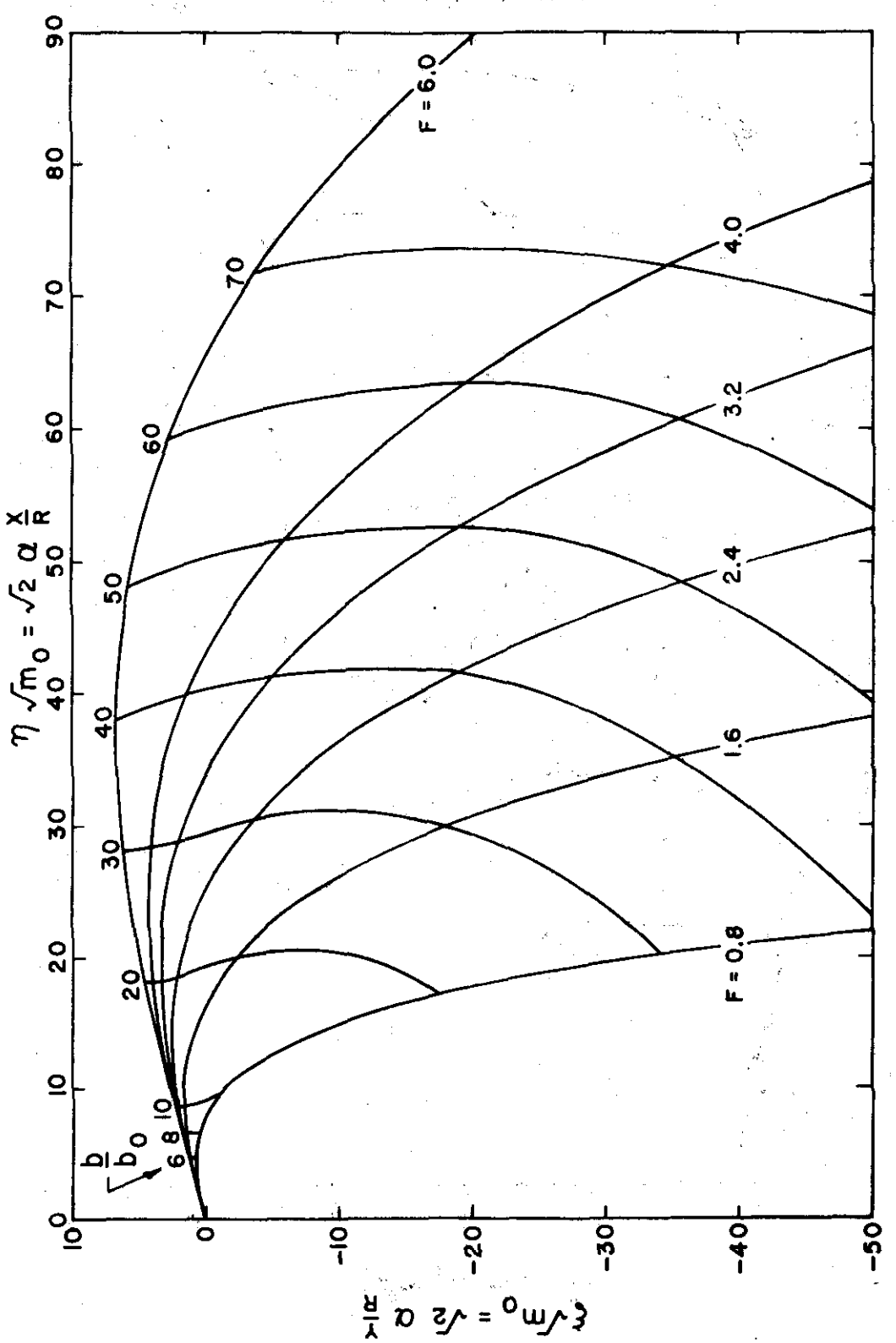

Fig. 3(f). $\theta = 15°$, $\Delta T = 15°F$

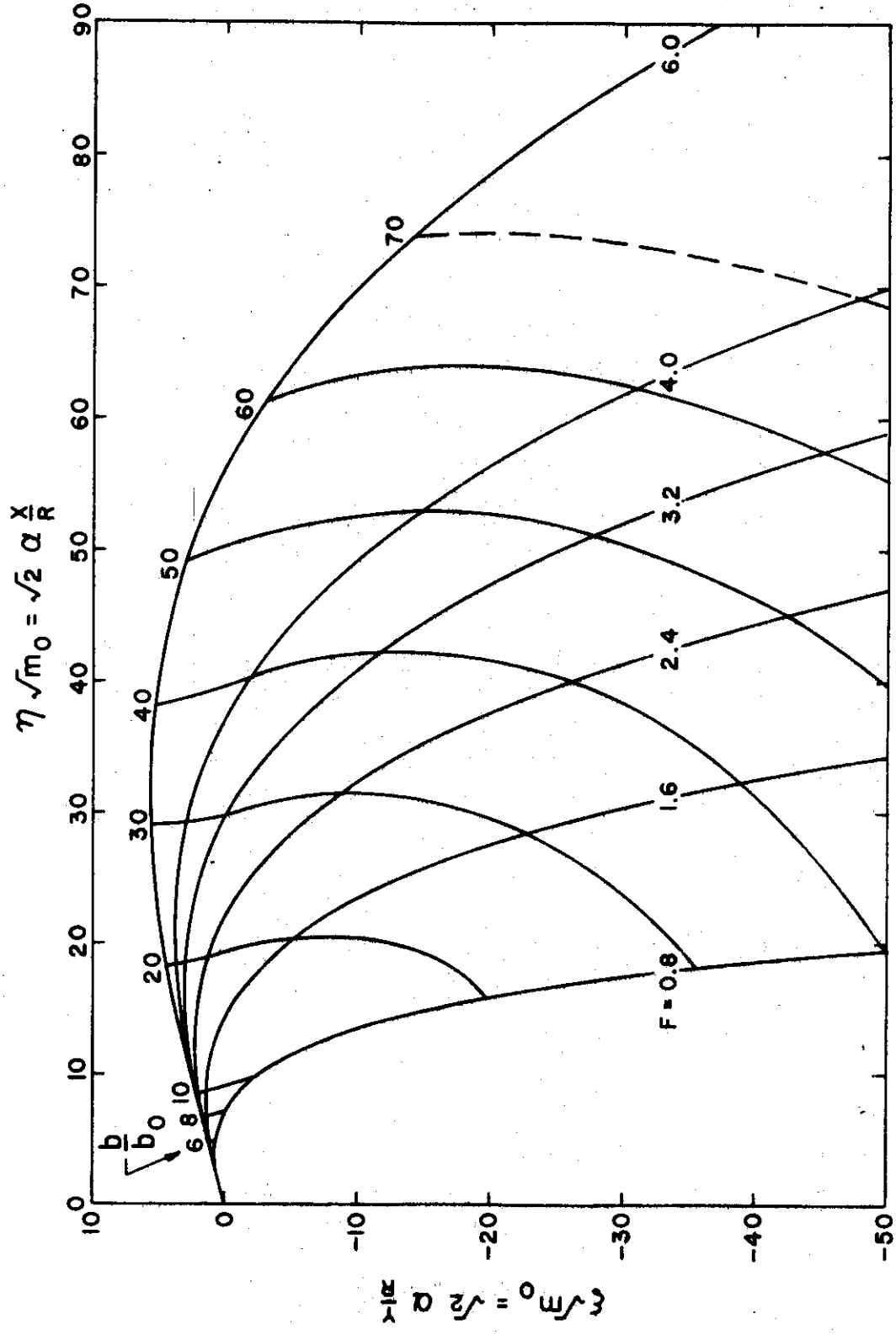

Fig. 3(g). $\theta = 15°$, $\Delta T = 20°F$

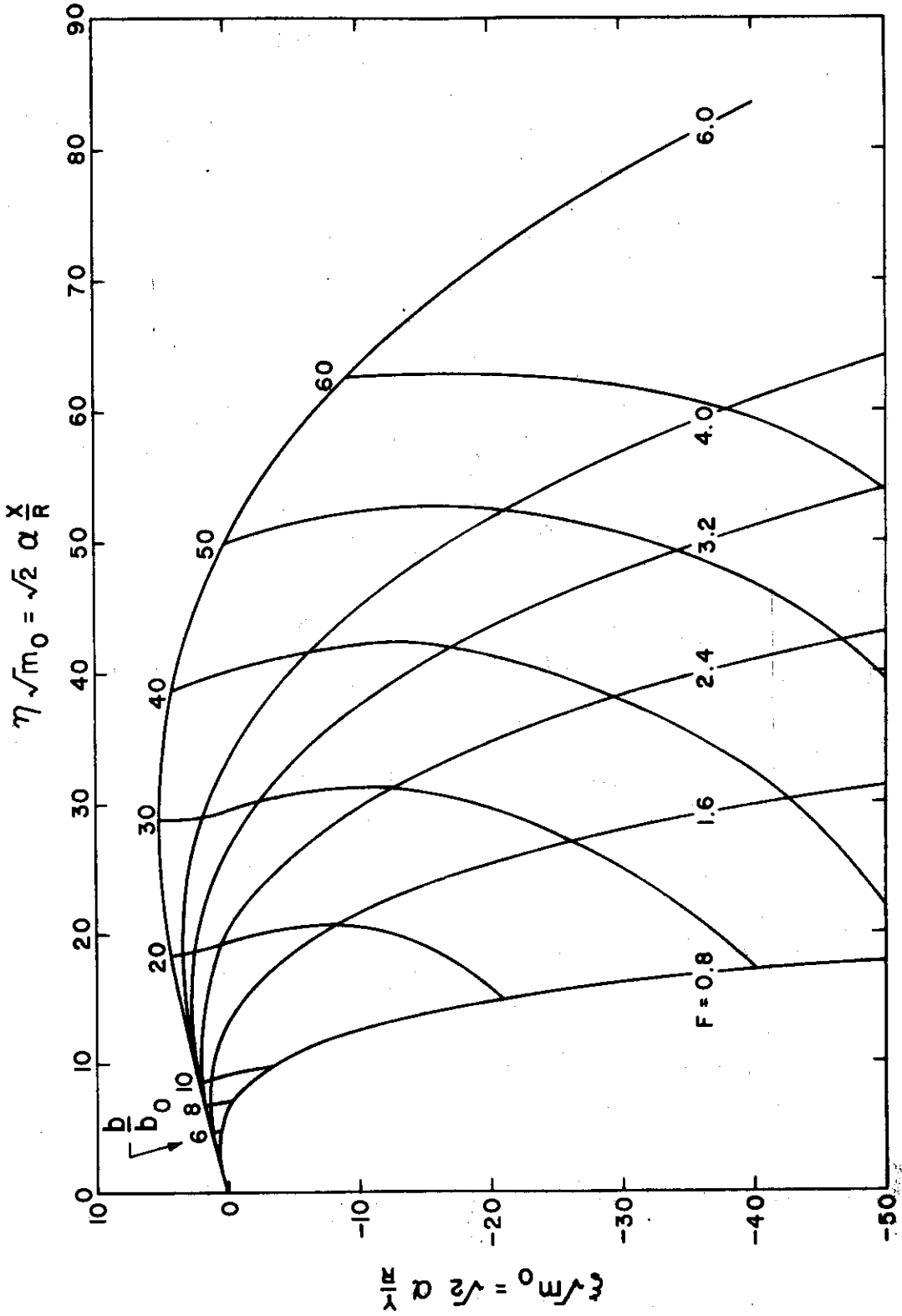

Fig. 3(h). $\theta = 15°$, $\Delta T = 25°F$

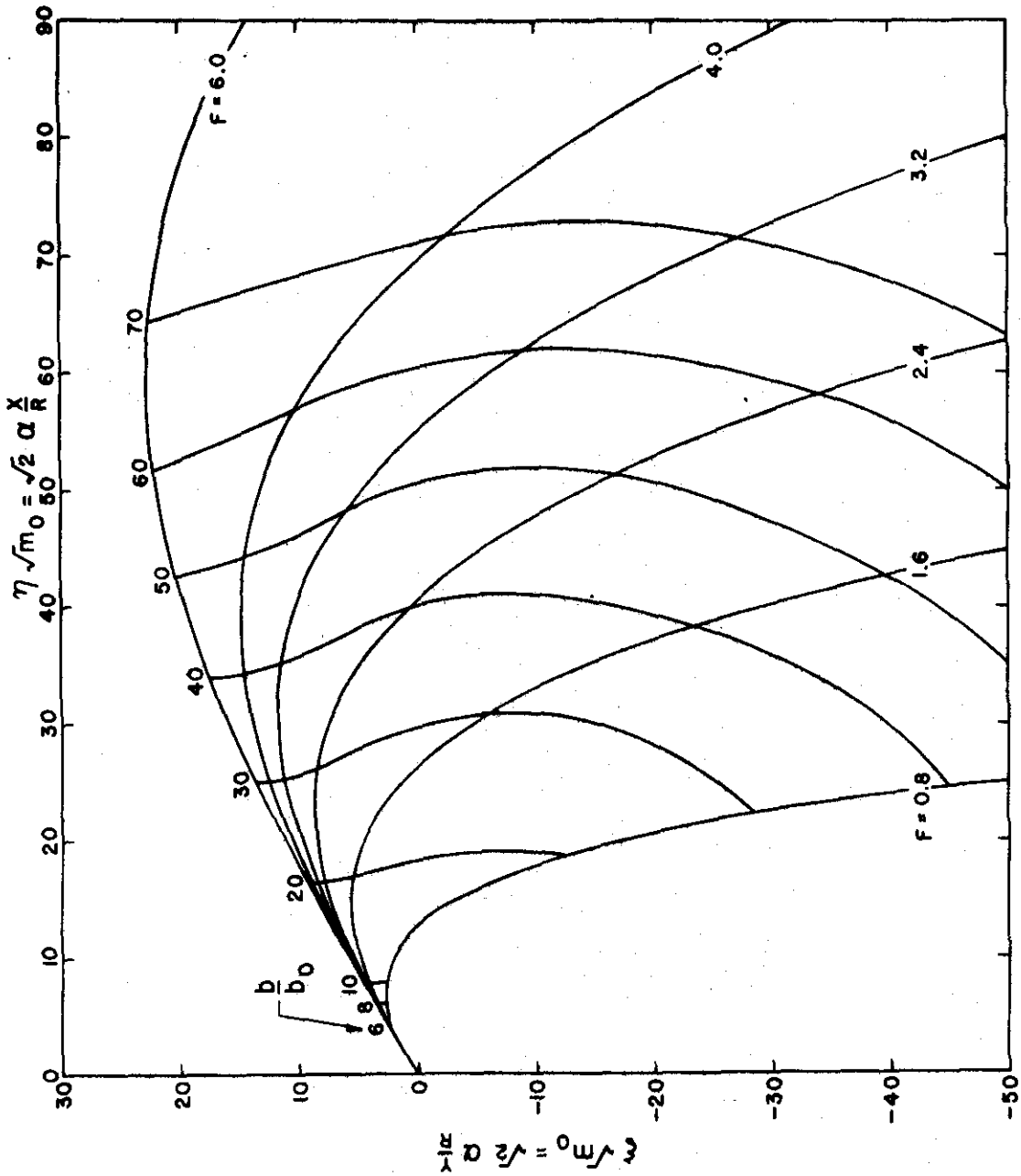

Fig. 3(i). $\theta = 30°$, $\Delta T = 10°F$

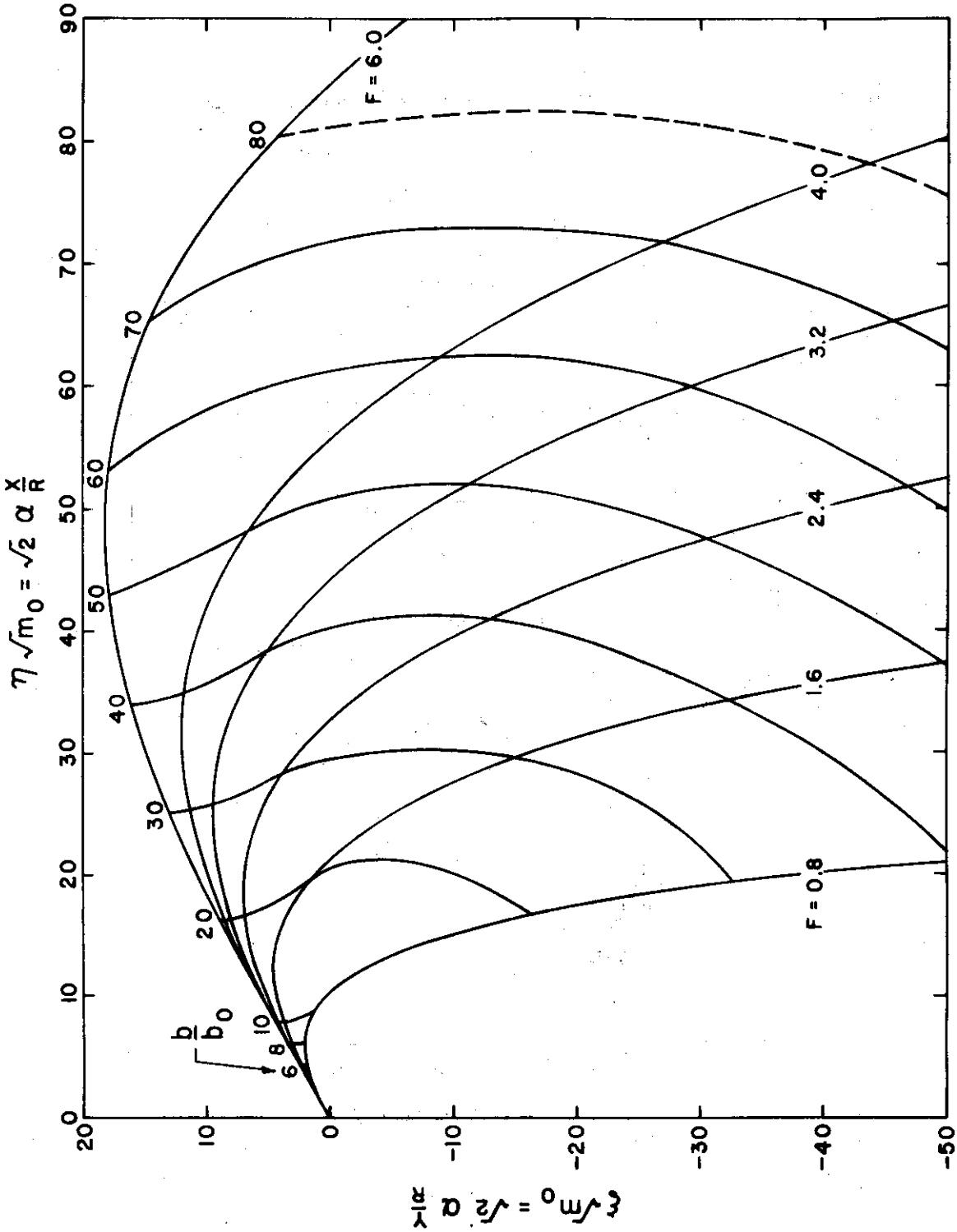

Fig. 3(j). $\theta = 30^{\circ}$, $\Delta T = 15^{\circ}F$

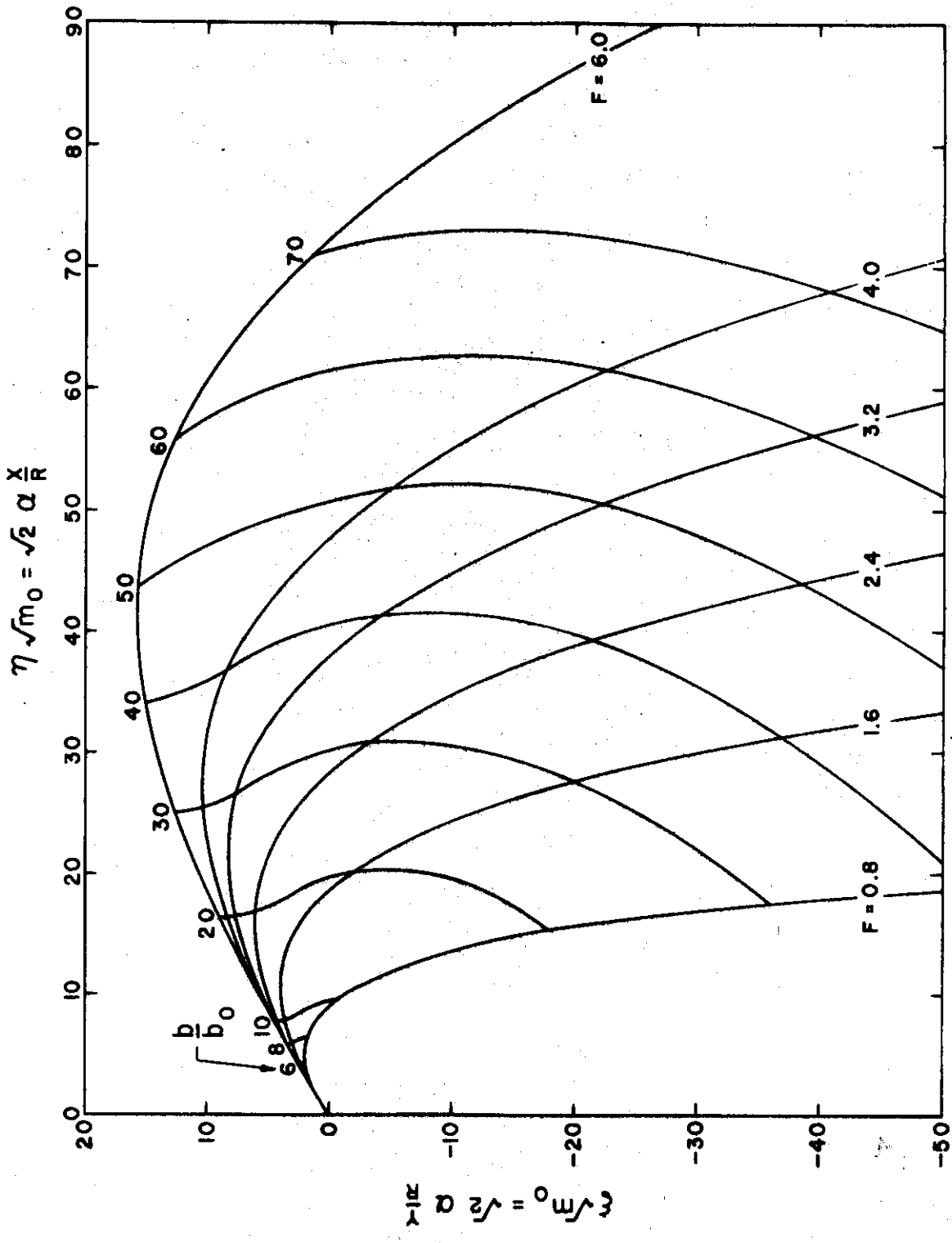

Fig. 3(k). $\theta = 30°$, $\Delta T = 20°F$

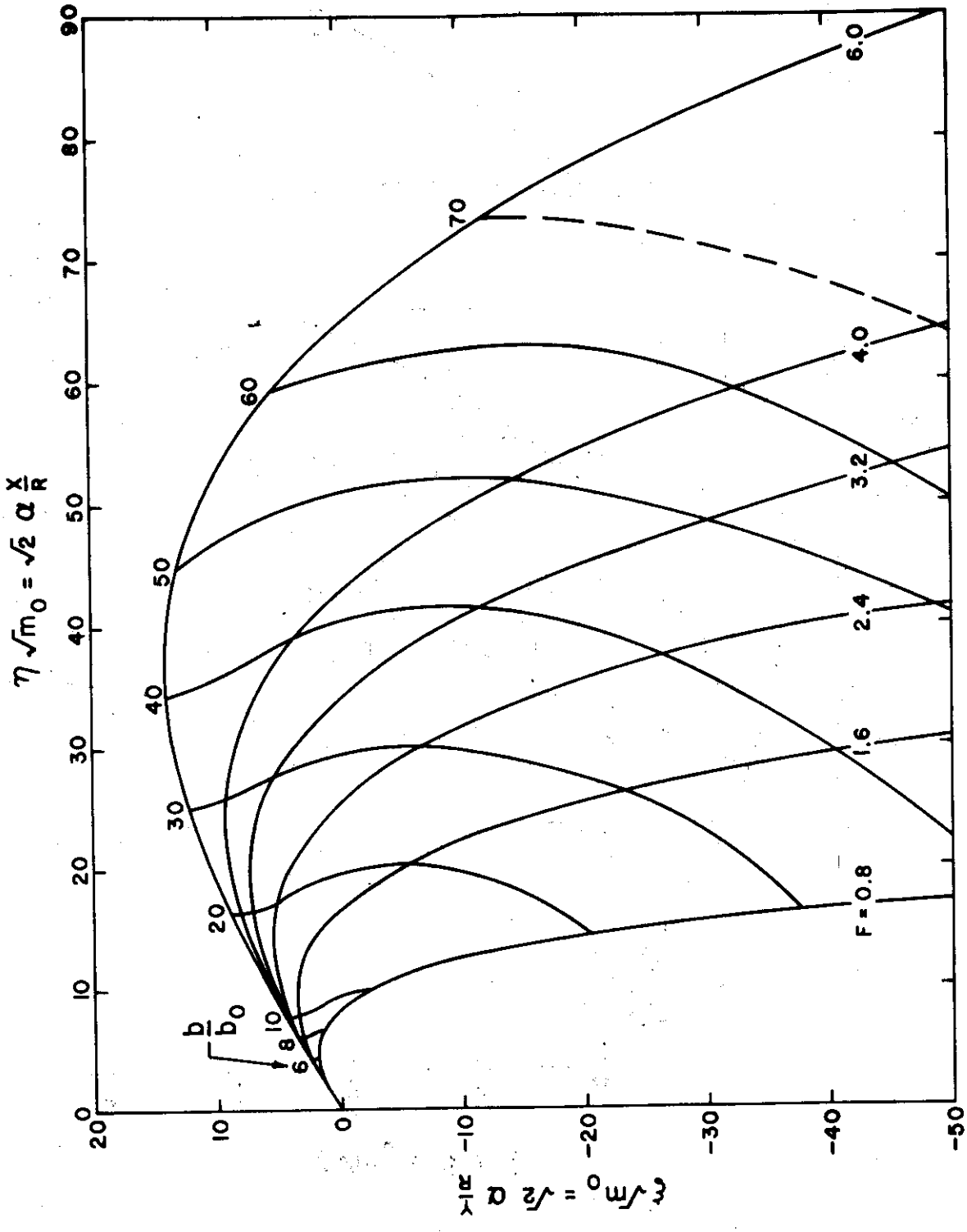

Fig. 3(1). $\theta = 30°$, $\Delta T = 25°F$

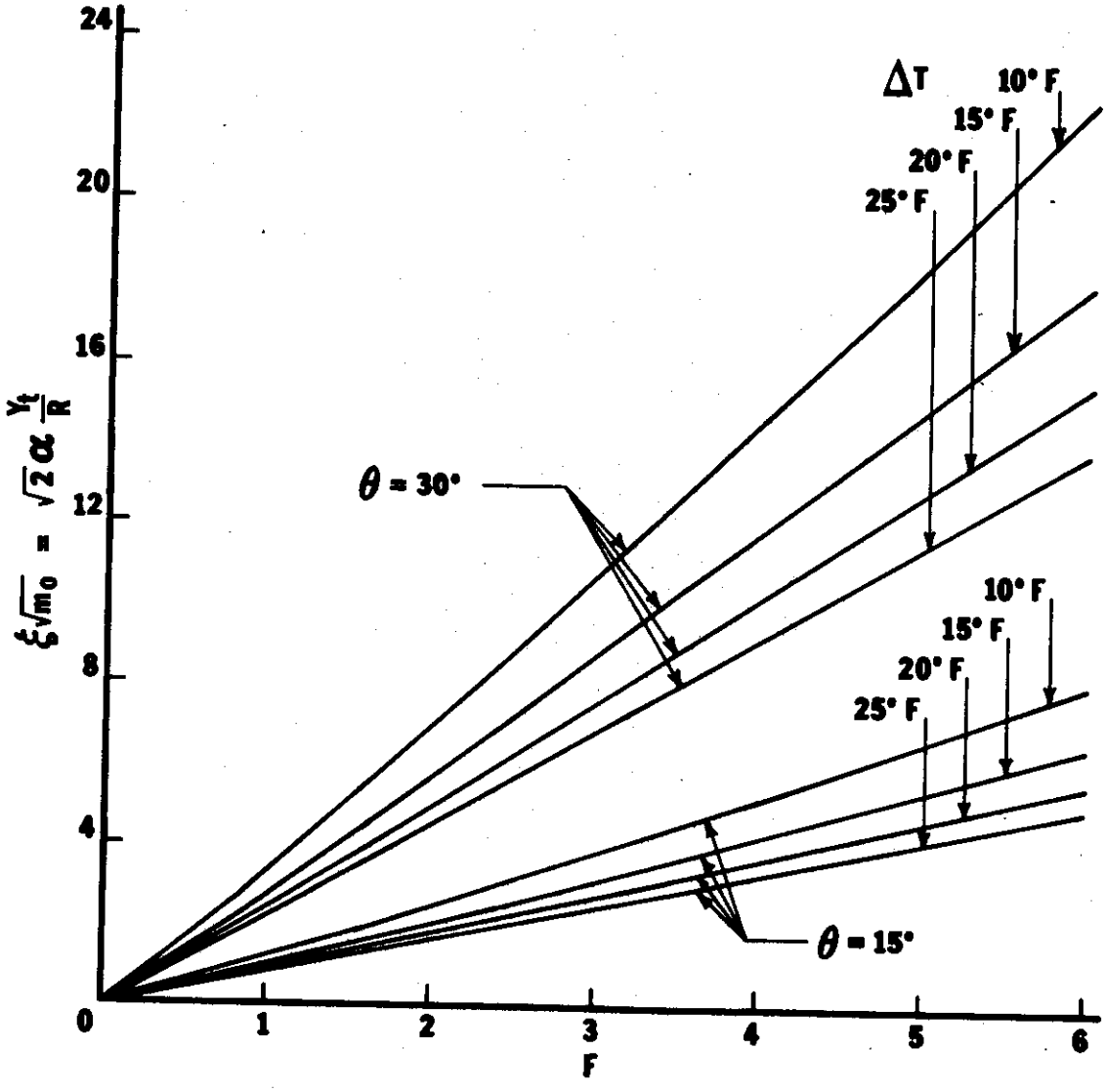

Fig. 4. Maximum rise of round jet

Figs. 5. Dilution along trajectory of round jet

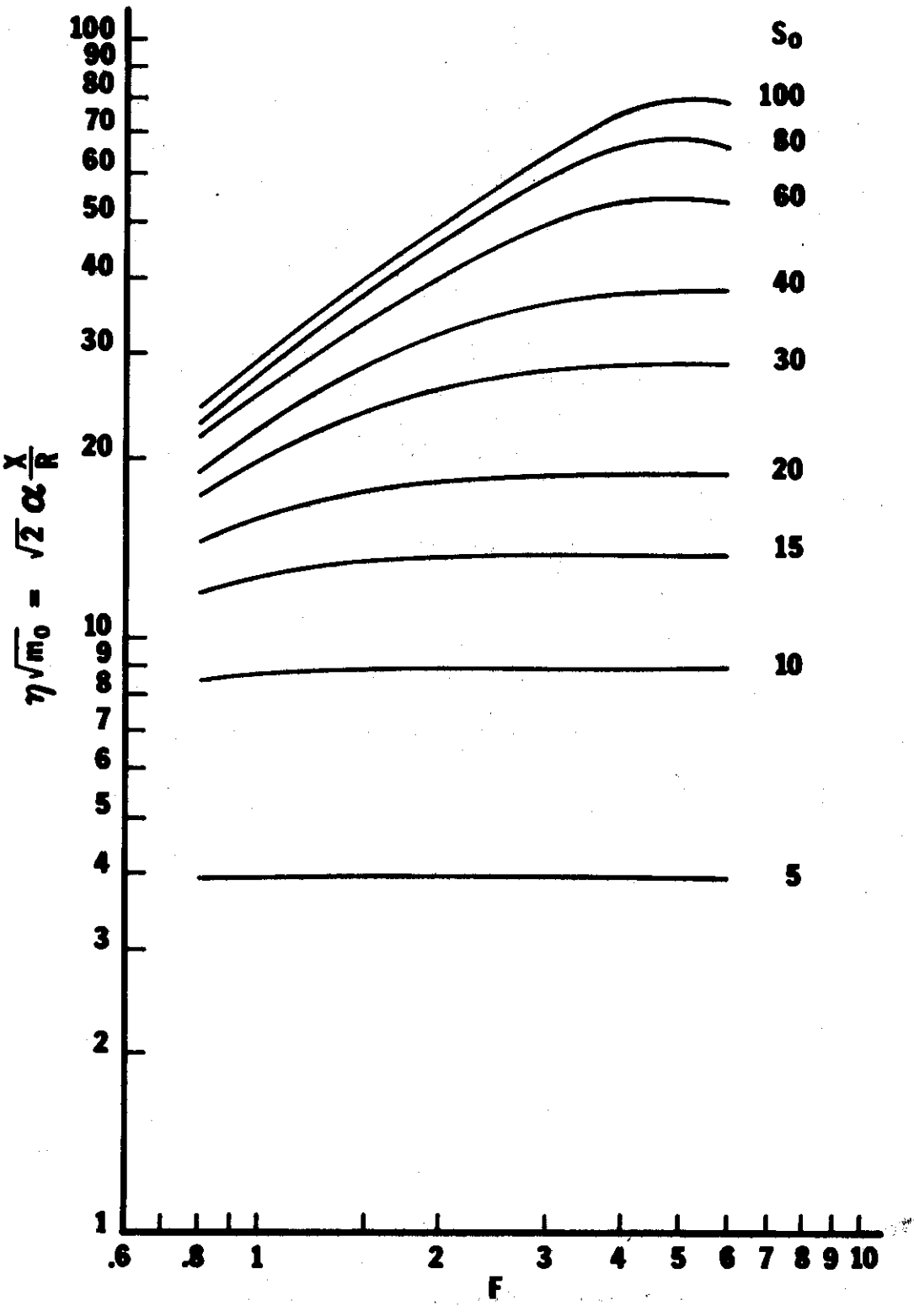

Fig. 5(a). $\theta = 0°$, $\Delta T = 10°F$

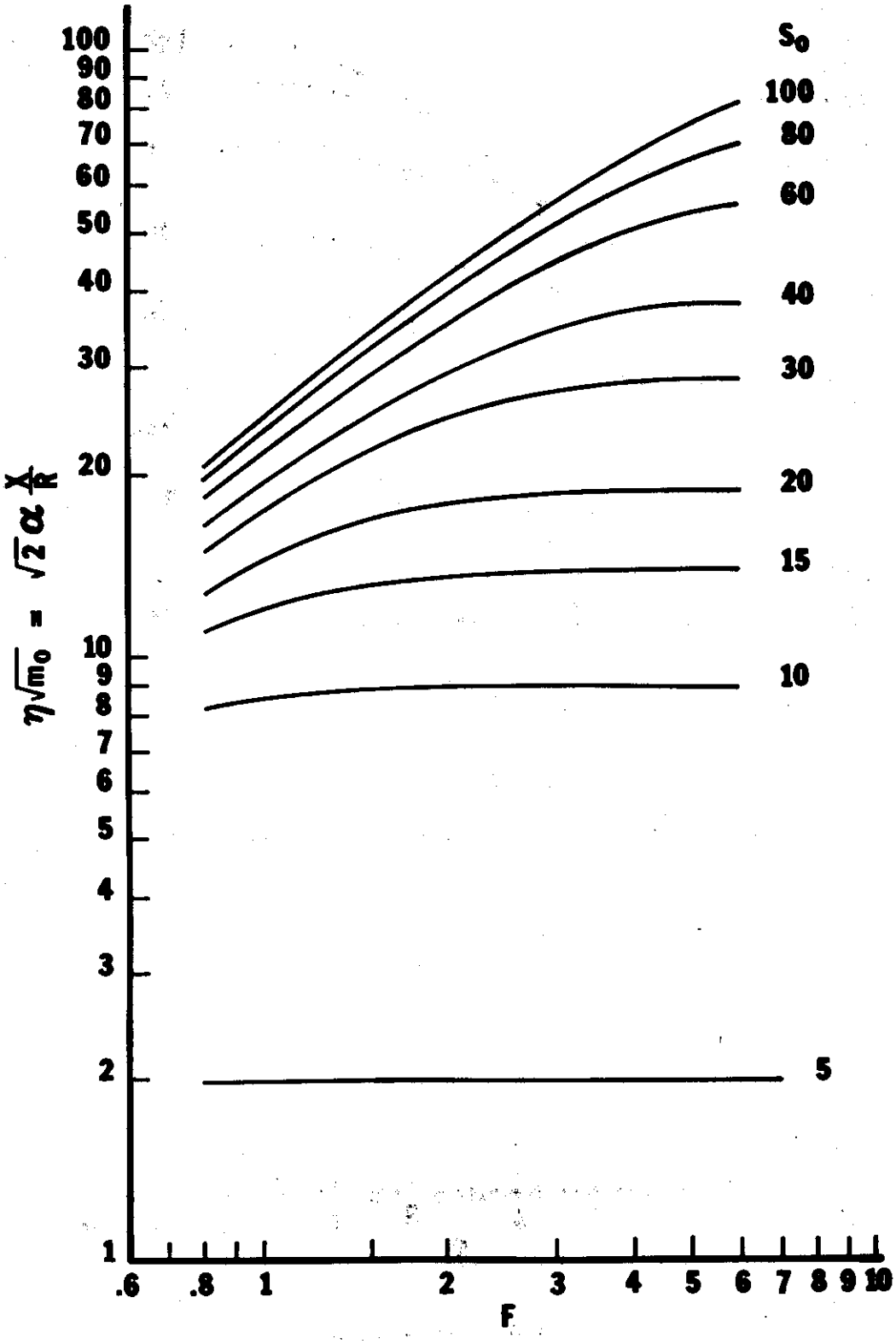

Fig. 5(b). $\theta = 0°$, $\Delta T = 15°F$

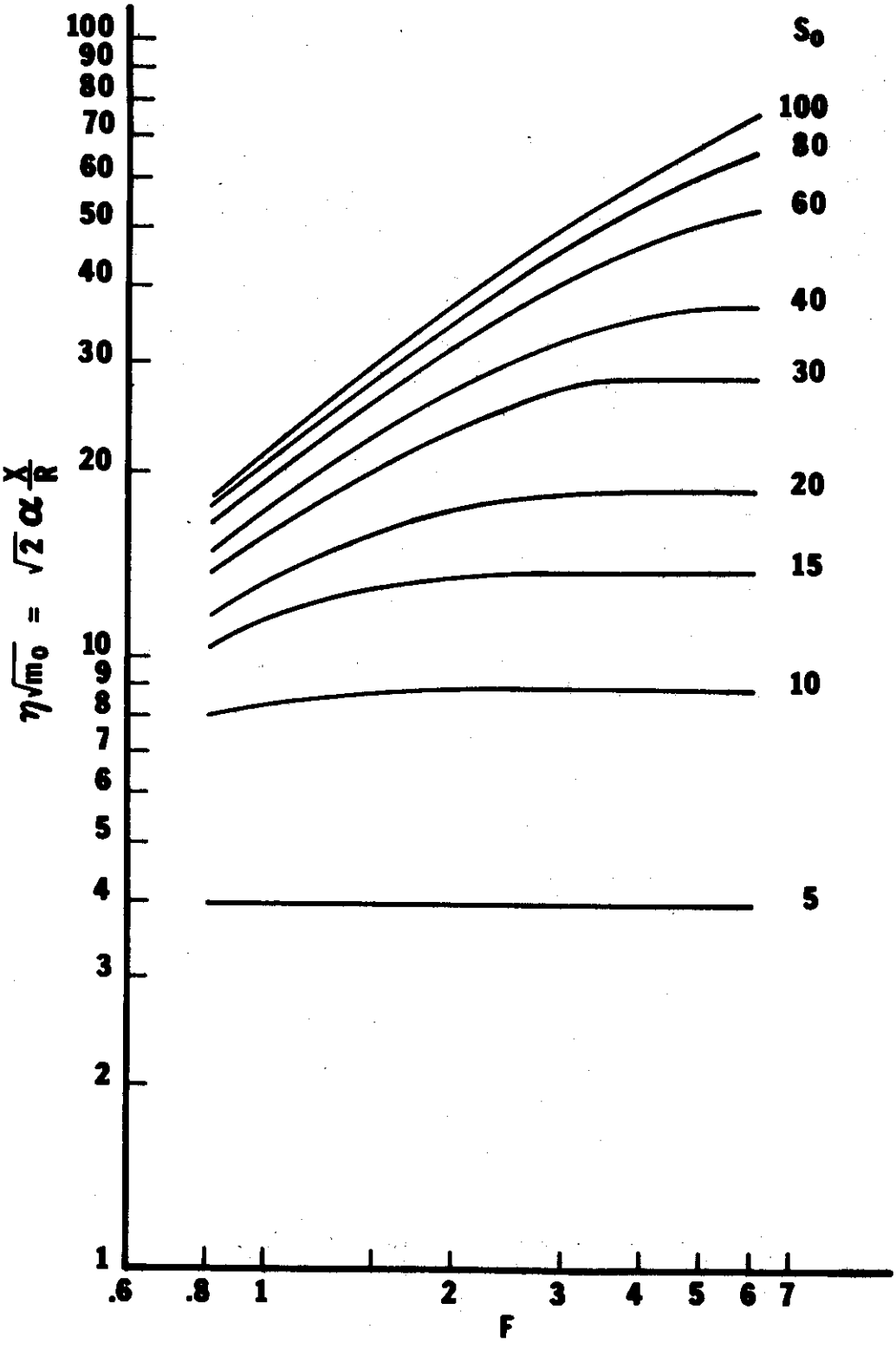

Fig. 5(c). $\theta = 0°$, $\Delta T = 20°F$

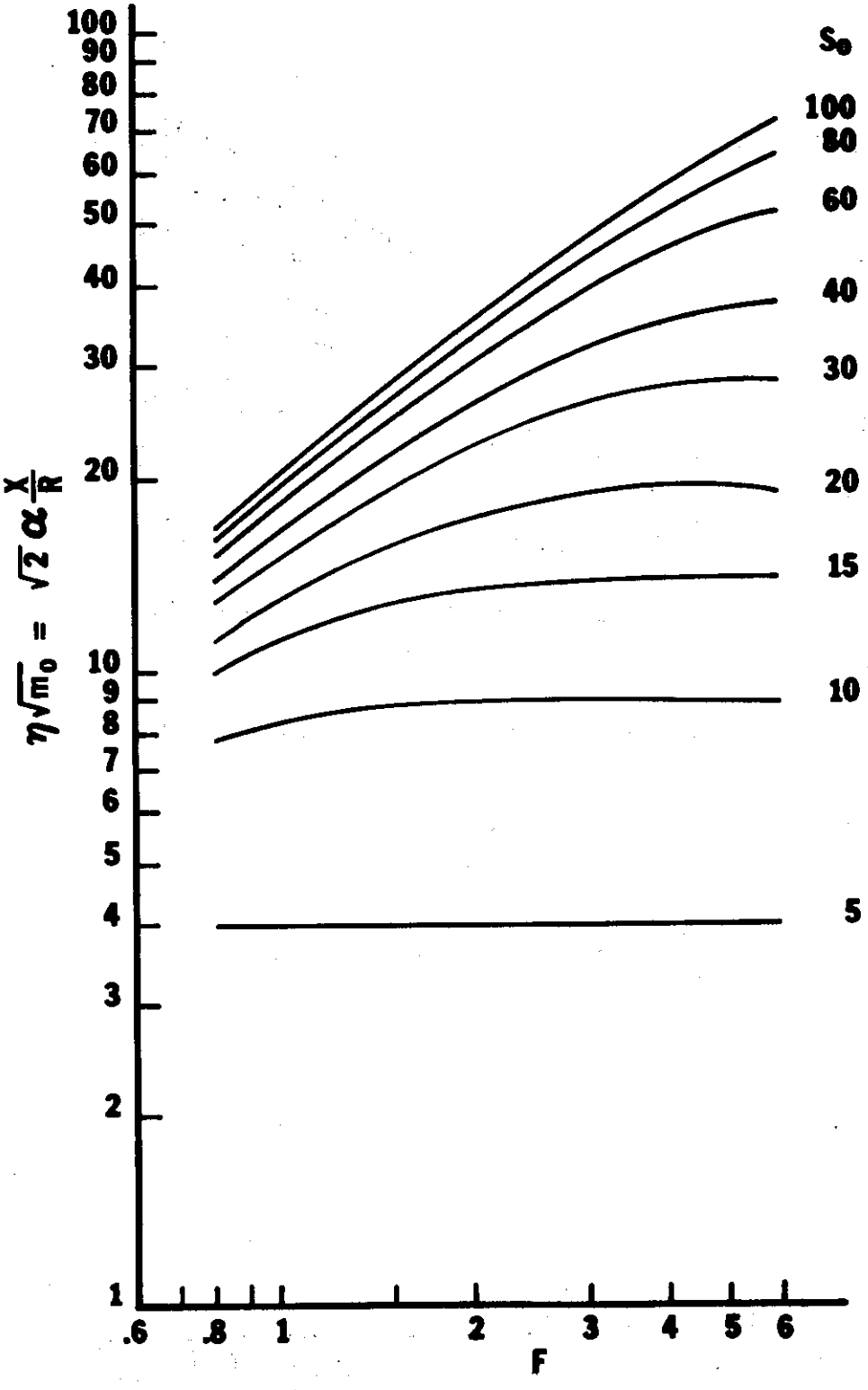

Fig. 5(d). $\theta = 0°$, $\Delta T = 25°F$

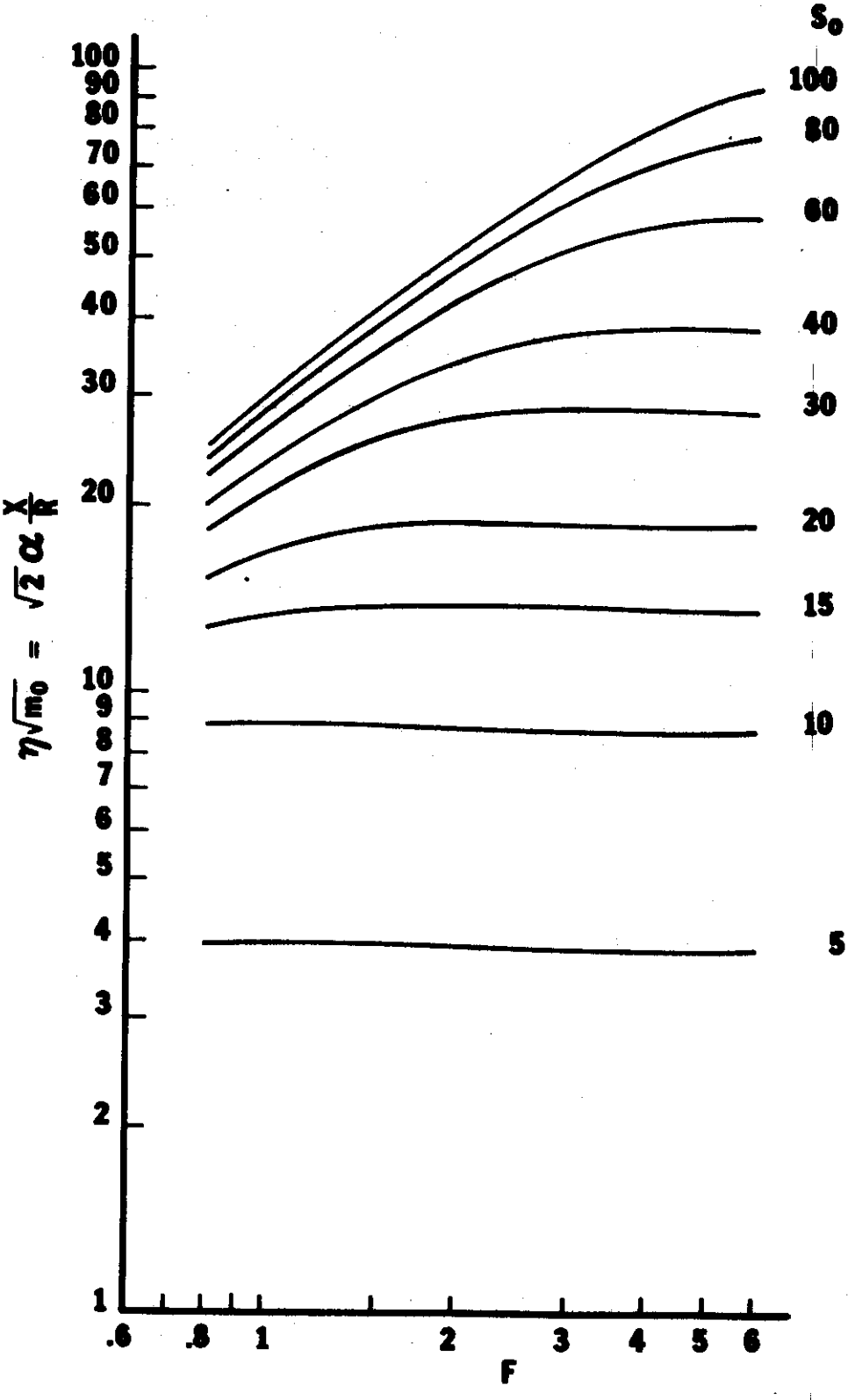

Fig. 5(e). $\theta = 15°$, $\Delta T = 10°F$

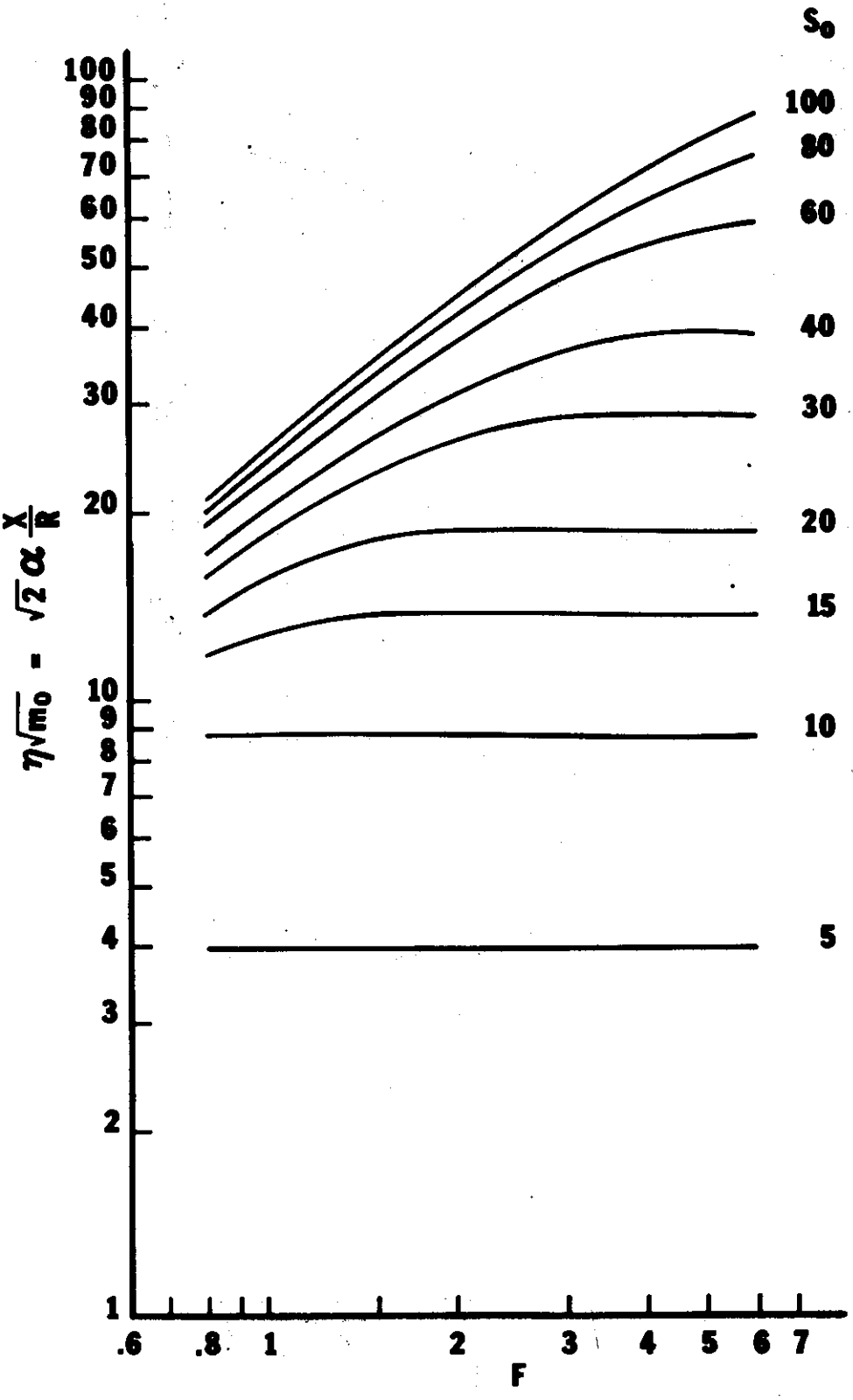

Fig. 5(f). $\theta = 15°$, $\Delta T = 15°F$

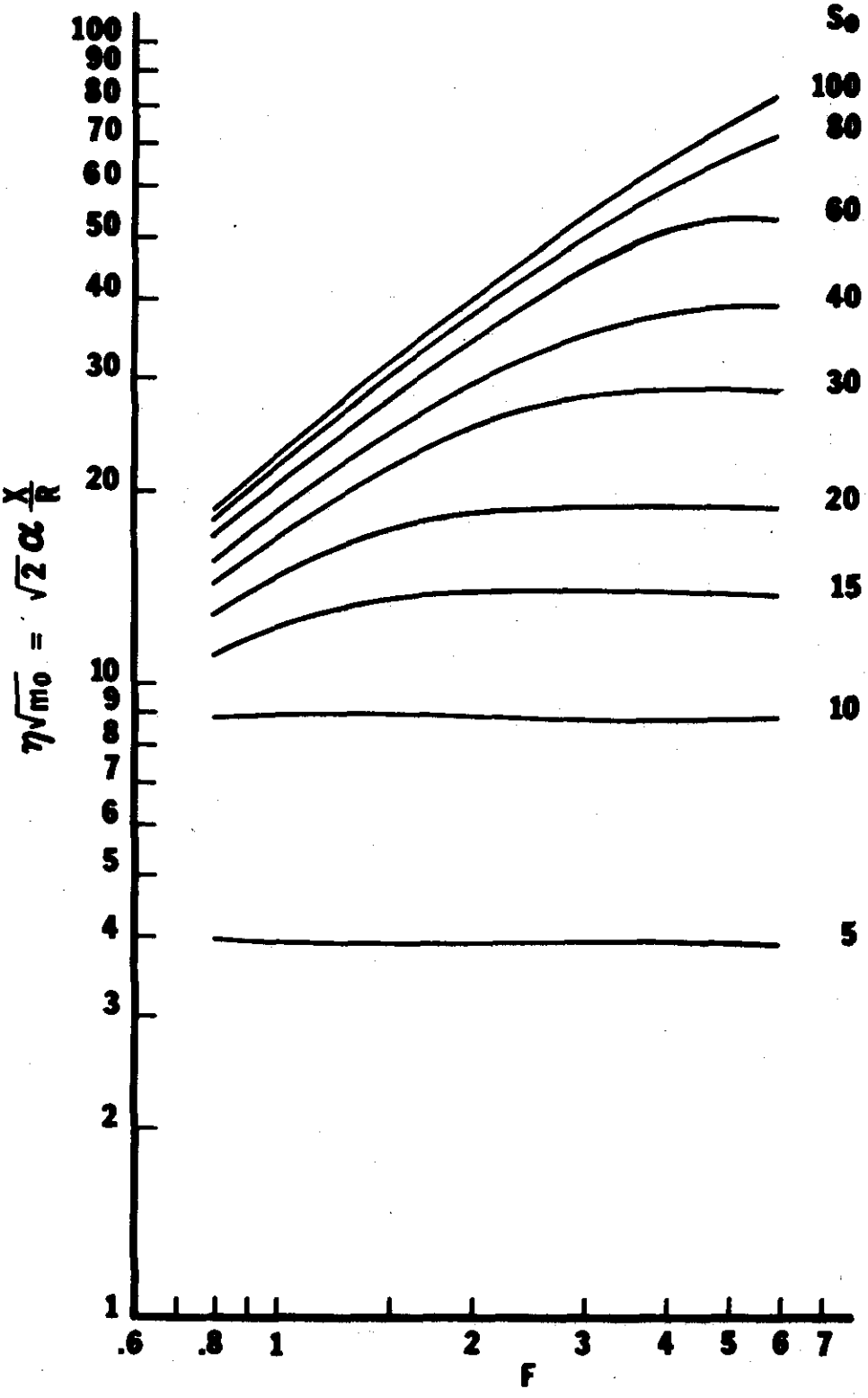

Fig. 5(g). $\theta = 15°$, $\Delta T = 20°F$

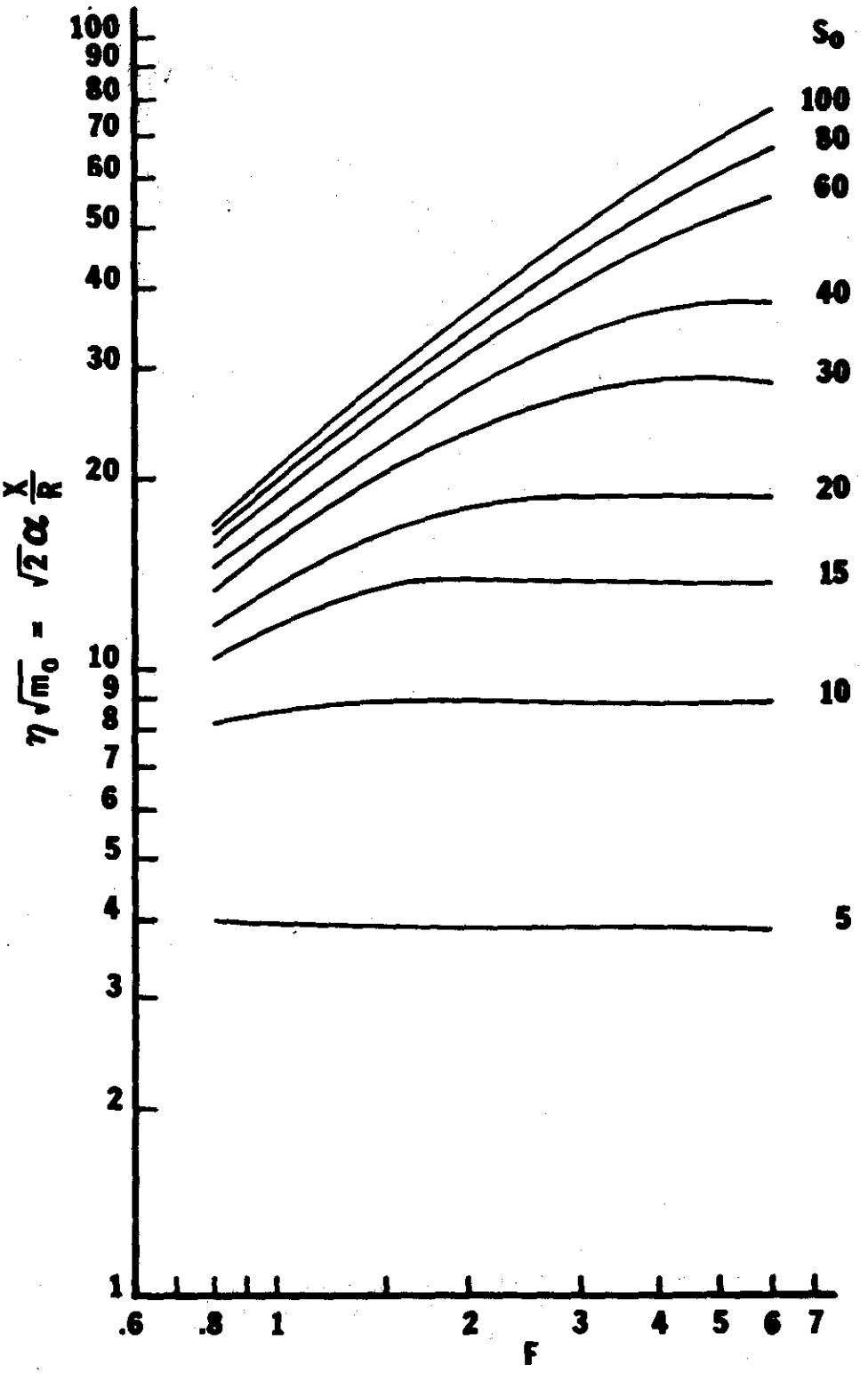

Fig. 5(h). $\theta = 15°$, $\Delta T = 25°$

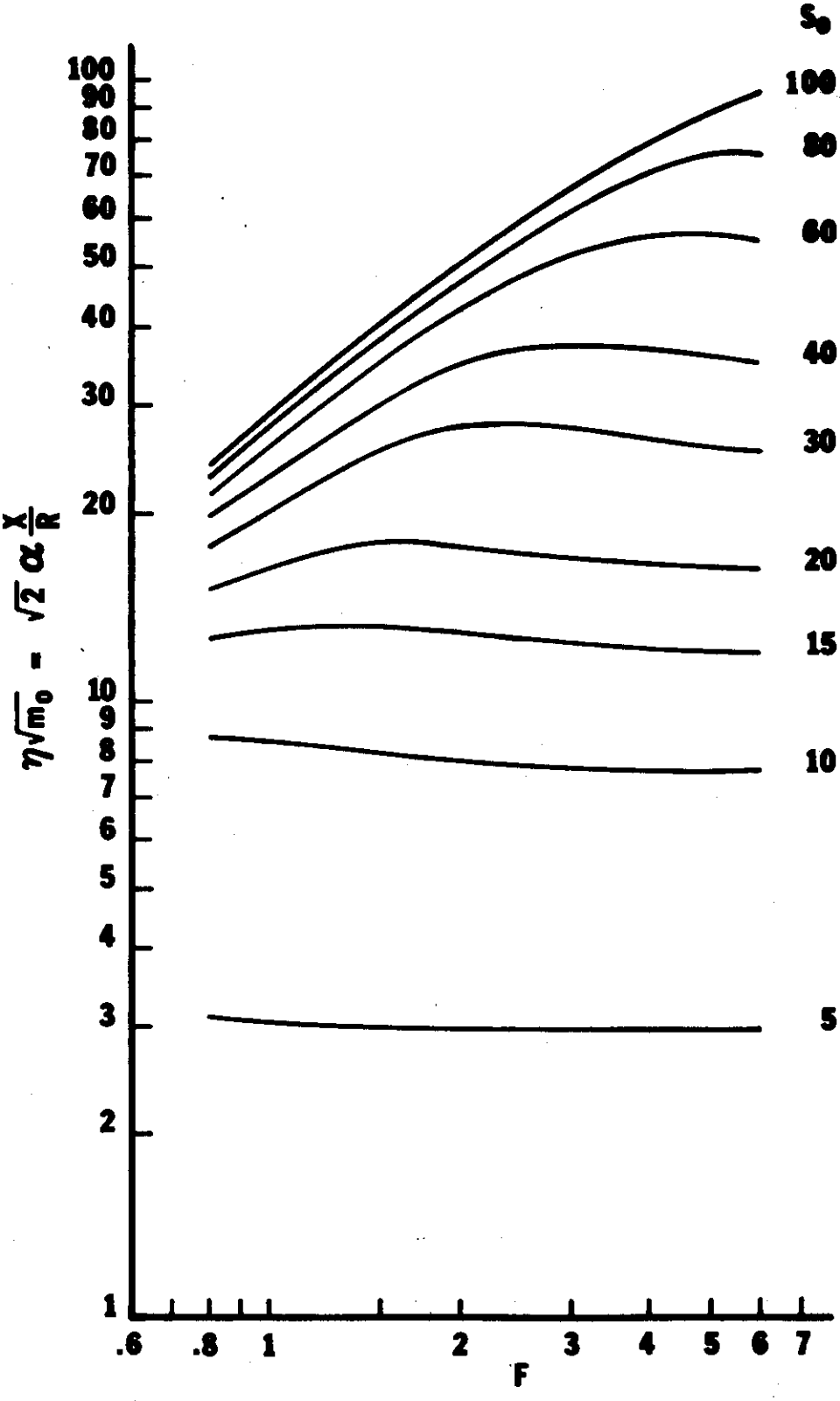

Fig. 5(i). $\theta = 30°$, $\Delta T = 10°F$

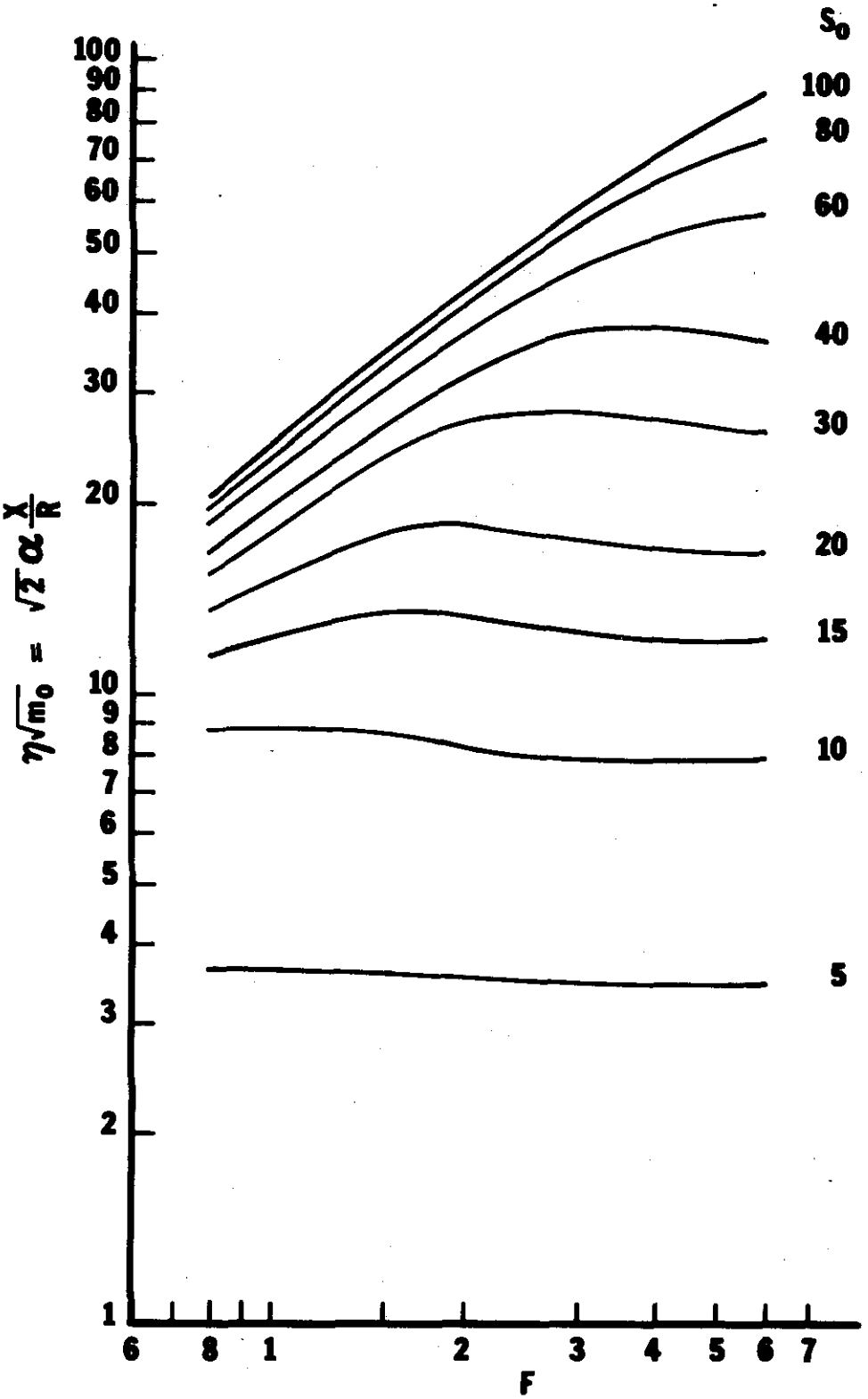

Fig. 5(j). $\theta = 30°$, $\Delta T = 15°F$

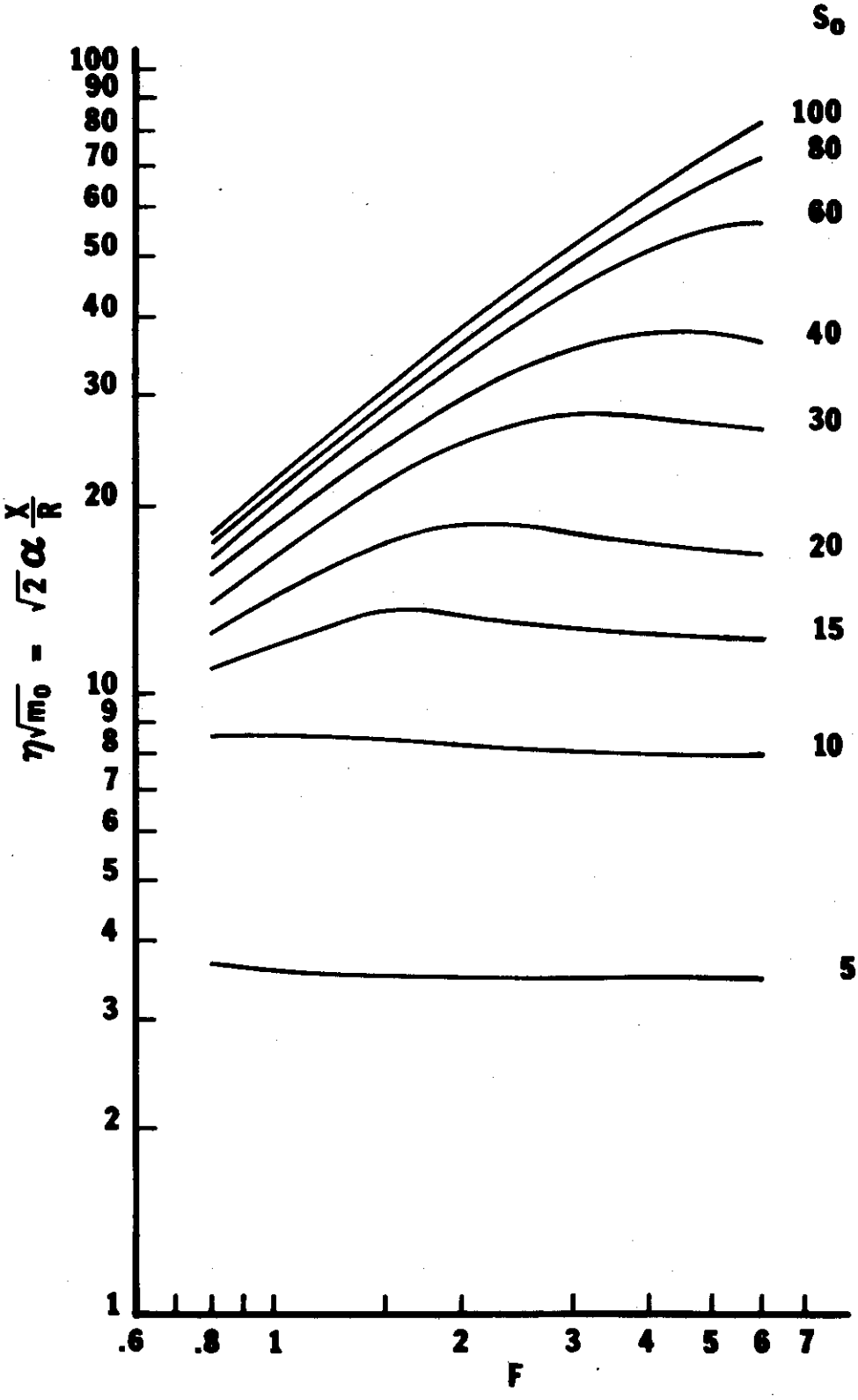

Fig. 5(k). $\theta = 30°$, $\Delta T = 20°F$

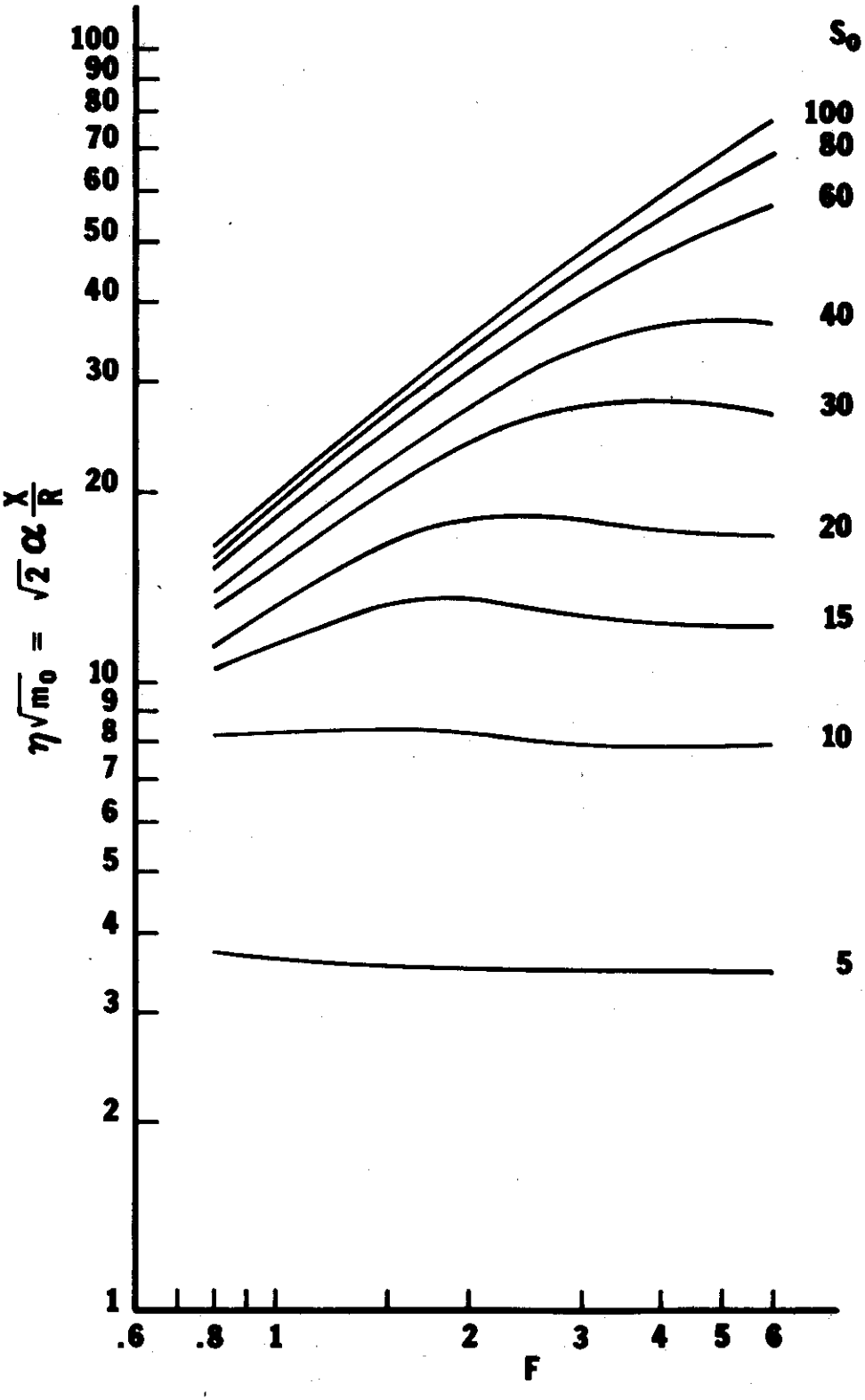

Fig. 5(1). $\theta = 30°$, $\Delta T = 25°F$

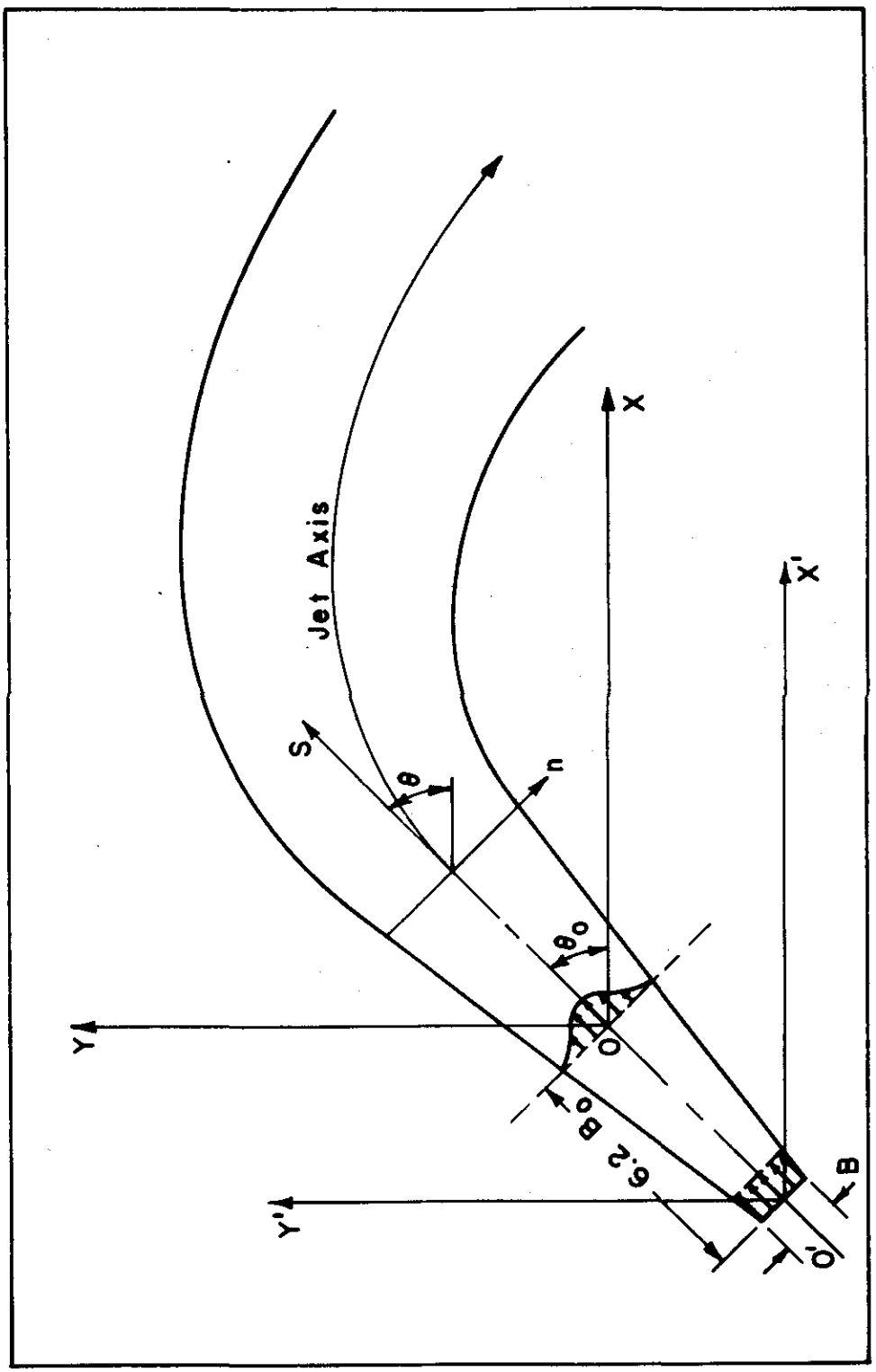

Fig. 6. Schematic diagram of slot jet

Figs. 7. Centerline trajectory and half-width of slot jet

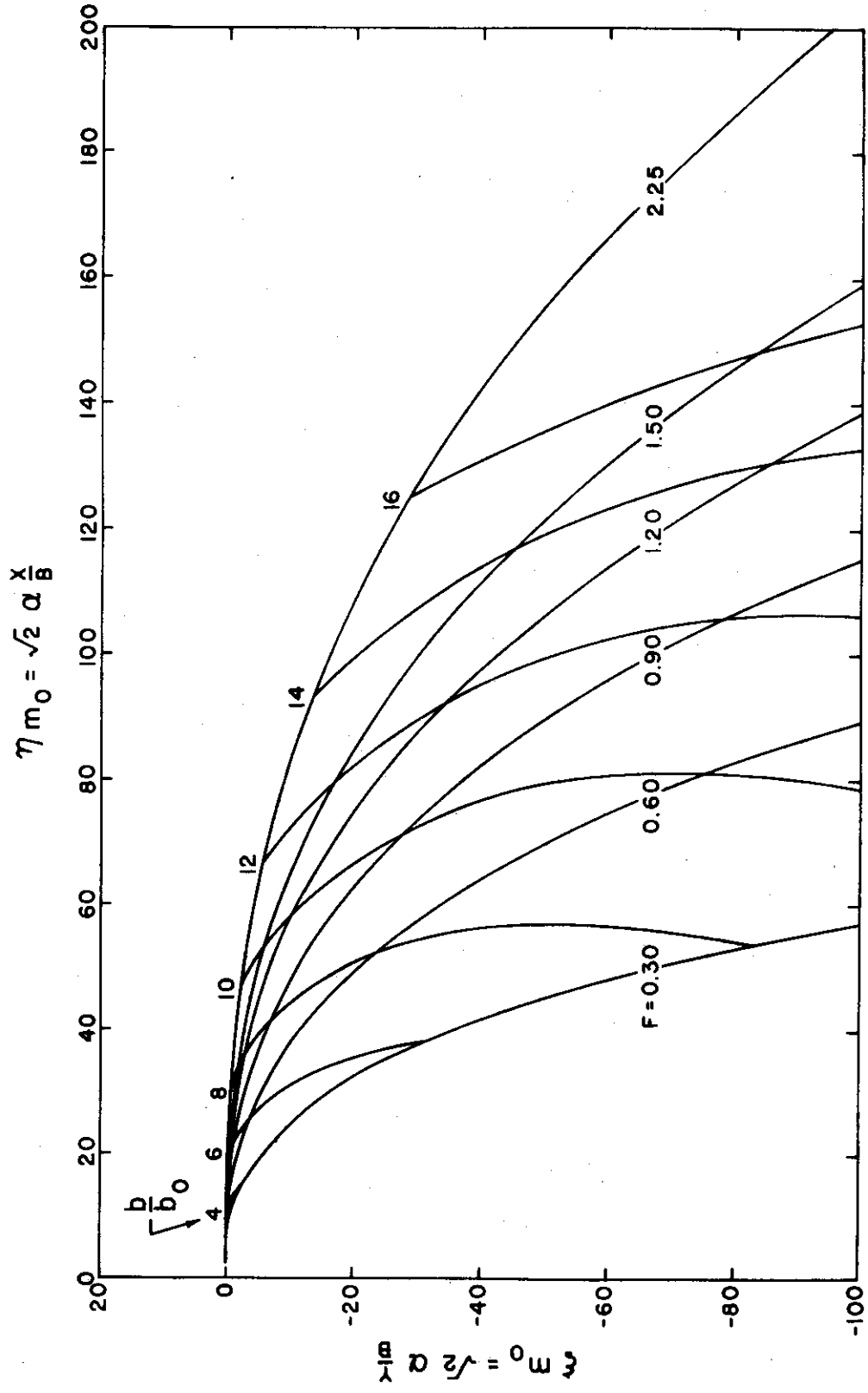

Fig. 7(a). $\theta = 0°$, $\Delta T = 10°F$

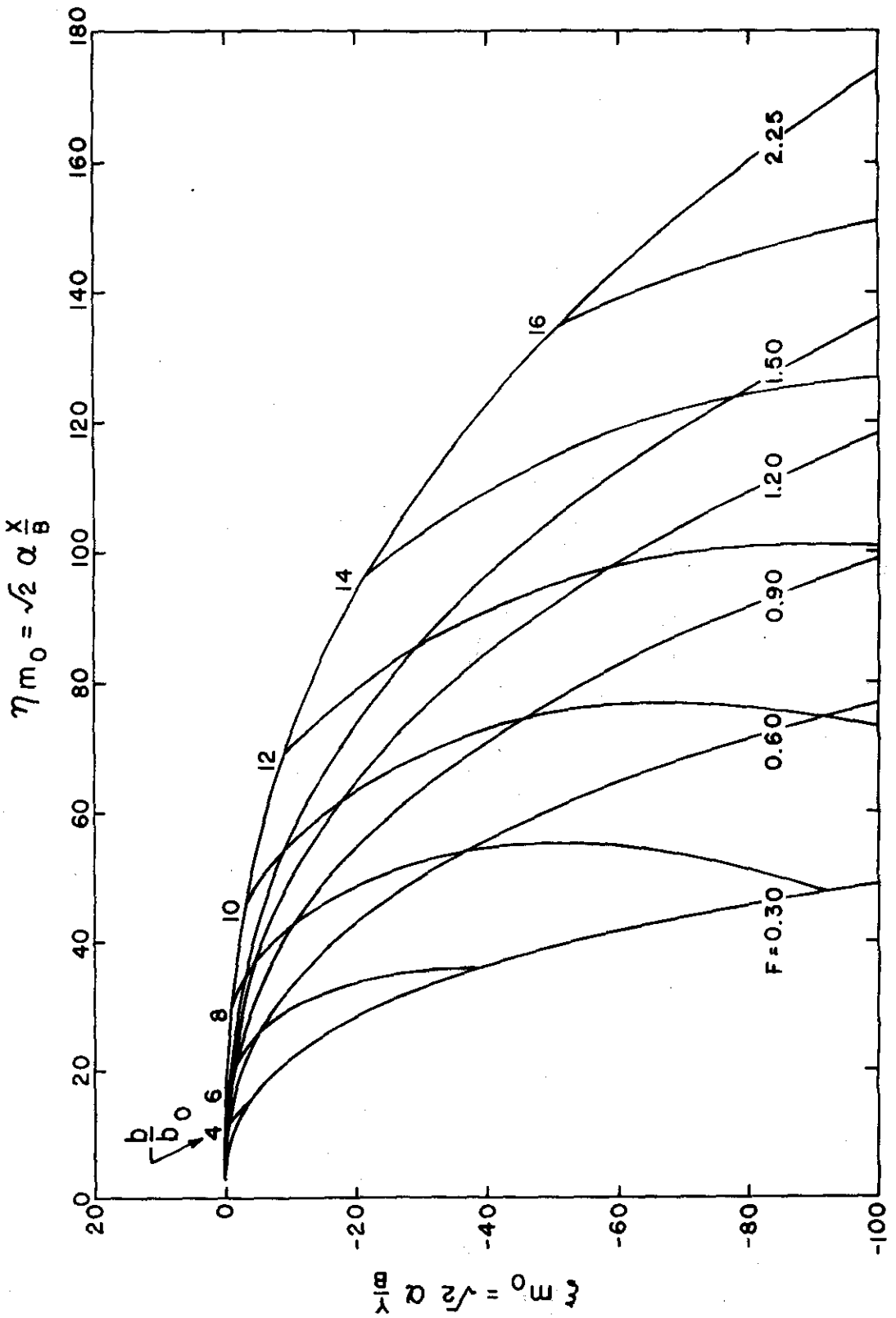

Fig. 7(b). $\theta = 0°$, $\Delta T = 15°F$

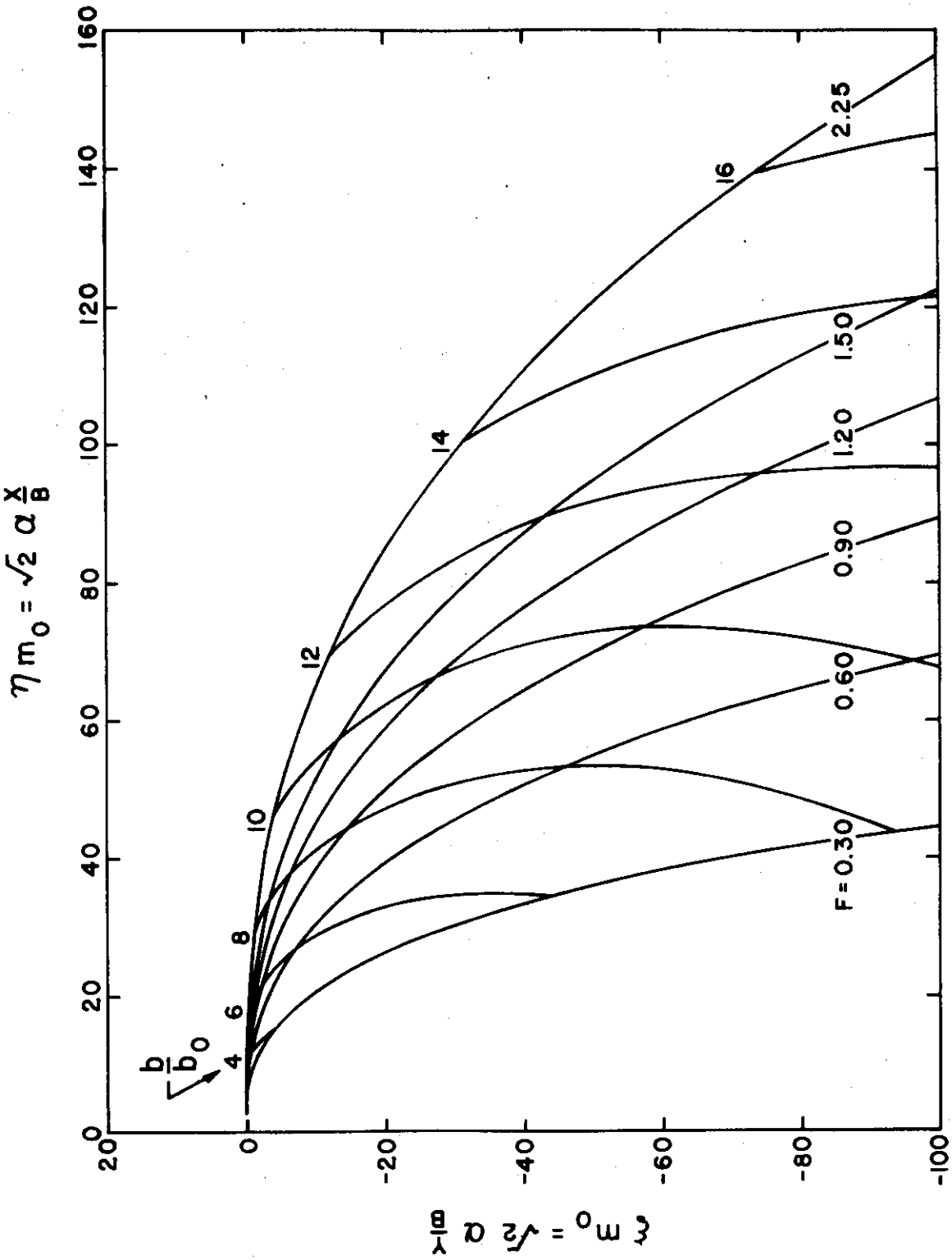

Fig. 7(c). $\theta = 0°$, $\Delta T = 20°F$

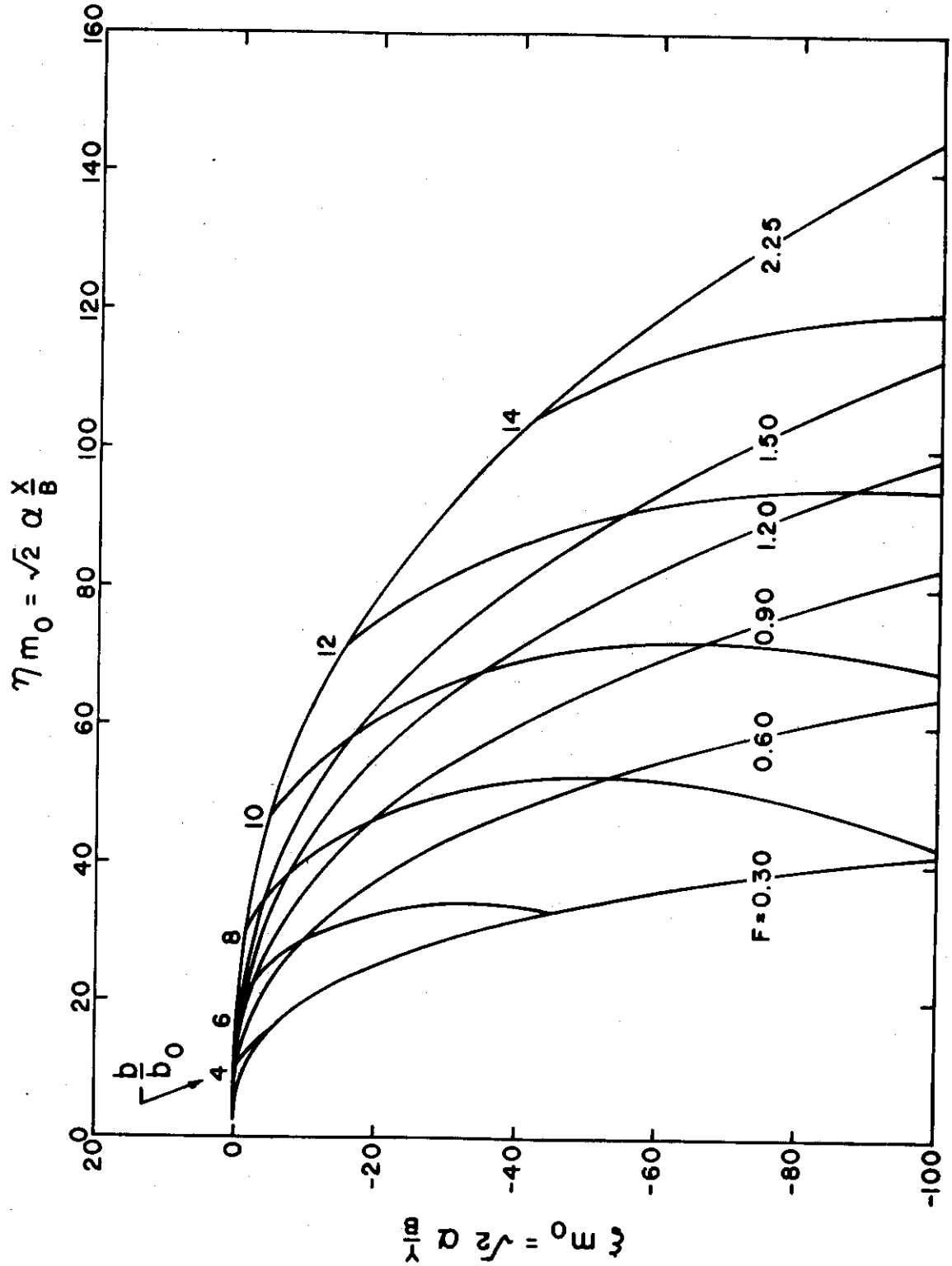

Fig. 7(d). $\theta = 0°$, $\Delta T = 25°F$

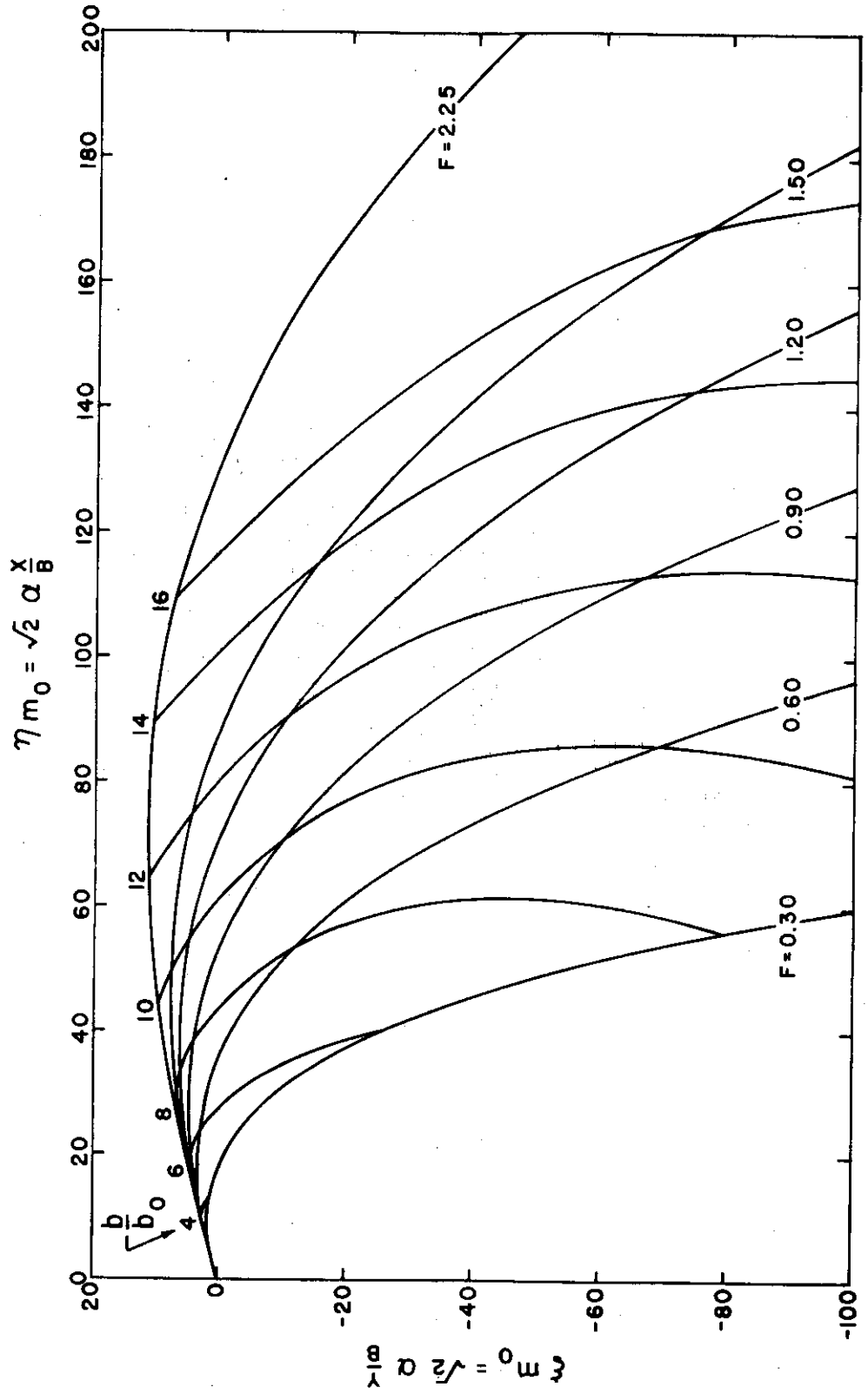

Fig. 7(e). $\theta = 15°$, $\Delta T = 10°F$

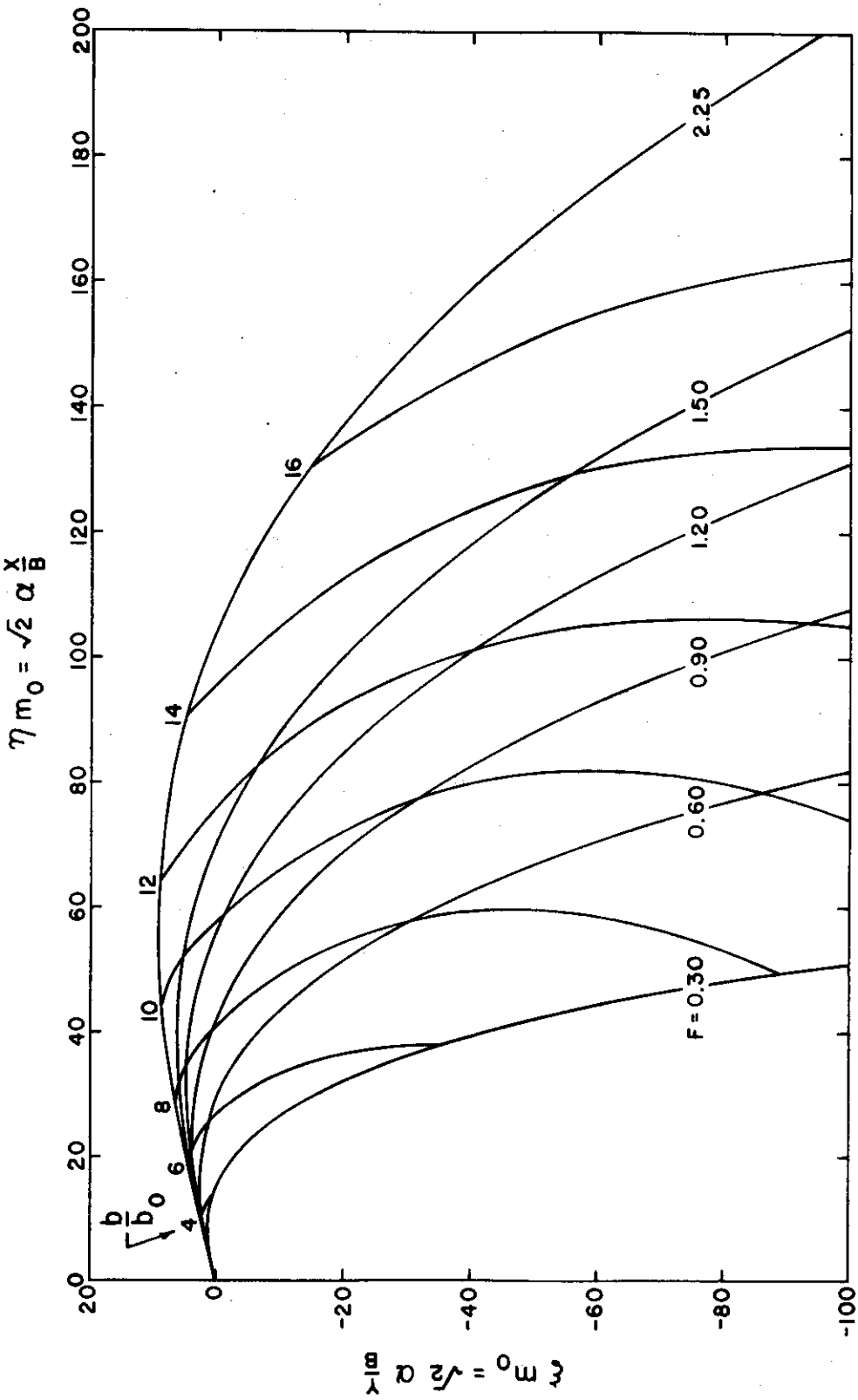

Fig. 7(f). $\theta = 15°$, $\Delta T = 15°F$

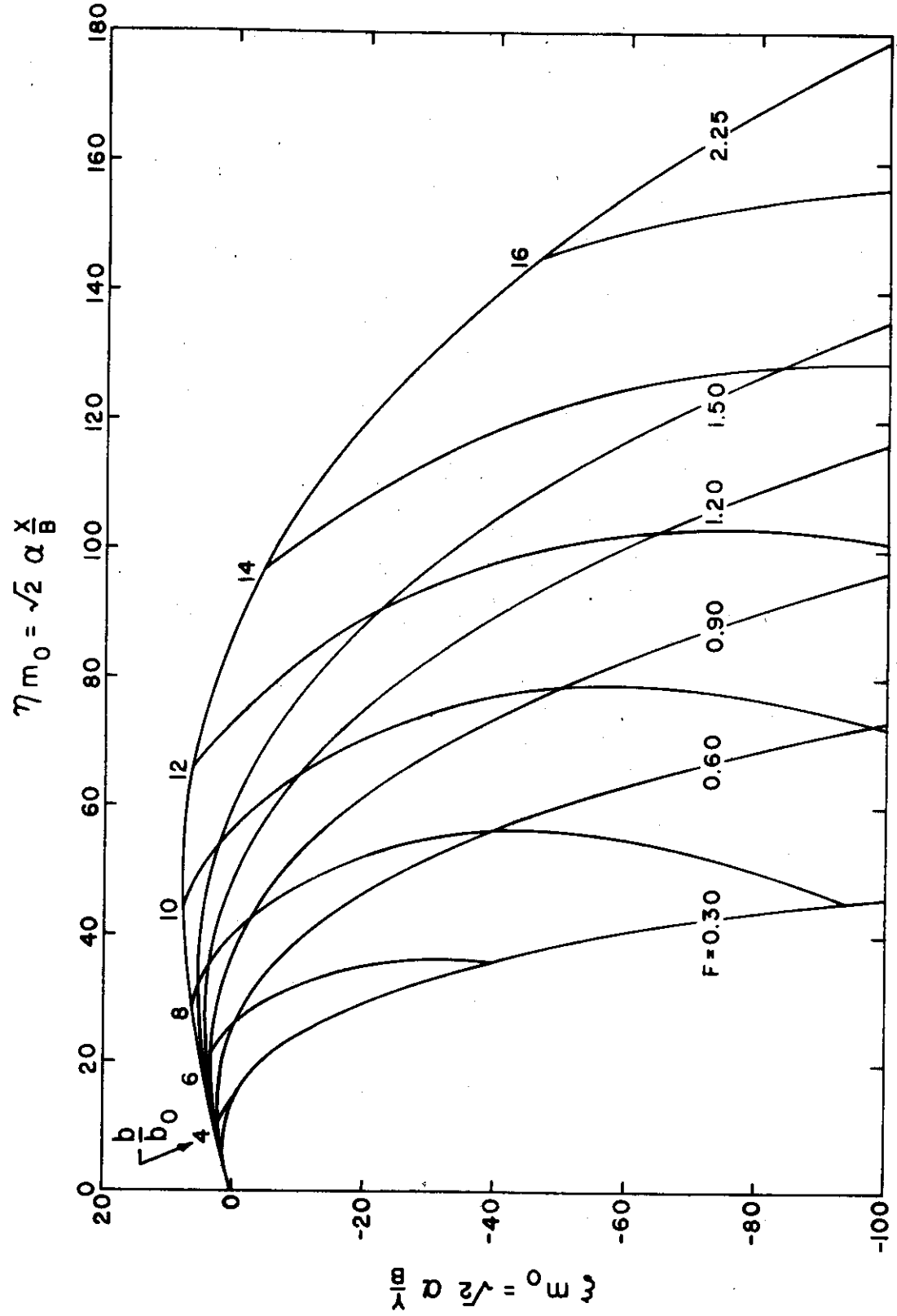

Fig. 7(g). $\theta = 15°$, $\Delta T = 20°F$

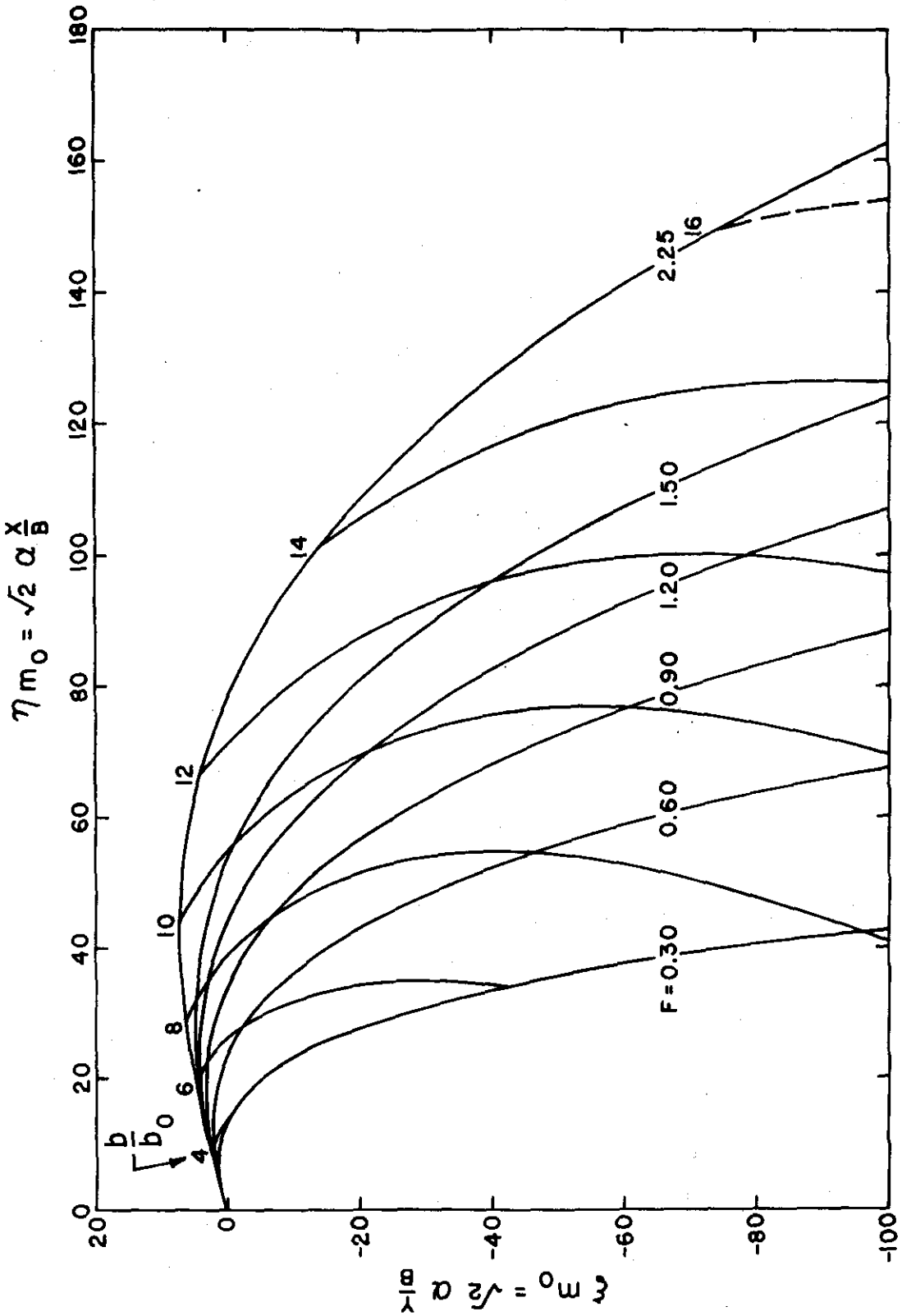

Fig. 7(h). $\theta = 15°$, $\Delta T = 25°F$

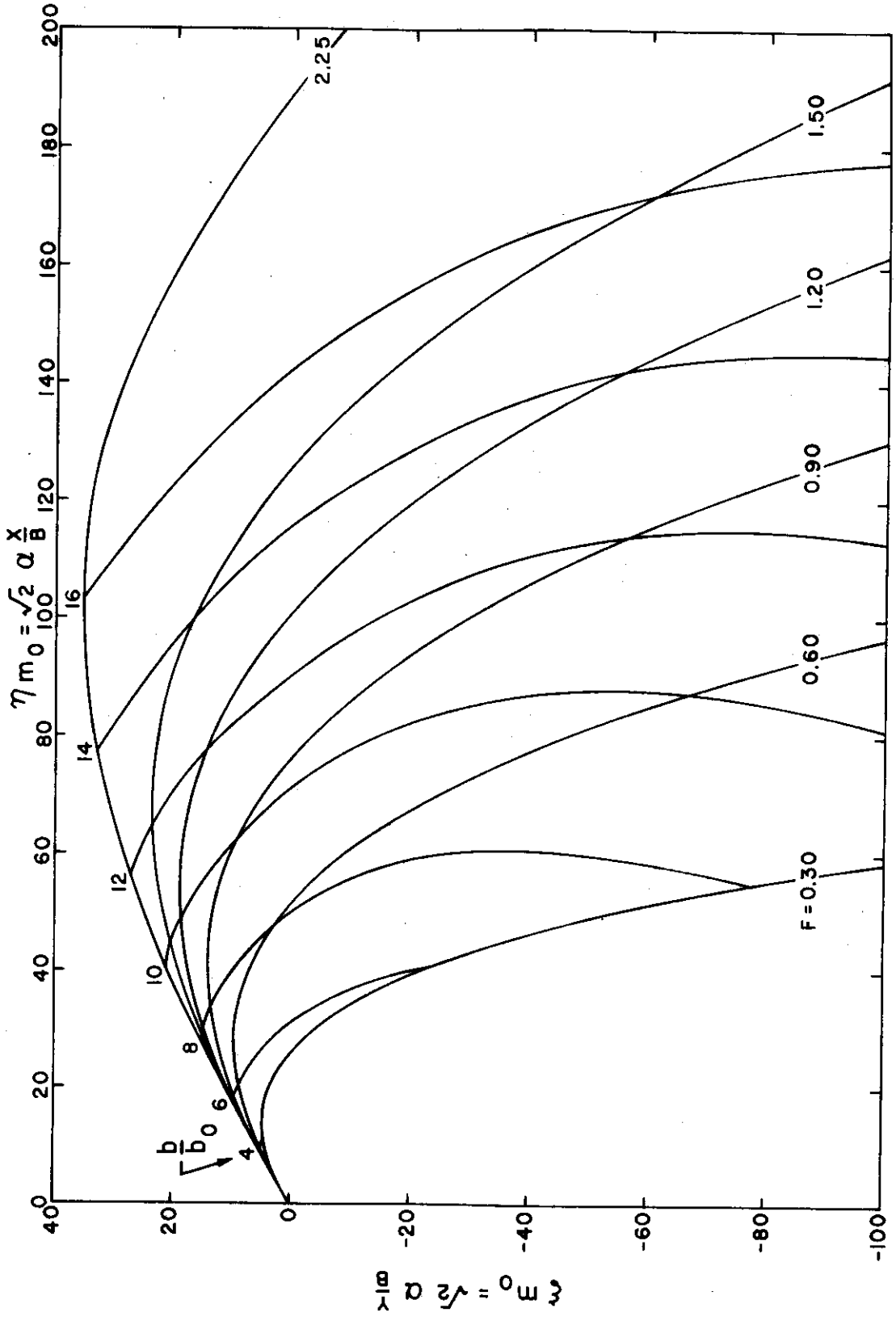

Fig. 7(i), $\theta = 30°$, $\Delta T = 10°F$

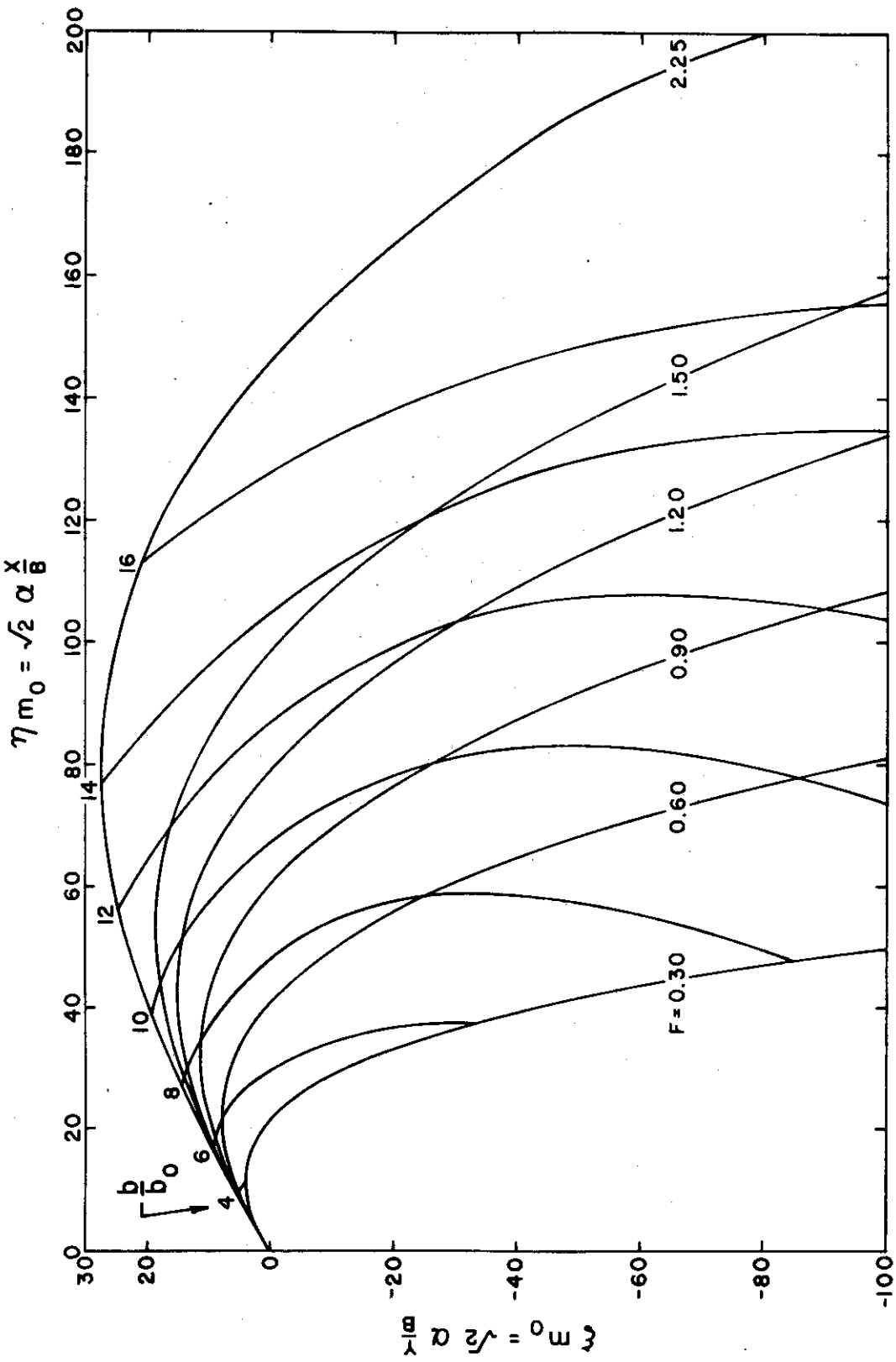

Fig. 7(j). $\theta = 30°$, $\Delta T = 15°F$

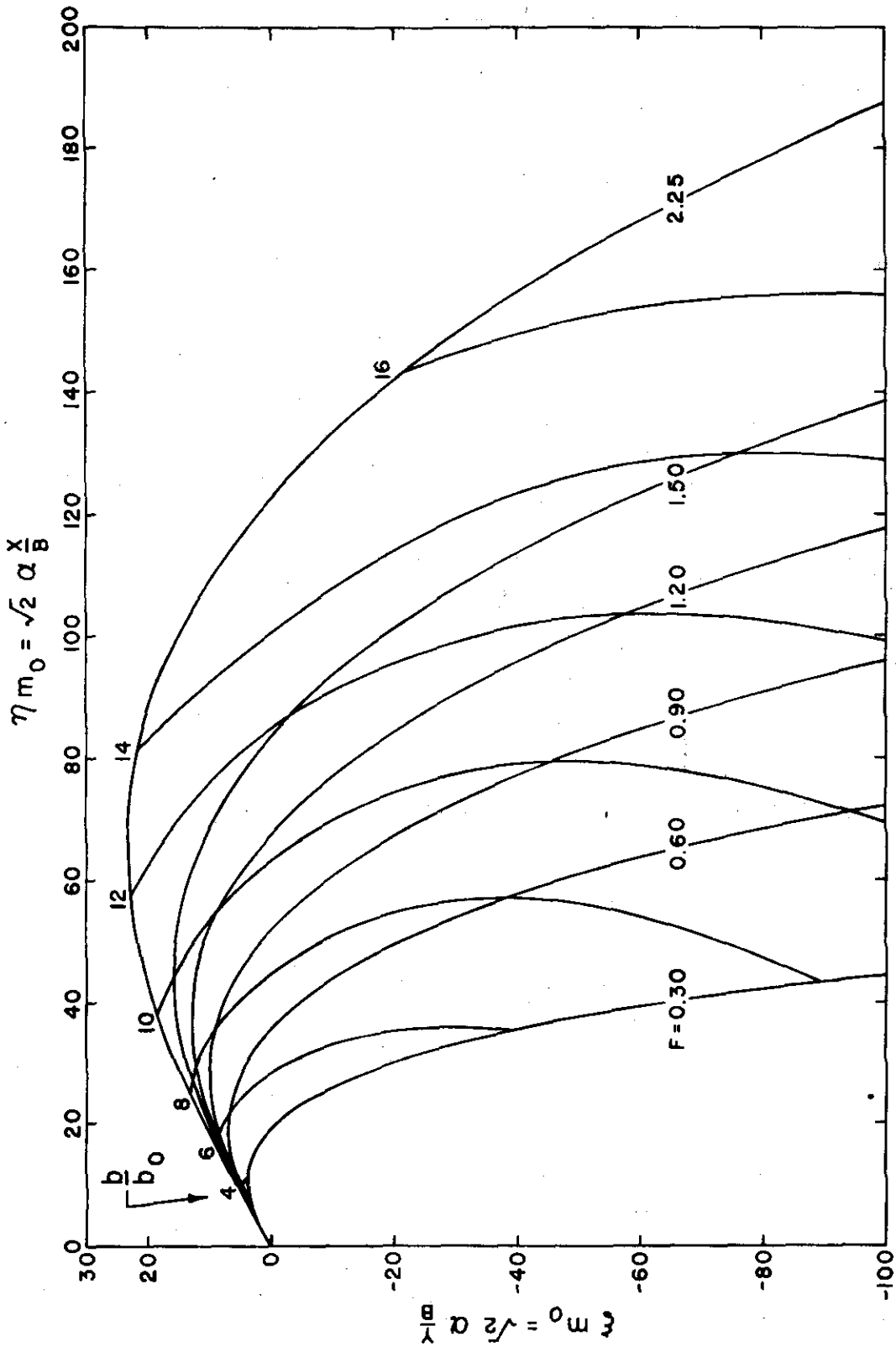

Fig. 7(k). $\theta = 30°$, $\Delta T = 20°F$

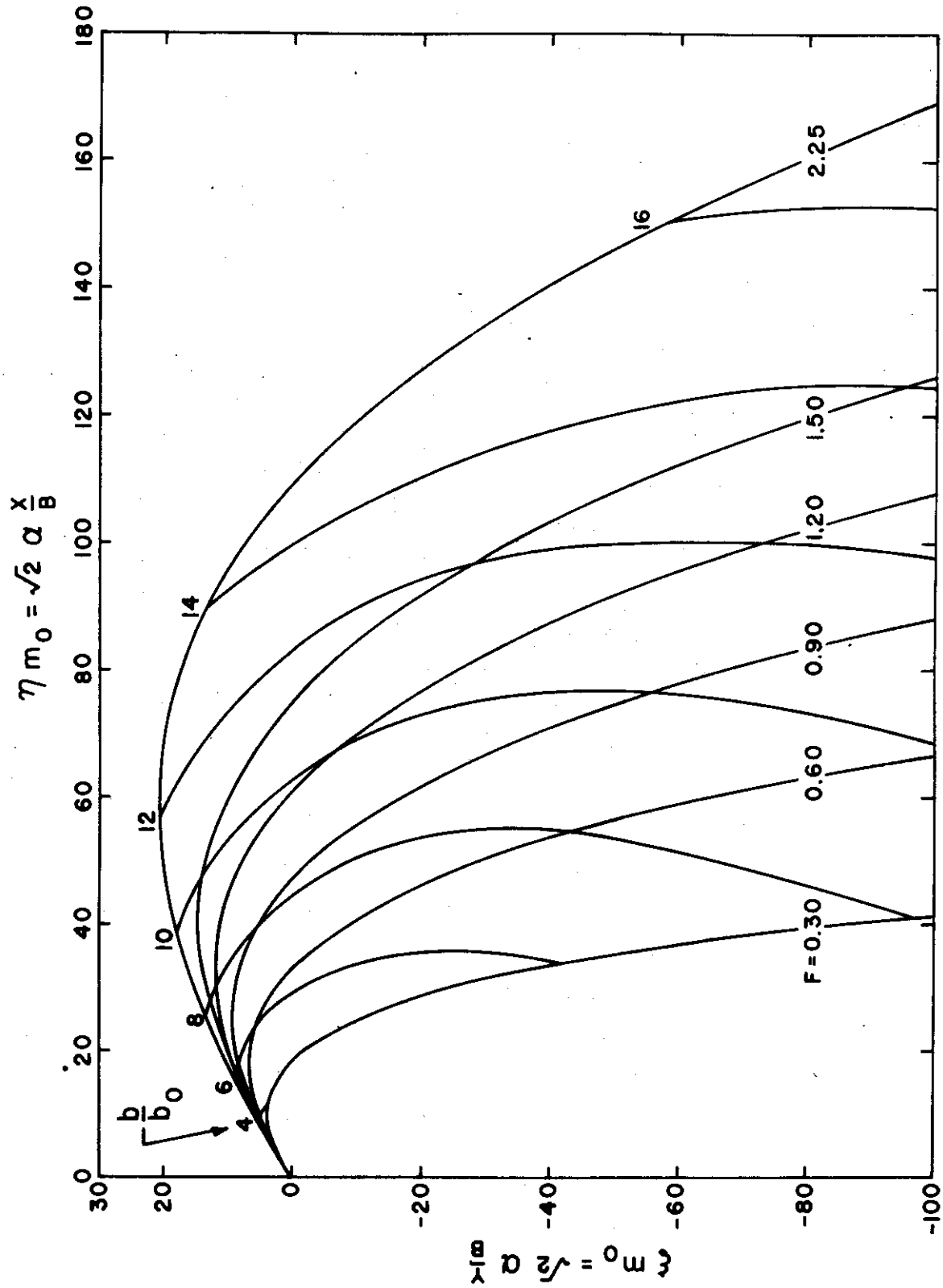

Fig. 7(1). $\theta = 30°$, $\Delta T = 25°F$

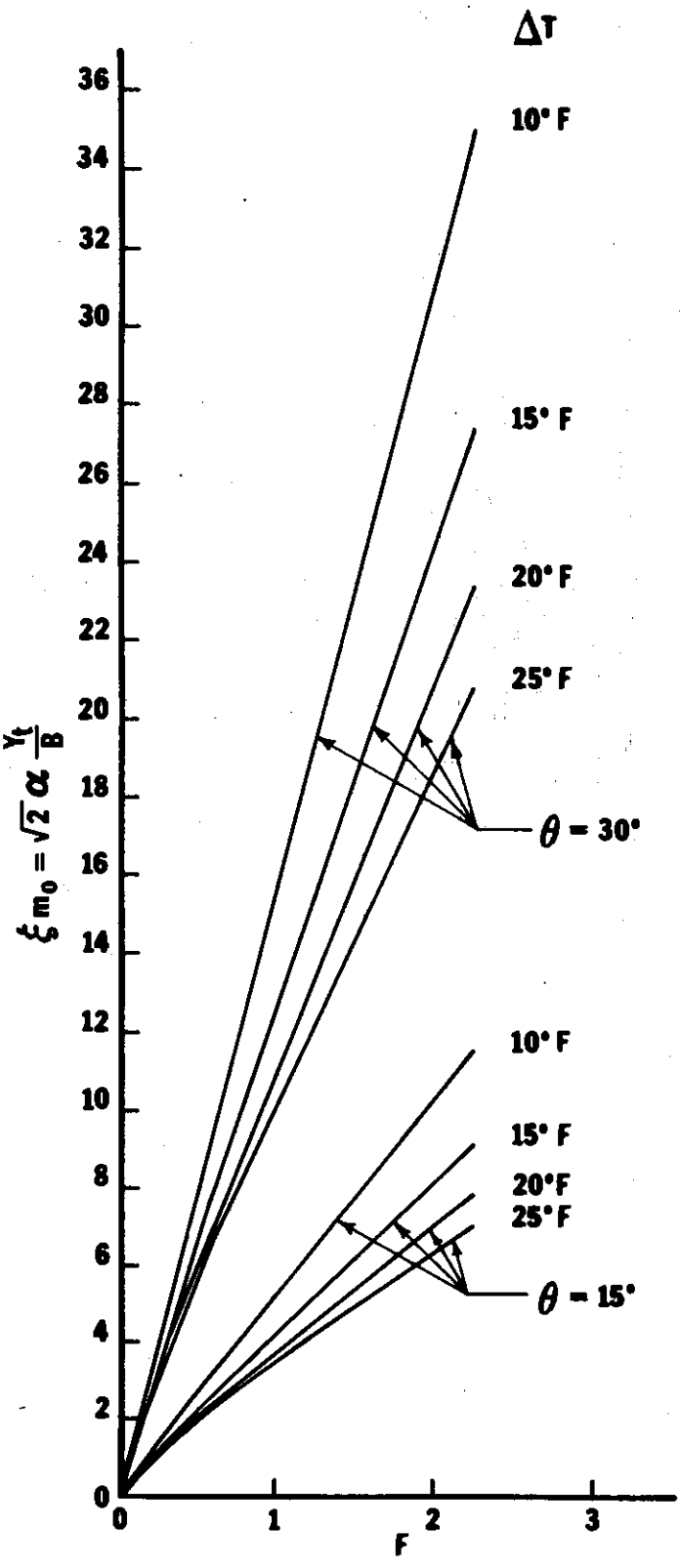

Fig. 8. Maximum rise of slot jet

Figs. 9. Dilution along trajectory of slot jet

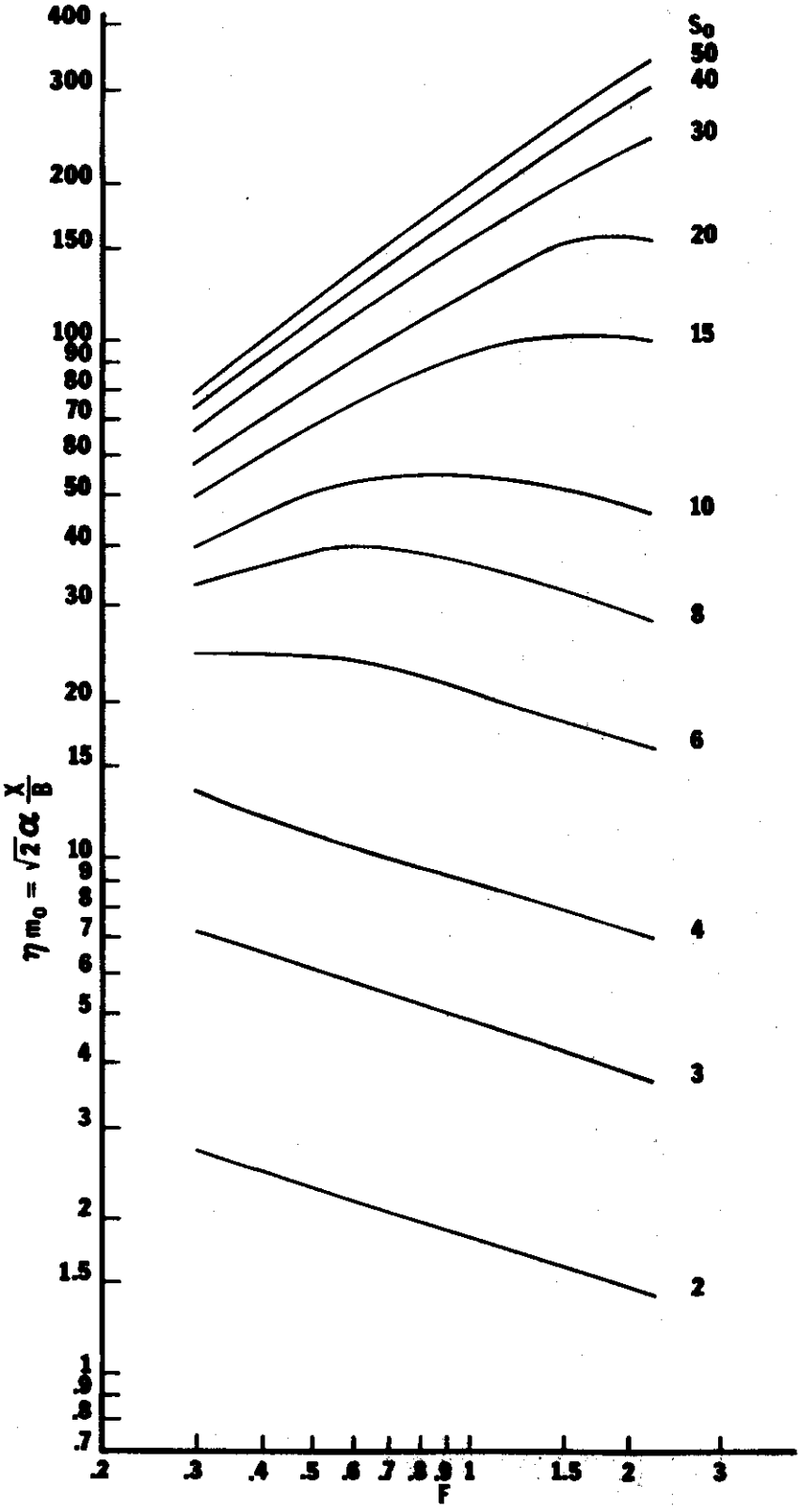

Fig. 9(a). $\theta = 0°$, $\Delta T = 10°F$

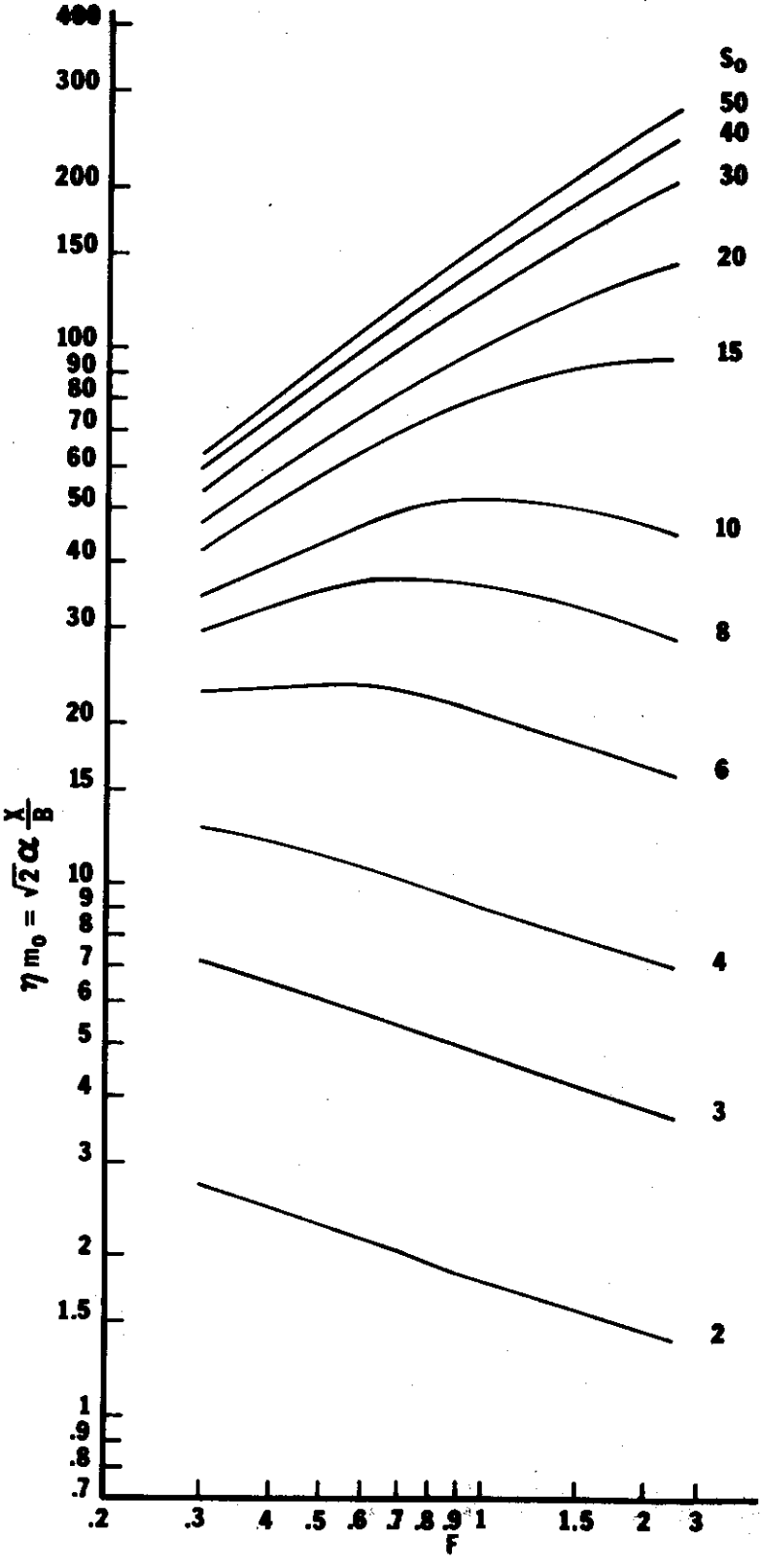

Fig. 9(b). $\theta = 0°$, $\Delta T = 15°F$

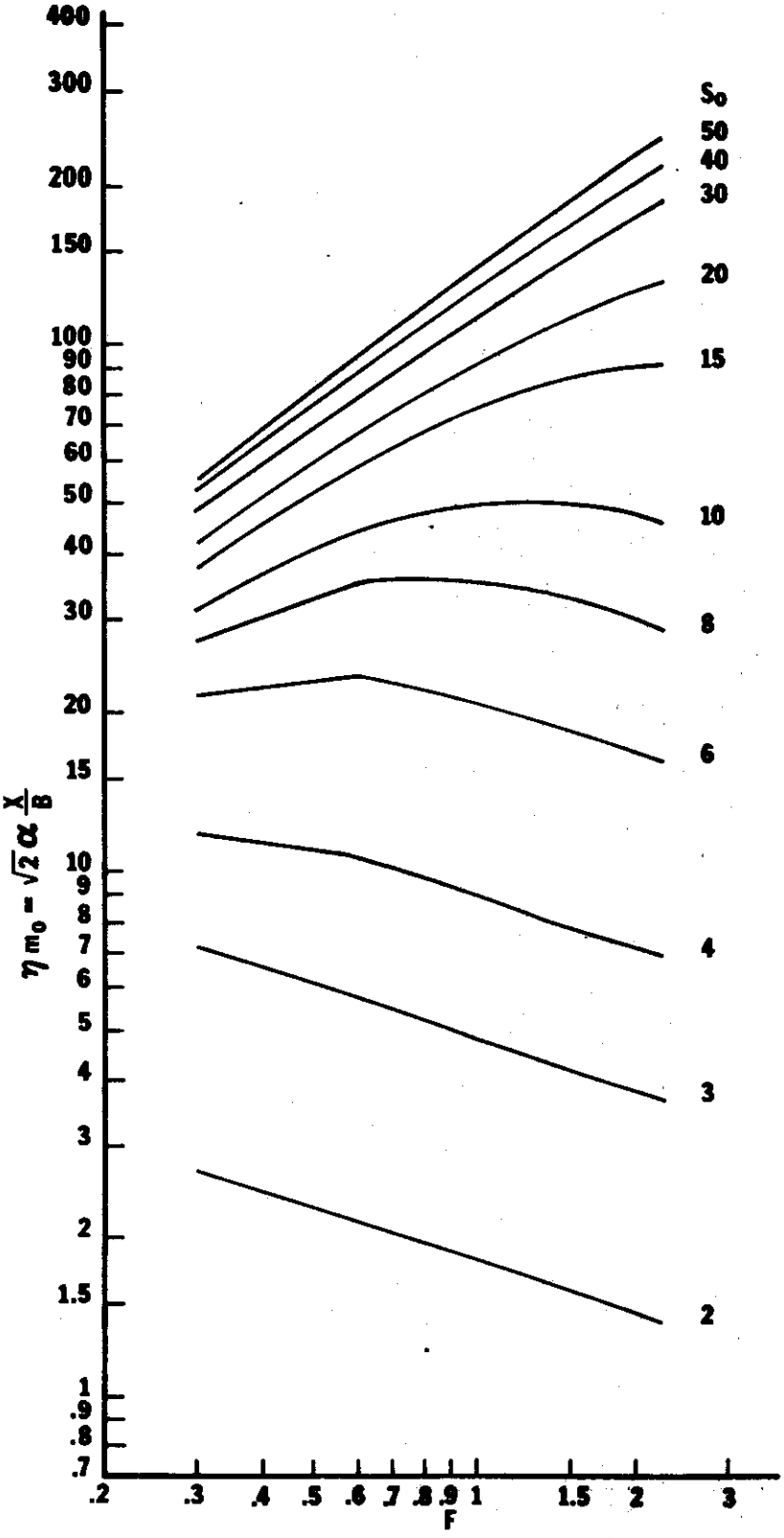

Fig. 9(c). $\theta = 0°$, $\Delta T = 20°F$

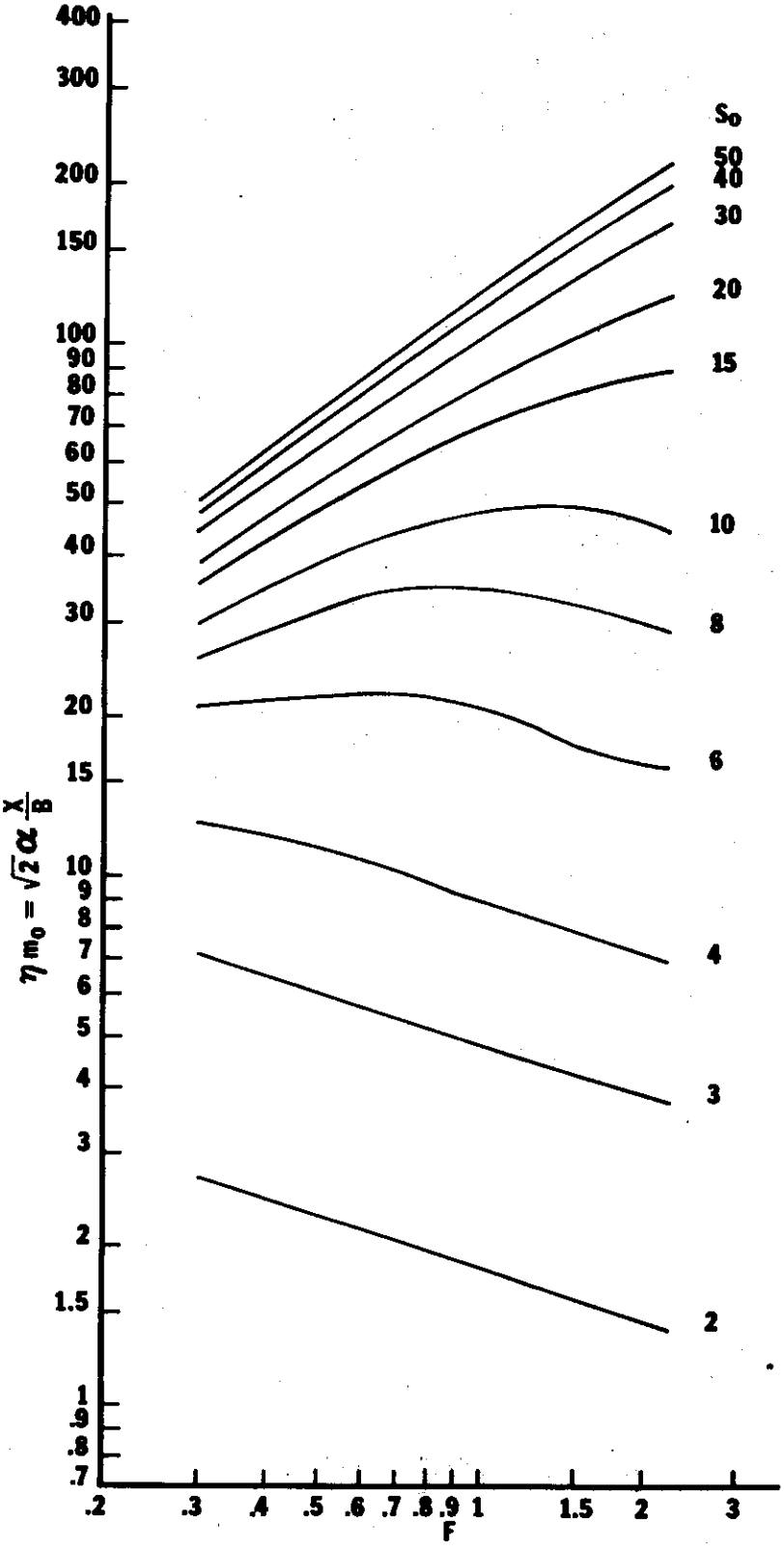

Fig. 9(d). $\theta = 0°$, $\Delta T = 25°F$

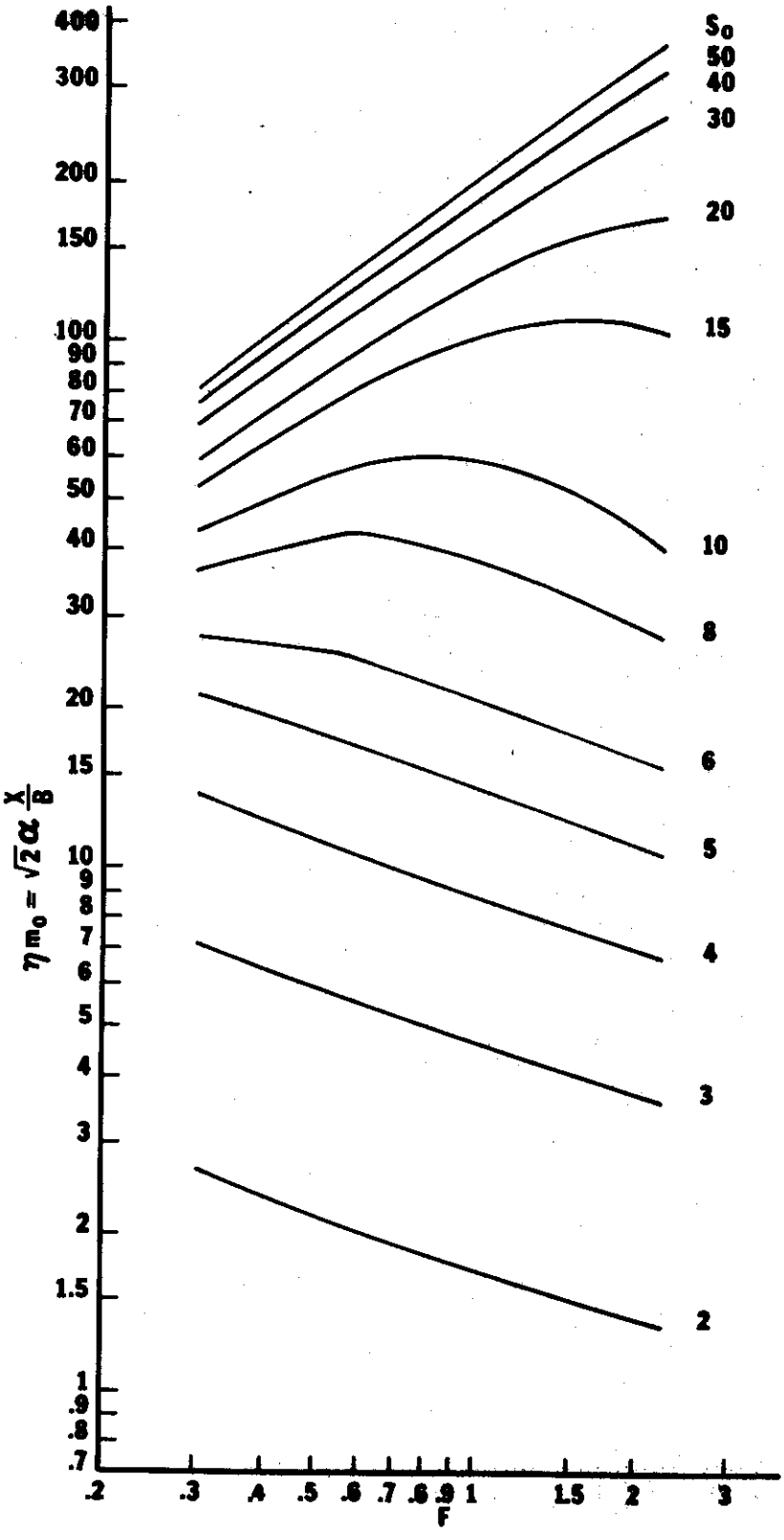

Fig. 9(e). $\theta = 15°$, $\Delta T = 10°F$

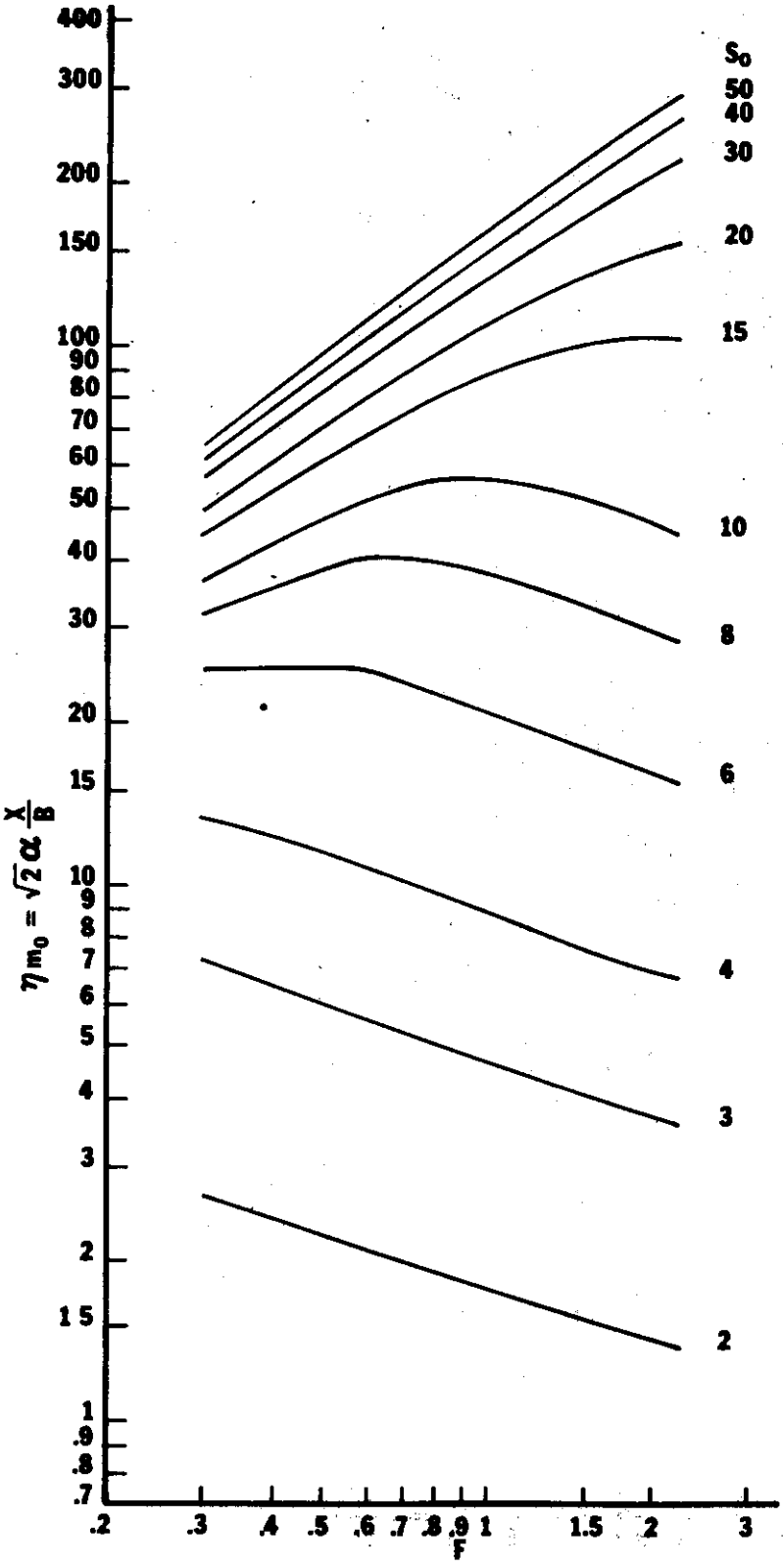

Fig. 9(f). $\theta = 15°$, $\Delta T = 15°F$

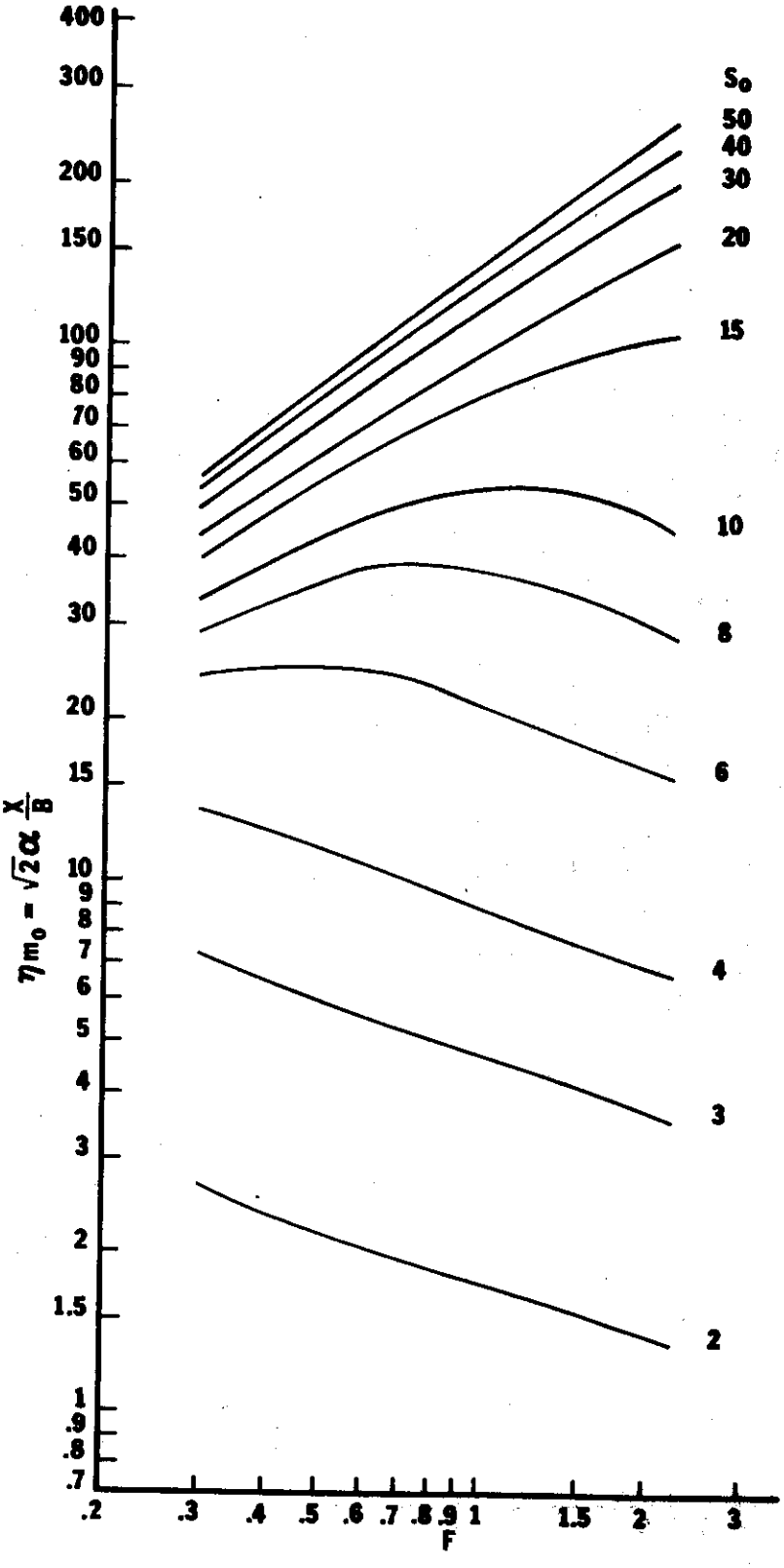

Fig. 9(g). $\theta = 15°$, $\Delta T = 20°F$

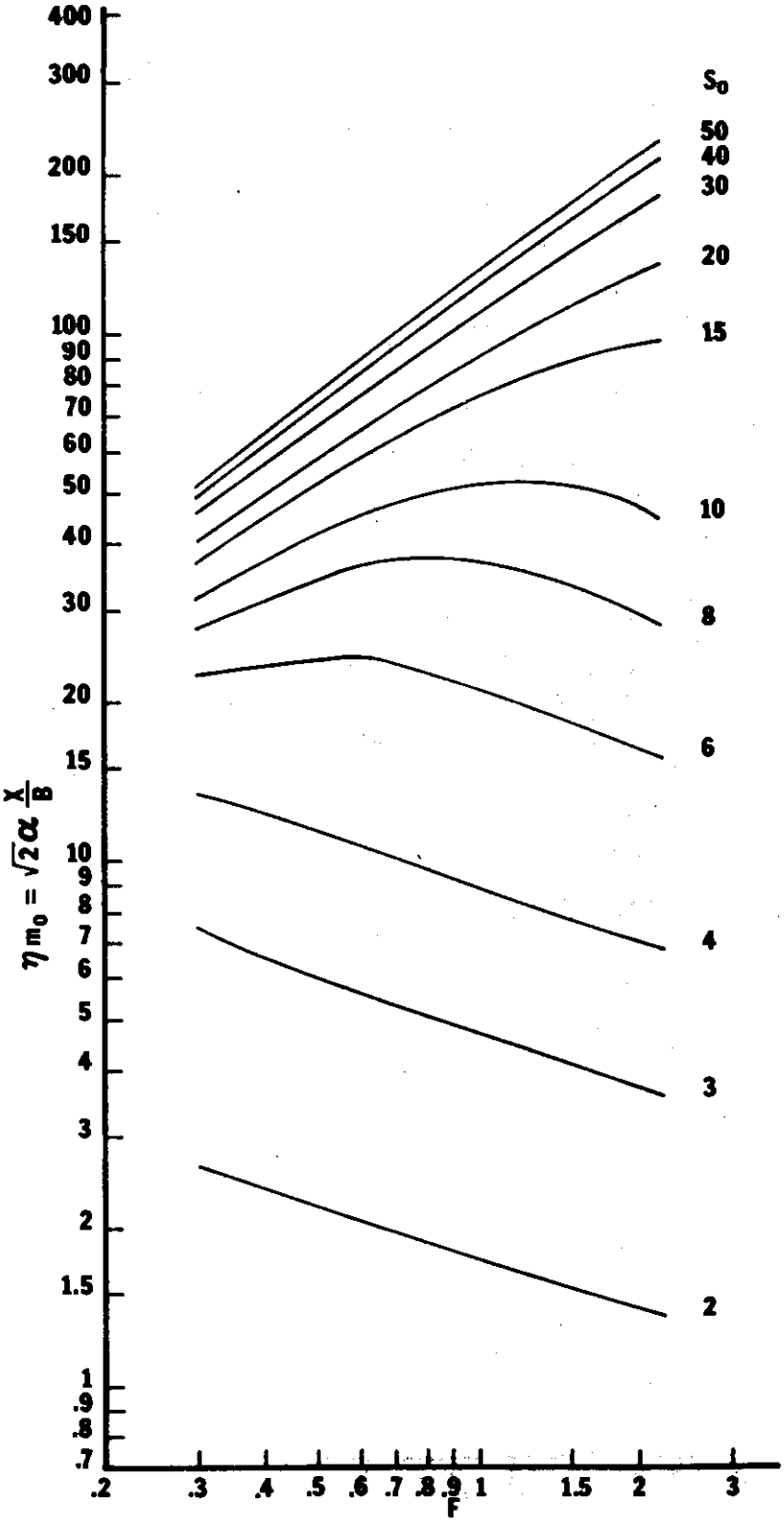

Fig. 9(h). $\theta = 15°$, $\Delta T = 25°F$

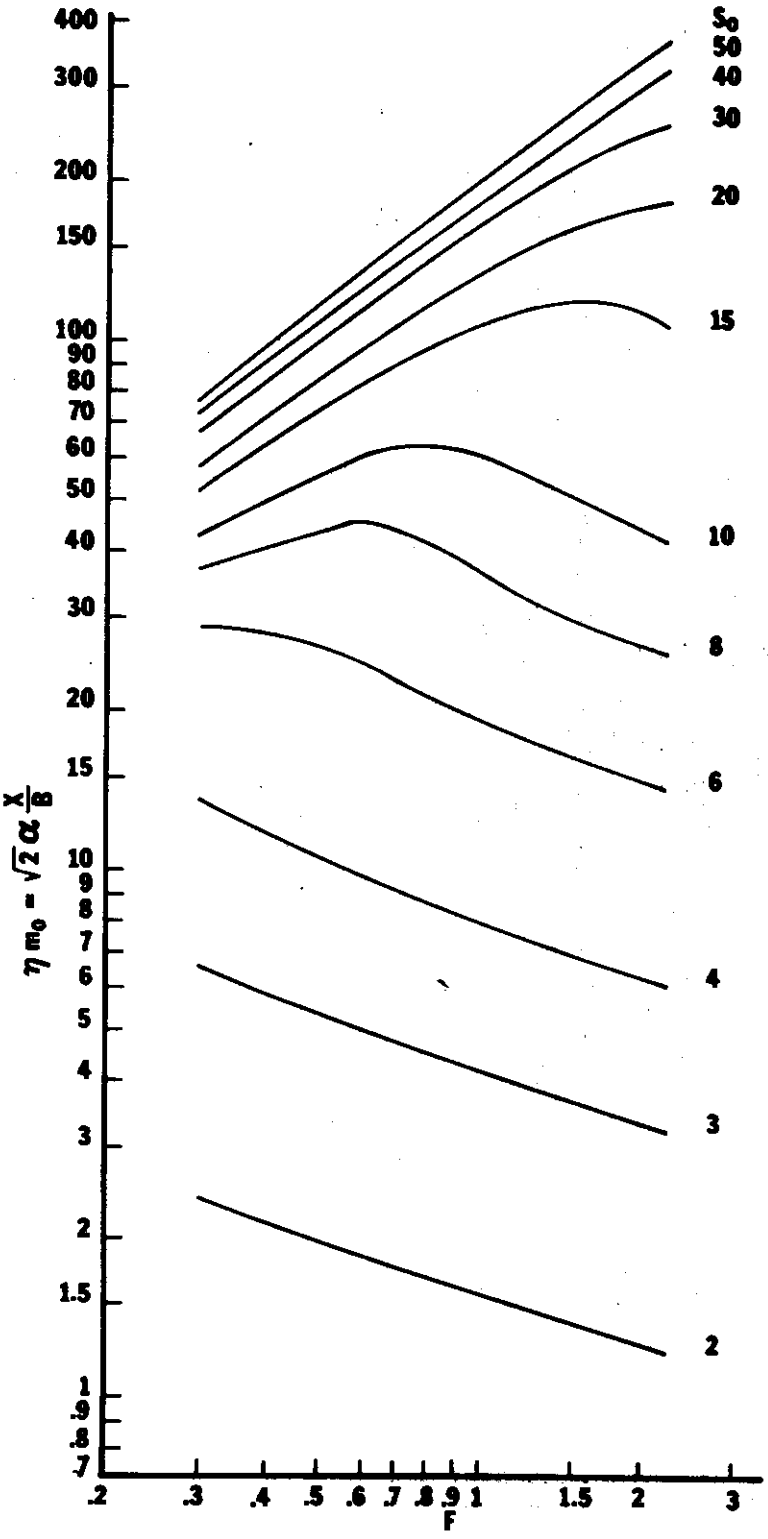

Fig. 9(i). $\theta = 30°$, $\Delta T = 10°F$

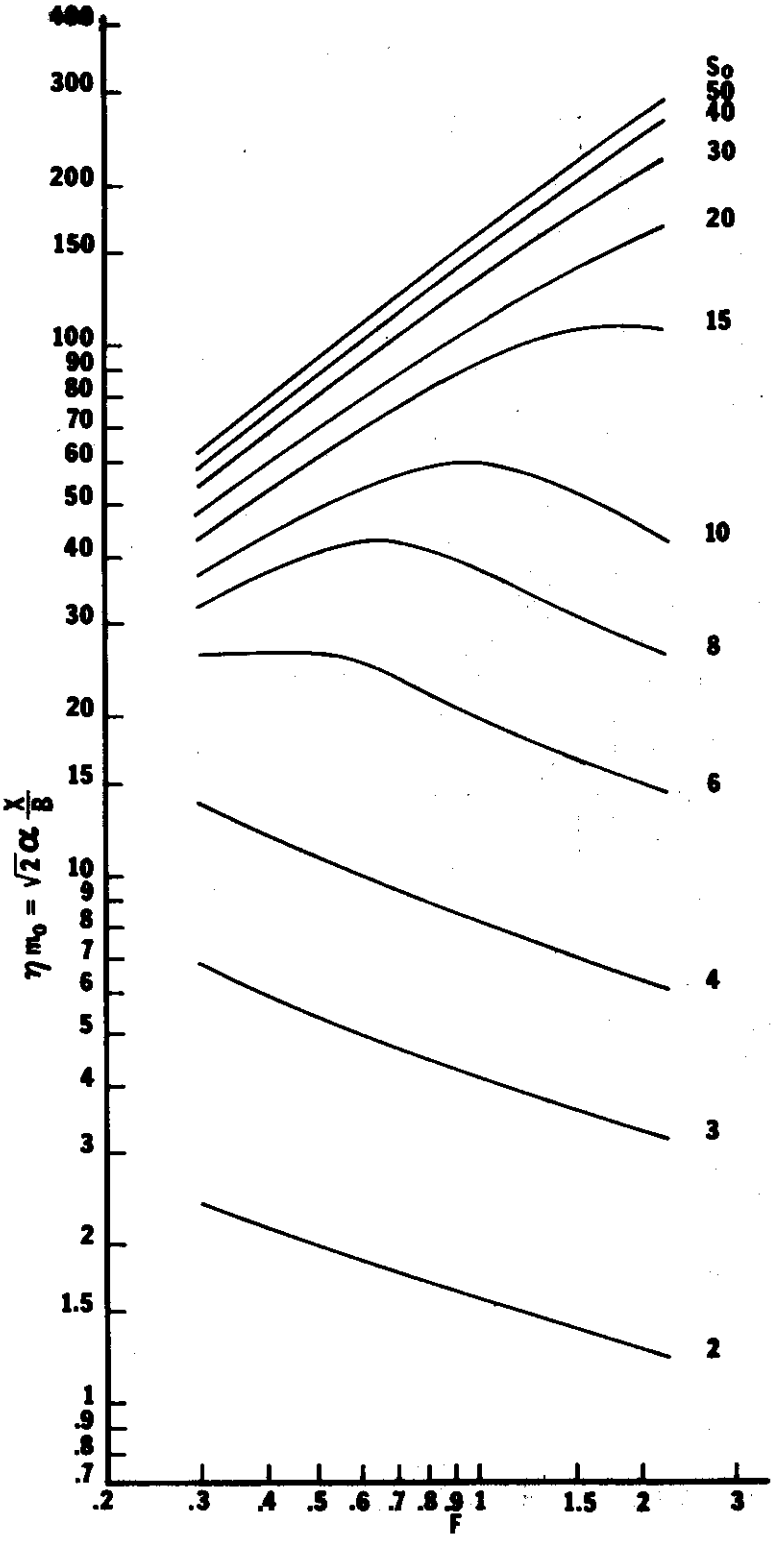

Fig. 9(j). $\theta = 30°F$, $\Delta T = 15°F$

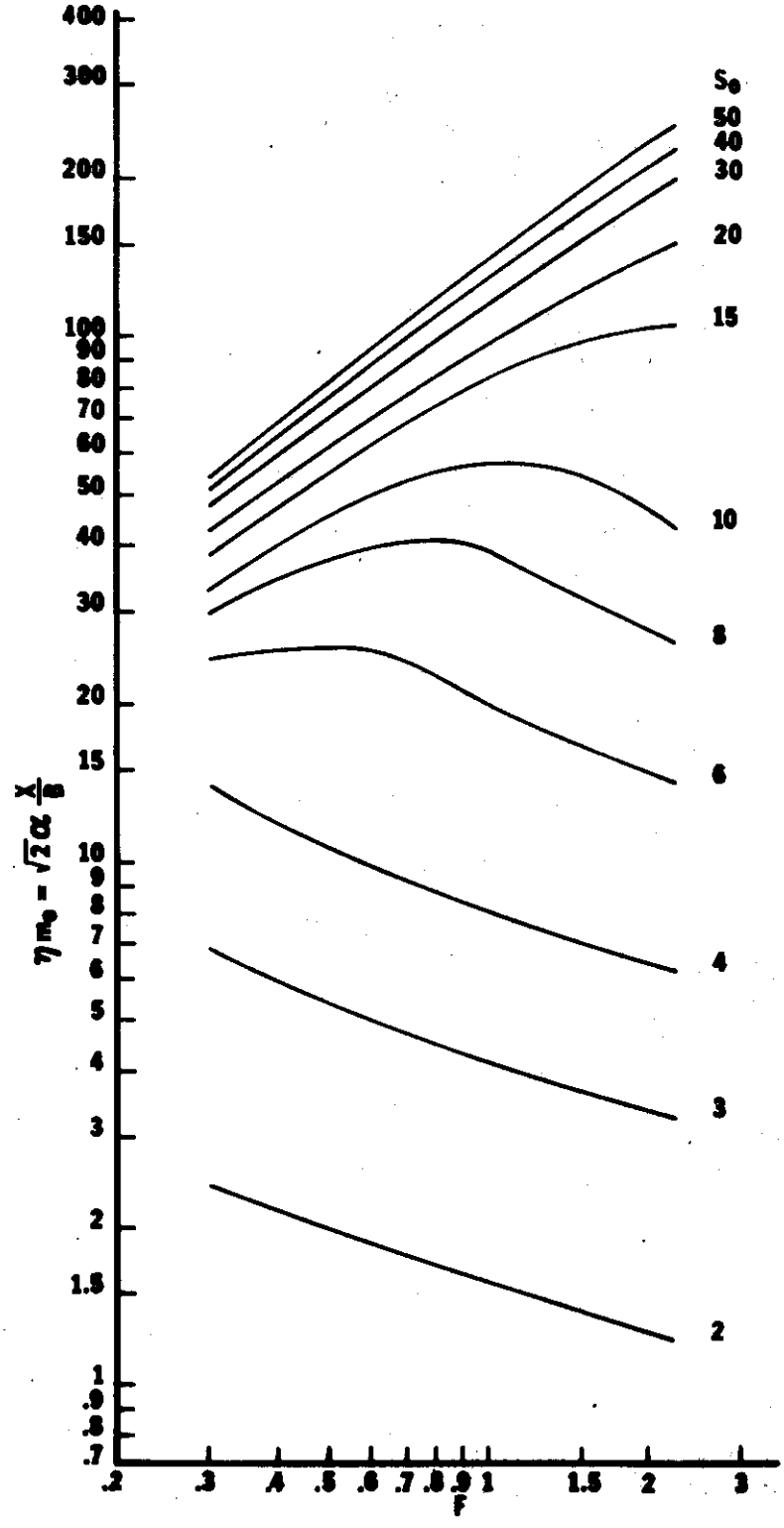

Fig. 9(k). $\theta = 30^\circ$, $\Delta T = 20^\circ F$

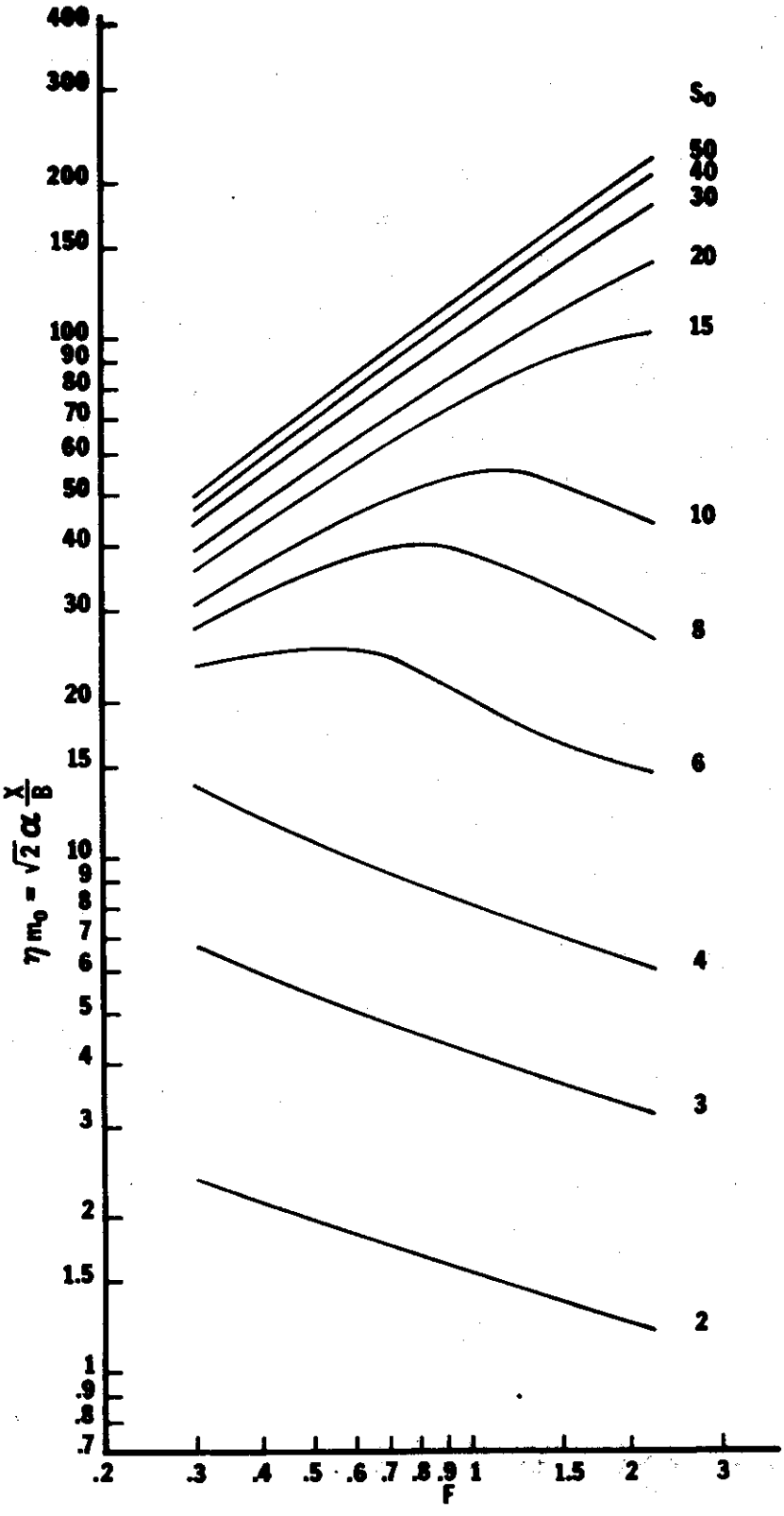

Fig. 9(1). $\theta = 30°$, $\Delta T = 25°F$